APPLICABILITY OF DIRECT EXTRACTION OF RATIONAL FUNCTION APPROXIMATION FOR AEROELASTIC FORCES BY FORCED VIBRATION METHOD

強制加振法による非定常空気力の有理関数近似直接同定に関する適用性

Doctoral Dissertation

Herry Irpanni

Department of Civil Engineering

Yokohama National university

Yokohama, Japan

March 2021

APPLICABILITY OF DIRECT EXTRACTION OF RATIONAL FUNCTION APPROXIMATION FOR AEROELASTIC FORCES BY FORCED VIBRATION METHOD

強制加振法による非定常空気力の有理関数近似直接同定に関する適用性

Herry Irpanni

A dissertation submitted in partial fulfillment of the requirements for the degree of Doctor Engineering

Academic Supervisor
Prof. Dr. Eng Hiroshi Katsuchi
Prof. Dr. Eng Hitoshi Yamada

Department of Civil Engineering
Yokohama National university
Yokohama, Japan

March 2021

Abstract

Aeroelastic forces are characterized by aeroelastic coefficients or flutter derivatives which are mostly obtained from wind tunnel experiments as a function of reduced frequency. Flutter derivatives extraction in frequency domain in a wind tunnel test by either a free or forced vibration method requires a recursive process for several wind speed. In frequency domain offer computational efficiency because the analysis is carried out in the selected mode. On the other hand, in time domain analysis is more convenient because nonlinear phenomena such as geometric nonlinearity of deck structure may be easily taken into account in the calculation. Aeroelastic force in frequency domain can be transformed to the time domain by using Rational Function Approximation (RFA). In this manner, it required linear and nonlinear optimization to extract RFA coefficients. Recently, direct extraction algorithm of RFA coefficients from wind tunnel experiments has been developed and RFA coefficients can be directly converted to flutter derivatives. This technique is less time-consuming and requires at least two wind speed that covers a wide range of reduce frequency of flutter derivatives.

This dissertation presents a fundamental investigation of the applicability of direct extraction of RFA coefficients for aeroelastic forces by forced vibration methods. This work is only limited to linear aeroelastic forces. The first step, a baseline study using secondary data of flutter derivatives of a truss deck, an edge girder deck, a twin deck, has been carried out to simulate appropriate wind speed combination and lag terms effect to extract a full set of the RFA coefficients. Aeroelastic forces are generated by using secondary tabular data of flutter derivatives and displacement time histories simulation. Applying RFA coefficient extractions procedure, new flutter derivatives can be obtained and the result is compared with experimental data. In this simulation, the phase lag between time histories and pre-set amplitude is neglected. Airfoil case shows a good agreement among eight flutter derivatives and proves that the RFA extraction algorithm is correct. The result shows that there is no relation between deck type and number of lag terms because lag terms are directly fitted. Two wind speed with one lag term is the minimum requirement for RFA extraction. One interesting point is that RFA extraction accuracy is limited to second-order polynomial of the flutter derivatives.

In the next step, wind tunnel experiments on a bluff body section model with B/D= 9.25:1 side ratio have been investigated by using one and two degrees of freedom experiments. The purpose of this experiment is to investigate the robustness of the direct extraction algorithm in terms of data length, pre-set amplitude and verify preliminary conclusions in numerical simulation. In the experiment, phase lag of displacement time histories and aeroelastic forces can be identified and the mechanism of wind speed combination can be verified. Free vibration was also conducted

to validate forced vibration experiment result. Extended Kalman filter weight global iteration was used to extract flutter derivatives in free vibration method. RFA extraction results are compared with classical approach of forced vibration and free vibration test results. In case of direct extraction, amplitude and phase lag are explicitly calculated. On the other hand, in RFA extractions, phase lag is implicitly calculated. There are some discrepancies between free and forced vibrations that might be caused by the airflow state. In the RFA extraction case, there is no effect on data length and discrepancies occur in case pre-set amplitude solely due to data processing. Results show that high-quality measurement data is an important matter to extract RFA coefficients. Based on the experimental result, it is confirmed that RFA extraction can be applied for a derivative that has a trend in a second-order polynomial.

Foreword

Three years living in Japan, learning fundamental knowledge of long-span bridges is a short time. I dedicate this dissertation to my beloved country Indonesia, which has many plans to develop a long-span bridge in the future. Even though the thesis discussion does not directly relate to the field reality, at least it may contribute as a reference.

I would like to sincerely thank to LPDP that financed my study and make it my dream comes true. I am grateful to my mother, who always gives me advice about the philosophy of life. I am also thankful to my wife and children that have sacrificed their time. I apologize that I miss a critical moment during my study.

I would like to sincerely thank to Prof. Dr. Eng Hiroshi Katsuchi, who gives me an opportunity to study for a doctoral degree at Yokohama National University under his guidance with zero wind engineering knowledge. Your patient in guiding me for three years in Japan is appreciated. May your goodness get the best reward from God. Without his guidance and persistent help, this dissertation would not have been possible.

I would like to sincerely thank to Prof. Dr. Eng Hitoshi Yamada, Associate Prof. Hitoshi Tamura. Associate Prof. Dyonisius M. Siringoringo, Ph.D. for their guidance, encouragement during my study in Japan.

I would like to show my greatest appreciation to Prof. Koichi Maekawa and Prof. Chikako Fujiyama for their constructive comments and some recommendations.

Finally, I would like to thank all of the structural laboratory members for their kind cooperation, support, and assistance.

Table of Contents

List of Figures

List of Tables

Chapter 1. Introduction

1.1 Motivation

Since the collapse of the old Tacoma bridge in 1940, research in wind engineering in the civil engineering area, especially in the long span bridge, has been increasing rapidly in a few decades. In a long-span bridge, aeroelastic force is more dominant than the earthquake force. Amplitude divergent during the wind-induced response of the bridge deck becomes the primary concern, particularly in the design phase.

The action of wind loads can be divided into two types, static and dynamic loads. In static case, such as lateral and vertical displacement can be easily prevented, i.e., by increasing the structural stiffness. On the other hand, dynamic loads need a depth investigation. In the wind dynamic, bridge response can be divided into two main types: limited-amplitude response (limited vibration) and divergent amplitude response vibrations (self-excited vibrations).

In the limited-amplitude case, it usually occurs due to the Karman vortex shedding phenomenon. When the oscillation frequency is equal to vortex shedding frequency, resonance will occur, which is called lock-in phenomenon. In this case, an enormous amplitude oscillation response will appear. The lock-in phenomenon will occur not only in the bridge deck but also in member parts of the bridge such as; stay cable, hanger, and lighting poles. Divergent amplitude response occurs only in the bridge deck, which is defined as a flutter or galloping phenomenon.

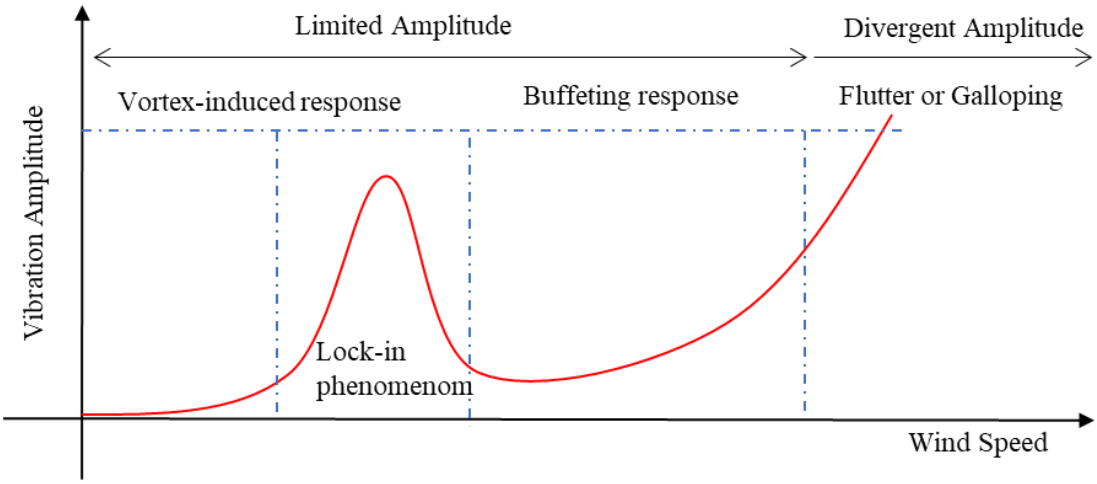

Fig. 1 Wind structure response against wind loading.

Aeroelastic forces of a bridge deck are characterized by aeroelastic coefficients [1] (flutter derivatives). Flutter derivatives are mostly obtained from a wind tunnel experiment with a scaled model of the bridge deck. Scanlan and Tomko [2] laid a fundamental theory to carry out flutter analysis in frequency domain. In this regard, the response of a structure is measured in every wind speed and the effectiveness of the restoring forces known as flutter derivatives is changing in a complex manner in every wind speed. Conducting wind tunnel experiments in frequency domain requires recursive procedure and time-consuming.

When a bridge deck is immersed in a wind field, a deck will be subjected to static and dynamic wind forces due to fluctuating wind speed. In frequency domain offer computational efficiency because the analysis is carried out in the selected mode. In time, domain analysis is more convenient because nonlinear phenomena such as geometric nonlinearity of deck structure may be easily taken into account in the calculation. Rational Function Approximation (RFA) will be used to model aeroelastic forces in time domain.

Thirty-five years later, a former student of Prof. Scanlan, Prof. Sarkar et al. [3]–[6] proposed a method to extract flutter derivative in time domain by employing RFA coefficients. This method is more direct and faster because it requires at least two wind speed to extract flutter derivatives through RFA. Another researcher, Siedziako and Øiseth [7] have been successful in obtaining a full set RFA coefficients using one wind speed subjected to random vibrations. The advantages of RFA extraction in wind tunnel experiments to extract flutter derivatives with less time consuming is mainly motivation in this thesis.

Nevertheless, flutter derivatives extraction in time domain could make some ambiguity in principle in identifying flutter derivatives in frequency domain because the response of a structure is measured in every wind speed and the aerodynamic response (flutter derivatives) will change in a complex manner at every wind speed. Some questions arise why flutter derivatives extraction in time domain by two wind speed combinations or one wind speed can cover wind range of reduced frequency and the applicability of direct extraction of RFA.

1.2 Aim and objectives

The thesis aims to find the applicability and mechanism of direct extraction of RFA coefficients by forced vibration method. In this manner, the effects of wind speed steps and the accuracy of flutter derivative extraction through the RFA coefficients were

investigated by numerical simulation and experimental. The objectives of this study are but not limited to:

1. To study the mechanism of direct extraction of RFA coefficients using different bridge deck types such as a streamlined deck, a truss deck, an edge girder deck by numerical simulation
2. To investigate some conditions in applying direct extraction of RFA coefficients such as data length of time histories, pre-set amplitude effect by wind tunnel experiments.

1.3 Dissertation outline

Dissertation outline is summarized as follows:

Chapter 2 will briefly summarize the current research related to the dissertation topic and presents system identification in frequency domain and time domain.

Chapter 3 presents the numerical simulation for the direct extraction of flutter derivatives with RFA. This chapter aims to investigate the number of lag terms and wind speed by using secondary data to understand the mechanism of wind speed combination.

Chapter 4 presents wind tunnel experiments for flutter derivative extraction in the time and frequency domain by forced vibration method. The purpose of this study is to investigate the applicability of RFA extraction in case of pre-set amplitude effect, data length and verify the mechanism of wind speed combination.

Chapter 5 presents concluding remarks of the dissertation and future works.

Chapter 2. Theoretical Background

2.1 Literature review

Aeroelastic forces are characterized by flutter derivatives. Free and forced vibration techniques are two distinct methods to extract flutter derivatives in a wind tunnel experiment. Although free vibration cannot accurately predict flutter derivatives in higher wind speed, a phenomenon that occurred at every wind speed, such as lock-in phenomenon, can be directly observed during experiments. Basically, in free vibration methods, flutter derivatives can be derived from a comparison between the structure's response in the wind off and wind on condition.

Many system identifications were introduced to identify flutter derivatives in free vibration experiments in frequency domain. In free vibration method, either a free decay or buffeting signal can be as an input. In free decay test, the flutter derivatives are based on free decay signals as a result of initial displacement. One method based on free decay signal is the Extended Kalman Filter with Weighted Global Iteration (EKWGI) [8]. This identification system is based on the Kalman filter technique [9], which is conducted in one degree of freedom (DOF) of heaving and torsional oscillation. By using modal information of each observation, data can be computed and finally combined with the same reduce frequency for each data to obtain flutter derivatives. Nevertheless, this method will work well in higher wind speed where a coupled vibrations will occur. Other techniques are the Iterative Least Square method (ILS) [10] and the Unified Least Square (ULS) method [11]. Each response of the structure in every wind speed is iterated in the space state model until convergence. However, these methods have disadvantages. In higher reduced wind speed because deck section will decay rapidly and causing data length to become short. In buffeting signal, the input uses only a steady random response of the deck section without any initial displacement. This mechanism will more represent a real bridge under wind flow. Some system identifications which are based on buffeting response are the Covariance Block Hankel matrix (CHBM) [12], stochastic system identification [13], [14]. The deck response is also compared between wind on and wind off conditions in order to extract flutter derivatives.

A forced vibration method has advantages more precisely in higher wind speed and straightforward. Flutter derivatives extraction is relatively easy by decomposing aerodynamic forces into the real part (aeroelastic stiffness) and imaginer part (aeroelastic

damping) in the complex plane. Aeroelastic forces can be measured either by load cells [13] or by pressure signals over the surface in the streamwise direction. The phase lag between displacement time histories aeroelastic forces is an important parameter in flutter derivatives extraction [14]. Many parameters can cause phase lag, such as sampling rate, instrumentation setup, and filters used [15]. By using surface pressure measurement, flow patterns around the bridge deck such as flow separation, flow reattachment, vortices formation can be easily investigated.

Aeroelastic forces commonly are described in frequency domain as a function of reduced frequency. On the other hand, the wind-induced response of the bridge is described in time domain. In the aeronautics field, Roger [15] proposes Least Square Rational Approximation (LS-RFA) and Karpel [16] introduces Minimum State of RFA (MS-RFA) to approximate aerodynamic forces of wing planes in time domain. In this case, linear and nonlinear parameter optimization has been required to identify RFA coefficients associated with the frequency-dependent aeroelastic forces, and the lag terms are essential things. Linear parameters are determined using least square techniques and nonlinear (lag term) are determined by the non-gradient method [17]. Lag terms can be optimized by using non-gradient and gradient methods in other to improve fitting accuracy [18]. In that paper, it argued different expressions of lag terms can be used. In aerospace science, there are many alternative methods can be used to convert frequency-domain aerodynamics into time-domain aerodynamics [19][20].

In bridge engineering, Fujino and coworkers applied MS-RFA to model bridge response in time domain [21]. There is a trade-off between approximation and lag terms. More lag terms are used, approximation error becomes smaller [22]. For example, the Akashi Kaikyo bridge used four lag terms to have good behavior of aeroelastic forces. Lag terms (aerodynamics root) are only mathematical expression that the behavior of aeroelastic response in frequency domain will fit in time domain. In this study, it has been concluded that one lag term for a streamlined deck, two lags for a box deck, and three lags for a conventional truss deck. Many studies have been conducted in bridge modeling in time domain to analyze flutter and buffeting response by using RFA. The equation of motion is expressed in the modal coordinate state-space form [23]–[25], and the wind-induced response of the bridge was also studied [26].

Chowdhury and Sarkar proposed an identification method of RFA coefficients directly from a wind tunnel test in free vibration [3]. In this technique, A direct identification method of RFA coefficients from wind tunnel experiments has been

presented by measuring aeroelastic force with surface pressures and displacement time history. In this technique, the formulation of aerodynamic aeroelastic forces using the Minimum Sate Rational Function Approximation (MS-RFA) in time domain was applied with inverse Laplace transformation, and then RFA coefficients were extracted by the Least Square method. In this technique, lag terms are not an important issue and require fewer wind speed combinations. This idea was based on Iterative Least Square (ILS) and convergency of eigenvalue, which is the characteristic of system identification in free vibration methods is neglected. In free vibration method of RFA extraction, it is questionable whether in higher wind speed where vertical vibration decay rapidly will affect the extraction.

Cao and Sarkar reformulated the identification method for forced vibration method in one degree of freedom (DOF) [4]. Time history information such as amplitude and phase lag explicitly calculated and was used in the extraction. The result shows there is a slight discrepancy result in the derivative of A_2^* and H_2^*.

Reformulated RFA formulation Sarkar & Bao has been successful in developing a formulation for two DOF [5] experiment. This formulation is more robust and phase lag independent. Time histories are included directly into the formulation where phase lag is calculated implicitly. It was said that at least two wind speed with one lag term is required to extract flutter derivatives. Some algorithm test has been performed to test the robustness of the algorithm of the formulation. It has been shown that the algorithm was accurate in predicting RFA coefficients. Sauder and Sarkar also extended the formulation for three DOF experiment [6]. In this technique, the formulation of aerodynamic self-excited forces using MS-RFA in time domain was applied with inverse Laplace transformation, and then RFA coefficients were obtained by the Least Square method. One of the advantages of this technique requires fewer wind speed. Only two wind speed with one lag term are demanded to extract flutter derivatives.

Siedziako and Øiseth [7] enhanced the identification procedure by using load cells to measure aeroelastic force during wind tunnel experiments. The purpose is to predict the self-excited drag force which contains nonlinear contributions more accurately. In this paper, they improve identification by making sure that the input lift force corresponds to predicted values of force components, and then aeroelastic forces equation in time domain is written in state-space. Therefore, RFA coefficients are obtained through the identification of the state space model. In this paper, they argued that the discrepancies of flutter derivatives between obtained RFA coefficients and references do not come from

errors in identification but indicate that the RFA extraction algorithm needs enhancement in the advanced model. In this experiment, the RFA coefficient was predicted before conducted the experiment and only one wind speed was used to extract RFA coefficients.

Flutter derivatives are unique coefficients that sometimes change in a complex manner with a higher-order polynomial. An initial study of numerical simulation using secondary data of flutter derivatives has been carried out to find which wind speed range are suitable for RFA extraction [27]. A combination of low and high wind speed categories gave a smaller error of discrepancy, and the increasing number of wind speed did not affect the result marginally. Further investigation using a wind tunnel experiment is needed to confirm the numerical calculation. Moreover, in the algorithm of RFA extractions [5], there is a significant improvement of formulation that is phase lag independent. However, the role of pre-set amplitudes and data length for RFA extractions needs to be clarified.

2.2 Equation motion of a bridge deck

Assuming that the bridge deck which has two DOF subjected to oncoming flow, vertical displacement, h, and torsional displacement, α. The bridge deck has mass m and moment of inertia I. Damping and stiffness coefficients of the heaving and torsional modes are defined as c_h, c_α, k_h, and k_α, respectively. Equation of motion can be described as:

$$\begin{aligned} m\ddot{h} + c_h\dot{h} + k_h h &= L_{ae} \\ I\ddot{\alpha} + c_\alpha\dot{\alpha} + k_\alpha\alpha &= M_{ae} \end{aligned} \tag{2.1}$$

where L_{se} and M_{se} are an aeroelastic force of lift and moment, respectively.

2.2.1 Formulation of aeroelastic forces for a streamlined deck

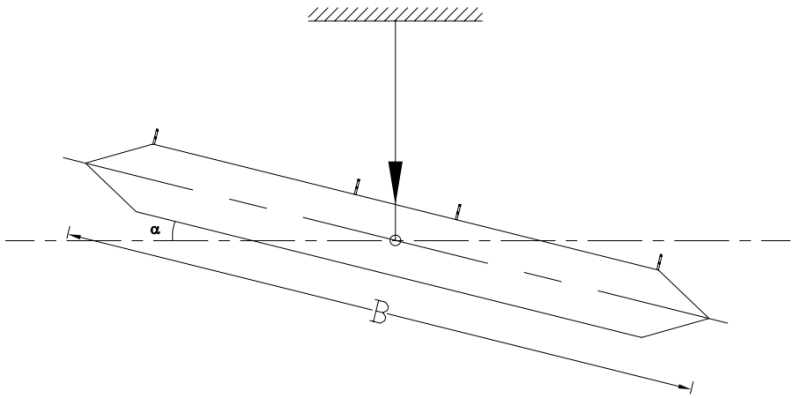

Fig. 2 Two degrees of freedom of bridge deck.

The behavior of self-excited force for a streamlined deck may be assumed to be similar to the Theodorsen [28] thin plate theory as follows:

$$L_{se} = \pi\rho b^2\left\{-\ddot{h} + U\dot{\alpha}\right\} + 2\pi\rho UbC(k)\left\{\dot{h} + U\alpha + \frac{b}{2}\dot{\alpha}\right\}$$
$$M_{se} = \pi\rho b^3\left\{-\frac{U}{2}\dot{\alpha} - \frac{b}{8}\ddot{\alpha}\right\} + \pi\rho Ub^2C(k)\left\{\dot{h} + U\alpha + \frac{b}{2}\dot{\alpha}\right\} \tag{2.2}$$

Where is deflection h and α are measured and defining complex sinusoidal motion can be defined as:

$$h = h_0 e^{i\omega t}$$
$$\alpha = \alpha_0 e^{i\omega t} \tag{2.3}$$

where b is the half width of the bridge deck. U and ρ are the mean wind speed and air density, respectively. $C(k)$ is known as Theodorsen's function which is defined as:

$$C(k) = F + Gi = \frac{H_1^{(2)}(k)}{H_1^{(2)}(k) + iH_0^{(2)}(k)} \tag{2.4}$$

F and G are the real and the imaginary parts of $C(k)$, respectively. $H_n^{(2)}(k)$ is Hankel function. $C(k)$ can be approximated by R.T Jones's formulation [29] as:

$$C(k) \approx 1 - \frac{0.165}{1 - \frac{0.0455}{k}i} - \frac{0.335}{1 - \frac{0.3}{k}i} \tag{2.5}$$

Unsteady aerodynamic coefficients of H_i^* and $A_i^*\,(i = 1,4)$ are called flutter derivatives that depend on deck shape and they can be connected with F and G as:

$$H_1^* = -2\pi\frac{F}{K}; \qquad H_2^* = \frac{-\pi}{2K}\left(1 + \frac{4G}{K} + F\right)$$
$$H_3^* = \frac{-\pi}{K}\left(\frac{2F}{K} - \frac{G}{2}\right); \qquad H_4^* = \frac{\pi}{2}\left(1 + \frac{4G}{K}\right)$$
$$A_1^* = \frac{\pi}{2}\frac{F}{K}; \qquad A_2^* = \frac{-\pi}{2K}\left(\frac{1}{4} - \frac{G}{K} - \frac{F}{4}\right) \tag{2.6}$$
$$A_3^* = \frac{\pi}{2K}\left(\frac{1}{32} + \frac{F}{K} - \frac{G}{4}\right); \quad A_4^* = \frac{-\pi}{2K}G$$

where $K = B\omega/U$ is reduced frequency and ω is circular frequency.

2.2.2 Formulation of aeroelastic forces for a bluff body

The Theodorsen thin plate theory is not appropriate for the bluff body. Therefore, Scanlan [30] proposed reduced frequency dependent flutter derivates. Self-excited force formulation can be written as:

$$\begin{aligned} L_{ae} &= \frac{1}{2}\rho U^2 B\left(KH_1^* \frac{\dot{h}}{U} + KH_2^* \frac{B\dot{\alpha}}{U} + K^2 H_3^* \alpha + K^2 H_4^* \frac{h}{B} \right) \\ M_{ae} &= \frac{1}{2}\rho U^2 B^2\left(KA_1^* \frac{\dot{h}}{U} + KA_2^* \frac{B\dot{\alpha}}{U} + K^2 A_3^* \alpha + K^2 A_4^* \frac{h}{B} \right) \end{aligned} \tag{2.7}$$

where B is the width of the bridge deck. In matrix form, the equation of motion of bridge deck can be written as:

$$\mathbf{M}\ddot{\mathbf{q}} + \mathbf{C}\dot{\mathbf{q}} + \mathbf{K}\mathbf{q} = \mathbf{V}_f \mathbf{Q}\mathbf{q} \tag{2.8}$$

Coefficient matrices in the equation (2.8) are defined as follows:

$$\begin{aligned} &\mathbf{M} = \begin{bmatrix} m_h & 0 \\ 0 & I_\alpha \end{bmatrix}, \quad \mathbf{C} = \begin{bmatrix} 2m_h\zeta_h\omega_h & 0 \\ 0 & 2I_\alpha\zeta_\alpha\omega_\alpha \end{bmatrix}, \quad \mathbf{K} = \begin{bmatrix} m_h\omega_h^2 & 0 \\ 0 & I_\alpha\omega_\alpha^2 \end{bmatrix}, \quad \mathbf{q} = \begin{bmatrix} h/B \\ \alpha \end{bmatrix} \\ &\mathbf{V}_f = \begin{bmatrix} \frac{1}{2}\rho U^2 B & 0 \\ 0 & \frac{1}{2}\rho U^2 B^2 \end{bmatrix}, \quad \mathbf{Q} = \begin{bmatrix} K^2 H_4^* + pKH_1^* & K^2 H_3^* + pKH_2^* \\ K^2 A_4^* + pKA_1^* & K^2 A_3^* + pKA_2^* \end{bmatrix} \end{aligned} \tag{2.9}$$

Where $p = sB/U = iK$, i and s are unit imaginary numbers and non-dimensional time, respectively. s can be defined as $s = Ut/B$.

2.3 Identification in frequency domain

2.3.1 Free vibration method

In this research, the identification of Flutter derivatives in frequency domain uses Extended Kalman Filter Global Weight Iteration (EKWGI). Expression of aeroelastic force can be described in other forms as:

$$\begin{Bmatrix} L_{ae} \\ M_{ae} \end{Bmatrix} = \pi\rho\omega^2 \begin{bmatrix} B^3 & 0 \\ 0 & B^4 \end{bmatrix} \left\{ \begin{bmatrix} L_{yI} & L_{\theta I} \\ M_{yI} & M_{\theta I} \end{bmatrix} \begin{Bmatrix} \dot{h}/\omega B \\ \dot{\alpha}/\omega B \end{Bmatrix} + \begin{bmatrix} L_{yR} & L_{\theta R} \\ M_{yR} & M_{\theta R} \end{bmatrix} \begin{Bmatrix} h/\omega B \\ \alpha/\omega B \end{Bmatrix} \right\} \tag{2.10}$$

Conversion to Scanlan format can be defined as:

$$H_1^* = 2\pi L_{yI};\ H_4^* = 2\pi L_{yR};\quad H_2^* = 2\pi L_{\theta I};\ H_3^* = 2\pi L_{\theta R}$$
$$A_1^* = 2\pi M_{yI};\ A_4^* = 2\pi M_{yR};\quad A_2^* = 2\pi M_{\theta I};\ A_3^* = 2\pi M_{\theta R}$$

Eight aeroelastic coefficients are unknown variables. In the algorithm of EKWGI, four displacement time histories and eight aeroelastic coefficients are described in state variable X as follows:

$$\begin{aligned} X &= \left\{ x_1, x_2, x_3, x_4, x_5, x_6, x_7, x_8, x_9, x_{10}, x_{11}, x_{12} \right\}^T \\ X &= \left\{ h, \alpha, \dot{h}, \dot{\alpha}, L_{yR}, L_{yI}, L_{\theta R}, L_{\theta I}, M_{yR}, M_{yI}, M_{\theta R}, M_{\theta I} \right\}^T \end{aligned} \tag{2.11}$$

State equations are

$$\begin{aligned} &\dot{x}_1 = x_3, \dot{x}_2 = x_4 \\ &\dot{x}_3 = \frac{\pi\rho B^3\omega^2}{m}\left(x_9 x_1 + \frac{1}{\omega} x_5 x_3 + x_{10} x_2 + \frac{1}{\omega} x_6 x_4 \right) - \omega^2 x_1 \\ &\dot{x}_4 = \frac{\pi\rho B^4\omega^2}{I}\left(x_{11} x_1 + \frac{1}{\omega} x_7 x_3 + x_{12} x_2 + \frac{1}{\omega} x_8 x_4 \right) - \omega^2 x_2 \\ &\dot{x}_5 = \dot{x}_6 = \dot{x}_7 = \dot{x}_8 = \dot{x}_9 = \dot{x}_{10} = \dot{x}_{12} = \dot{x}_{12} = 0 \end{aligned} \tag{2.12}$$

Based on the relation above, the EKWGI algorithm can be used [9] and flutter derivatives can be extracted.

2.3.2 Forced vibration method

The identification procedure in forced vibration method is straightforward. Aeroelastic forces are decomposed into real and imaginary parts. Supposed that heaving and torsional oscillation can be expressed as:

$$\begin{aligned} h &= h_0 \sin\left(\omega_h t\right) \\ \alpha &= \alpha_0 \sin\left(\omega_\alpha t\right) \end{aligned} \tag{2.13}$$

Where h_0 and α_0 are the vertical and torsional amplitudes, respectively, and corresponding the vertical and torsional frequency can be described as $\omega_h = 2\pi f_h$ and $\omega_\alpha = 2\pi f_\alpha$, respectively. The lift and moment forces associated with heaving oscillation can be expressed as:

$$L_{ae}^{h} = L_0^{h} \sin\left(\omega_h t - \theta_L^{h}\right)$$
$$M_{ae}^{h} = M_0^{h} \sin\left(\omega_h t - \theta_M^{h}\right) \tag{2.14}$$

L_0^h and M_0^h are the amplitudes of the fluctuating lift and moment associated with heaving oscillation, respectively. θ_L^h is the phase lag between the lift force and the heaving oscillation. θ_M^h is the phase lag between the moment and the heaving oscillation. Flutter derivatives related to the heaving motion are given as:

$$H_1^* = \frac{L_0^h}{h_0}\frac{\sin\theta_L^h}{qK^2}; \quad H_4^* = \frac{L_0^h}{h_0}\frac{\cos\theta_L^h}{qK^2}$$
$$A_1^* = \frac{M_0^h}{h_0}\frac{\sin\theta_M^h}{qBK^2}; \quad A_4^* = \frac{M_0^h}{h_0}\frac{\cos\theta_M^h}{qBK^2} \tag{2.15}$$

Where $q = 1/2\,\rho U^2$ is dynamic pressure. The lift and moment forces associated with torsional oscillation can be expressed as:

$$L_{ae}^{\alpha} = L_0^{\alpha} \sin\left(\omega_\alpha t - \theta_L^{\alpha}\right)$$
$$M_{ae}^{\alpha} = M_0^{\alpha} \sin\left(\omega_\alpha t - \theta_M^{\alpha}\right) \tag{2.16}$$

L_0^α and M_0^α are the amplitudes of the fluctuating lift and moment associated with torsional oscillation, respectively. θ_L^α is the phase lag between the lift force and the torsional oscillation and θ_M^α is the phase lag between the moment and the torsional oscillation. Flutter derivatives related to torsional motion are given as:

$$H_2^* = \frac{L_0^\alpha}{\alpha_0}\frac{\sin\theta_L^\alpha}{qBK^2}; \quad H_3^* = \frac{L_0^\alpha}{\alpha_0}\frac{\cos\theta_L^\alpha}{qBK^2}$$
$$A_2^* = \frac{M_0^\alpha}{\alpha_0}\frac{\sin\theta_M^\alpha}{qB^2K^2}; \quad A_3^* = \frac{M_0^\alpha}{\alpha_0}\frac{\cos\theta_M^\alpha}{qB^2K^2} \tag{2.17}$$

2.4 Identification in time domain

RFA was firstly introduced by Roger [15] with the formulation as:

$$\mathbf{Q}(p) = \mathbf{A}_0 + \mathbf{A}_1 p + \sum_{l=1}^{nl} \mathbf{A}_{l+1}\frac{1}{p+\lambda_l} \tag{2.18}$$

where $\mathbf{A}_0$ and $\mathbf{A}_1$ represent aerodynamic stiffness and damping matrices, respectively and $\mathbf{A}_{l+1}/p+\lambda_l$ represents lag terms. In minimum state equation, RFA can be written as [16]:

$$\mathbf{Q}(p) = \mathbf{A}_0 + \mathbf{A}_1 p + \mathbf{D}\left(p\mathbf{I} + \mathbf{R}\right)^{-1}\mathbf{E} \tag{2.19}$$

where **R** is a matrix containing the lag term coefficients. **D** and **E** are rectangular matrices. **I** is an identity matrix. Equation (2.19) can be rewritten for a single element of **Q** as:

$$\mathbf{Q}(p)=\left(\mathbf{A}_0\right)_{ij}+\left(\mathbf{A}_1\right)_{ij}\,p+\sum_{l=1}^{nl}\left(\mathbf{D}\right)_{il}\left(\mathbf{E}\right)_{lj}\mathbf{A}_{l+1}\frac{1}{p+\lambda_l} \tag{2.20}$$

Introducing that $\mathbf{F}\left(=\mathbf{D}\times\mathbf{E}\right)$ is the rational function coefficient matrices [3], equation (11) can be rewritten as:

$$\mathbf{Q}(p)=\mathbf{A}_0+\mathbf{A}_1 p+\frac{\mathbf{F}p}{p+\lambda} \tag{2.21}$$

The equation of motion of bridge deck (2.7) can be derived in the Laplace domain as:

$$\left(\mathbf{M}s^2+\mathbf{C}s+\mathbf{K}\right)L\left(q\right)=\mathbf{V}_f\mathbf{Q}L\left(q\right) \tag{2.22}$$

where L denotes of Laplace operator. Using RFA, the right-hand side of equation (2.22) can be described as:

$$\begin{aligned}\hat{L}_{ae}&=\frac{1}{2}\rho U^2 B\left\{\left(\left(A_0\right)_{11}+\left(A_1\right)_{11}\,p+\frac{\left(F\right)_{11}p}{p+\lambda}\right)\hat{h}/B+\left(\left(A_0\right)_{12}+\left(A_1\right)_{12}\,p+\frac{\left(F\right)_{12}p}{p+\lambda}\right)\hat{\alpha}\right\}\\ \hat{M}_{ae}&=\frac{1}{2}\rho U^2 B^2\left\{\left(\left(A_0\right)_{21}+\left(A_1\right)_{21}\,p+\frac{\left(F\right)_{21}p}{p+\lambda}\right)\hat{h}/B+\left(\left(A_0\right)_{22}+\left(A_1\right)_{22}\,p+\frac{\left(F\right)_{22}p}{p+\lambda}\right)\hat{\alpha}\right\}\end{aligned} \tag{2.23}$$

In time-domain modeling, past researchers use linear and nonlinear optimization to obtain RFA coefficients, (^) denotes the transformation in the Laplace domain. Omitting denominator part and applying inverse Laplace transform equation, equation (2.23) can be rewritten as:

$$\begin{aligned}\dot{L}_{ae}+\lambda_L\frac{U}{B}L_{se}&=\frac{1}{2}\rho U^2 B\left\{\left(\frac{U}{B}\right)\boldsymbol{\psi}_1\mathbf{q}+\boldsymbol{\psi}_2\dot{\mathbf{q}}+\left(\frac{B}{U}\right)\boldsymbol{\psi}_3\ddot{\mathbf{q}}\right\}\\ \dot{M}_{ae}+\lambda_M\frac{U}{B}M_{se}&=\frac{1}{2}\rho U^2 B^2\left\{\left(\frac{U}{B}\right)\boldsymbol{\psi}_4\mathbf{q}+\boldsymbol{\psi}_5\dot{\mathbf{q}}+\left(\frac{B}{U}\right)\boldsymbol{\psi}_6\ddot{\mathbf{q}}\right\}\end{aligned} \tag{2.24}$$

Where

$$\begin{aligned}&\boldsymbol{\psi}_1=\left[\lambda_L\left(A_0\right)_{11}\quad\lambda_L\left(A_0\right)_{12}\right];\\ &\boldsymbol{\psi}_2=\left[\left(A_0\right)_{11}+\lambda_L\left(A_1\right)_{11}+\left(F\right)_{11}\quad\left(A_0\right)_{12}+\lambda_L\left(A_1\right)_{12}+\left(F\right)_{12}\right]\\ &\boldsymbol{\psi}_3=\left[\left(A_1\right)_{11}\quad\left(A_1\right)_{12}\right];\boldsymbol{\psi}_4=\left[\lambda_M\left(A_0\right)_{21}\quad\lambda_M\left(A_0\right)_{22}\right]\\ &\boldsymbol{\psi}_5=\left[\left(A_0\right)_{21}+\lambda_M\left(A_1\right)_{21}+\left(F\right)_{21}\quad\left(A_0\right)_{22}+\lambda_M\left(A_1\right)_{22}+\left(F\right)_{22}\right];\\ &\boldsymbol{\psi}_6=\left[\left(A_1\right)_{21}\quad\left(A_1\right)_{22}\right]\end{aligned} \tag{2.25}$$

The equation above can be extracted in a different way. For the sake of simplicity, only lift force will be demonstrated.

$$L_{ae}(t)=\frac{1}{2}\rho U^2 B\left\{\mathbf{A}_0\mathbf{q}+\frac{B}{U}\mathbf{A}_1\dot{\mathbf{q}}+\mathbf{F}\left(\mathbf{q}-\frac{\lambda_L U}{B}\int_0^t e^{-\frac{U}{B}\lambda_L(t-\tau)}\mathbf{q}(\tau)d\tau\right)\right\} \tag{2.26}$$

Self-excited forces in time domain contain convolution integrals, defines as follows:

$$\mathbf{Z}=\mathbf{q}-\frac{\lambda_L U}{B}\int_0^t e^{-\frac{U}{B}\lambda_L(t-\tau)}\mathbf{q}(\tau)d\tau \tag{2.27}$$

The first derivative of the equation above has been shown in some literature [25], [31] as follows:

$$\dot{\mathbf{Z}}=\dot{\mathbf{q}}-\frac{\lambda_L U}{B}\mathbf{Z} \tag{2.28}$$

Equation (2.25) can be rewritten in matrix form matrix as:

$$\begin{aligned}
&\mathbf{A}_L=\begin{bmatrix}\boldsymbol{\psi}_1 & \boldsymbol{\psi}_2 & \boldsymbol{\psi}_3 & -\lambda_L\end{bmatrix},\\
&\mathbf{X}_L^T=\frac{1}{2}\rho U^2 B\begin{bmatrix}\left(\frac{U}{B}\right)\mathbf{q} & \dot{\mathbf{q}} & \left(\frac{B}{U}\right)\ddot{\mathbf{q}} & \frac{2L_{se}}{\rho U B^2}\end{bmatrix}, \quad b_L=\dot{L}_{se}\\
&\mathbf{A}_M=\begin{bmatrix}\boldsymbol{\psi}_4 & \boldsymbol{\psi}_5 & \boldsymbol{\psi}_6 & -\lambda_M\end{bmatrix},\\
&\mathbf{X}_M^T=\frac{1}{2}\rho U^2 B^2\begin{bmatrix}\left(\frac{U}{B}\right)\mathbf{q} & \dot{\mathbf{q}} & \left(\frac{B}{U}\right)\ddot{\mathbf{q}} & \frac{2M_{se}}{\rho U B^3}\end{bmatrix}, b_M=\dot{M}_{se}
\end{aligned} \tag{2.29}$$

Equation (2.29) can be solved by the least square method as:

$$\mathbf{A}_L=\left(b_{L(1x1)}\mathbf{X}_{L(1x7)}^T\right)\left(\mathbf{X}_{L(7x1)}\mathbf{X}_{L(1x7)}^T\right)^{-1}, \quad \mathbf{A}_M=\left(b_{M(1x1)}\mathbf{X}_{M(1x7)}^T\right)\left(\mathbf{X}_{M(7x1)}\mathbf{X}_{M(1x7)}^T\right)^{-1} \tag{2.30}$$

Conversion from RFA matrix to flutter derivatives can be done as:

$$\begin{aligned}
&H_1^*=i(Q_{11})/K^2, H_2^*=i(Q_{12})/K^2, H_3^*=(Q_{12})/K^2, H_4^*=(Q_{11})/K^2\\
&A_1^*=i(Q_{21})/K^2, A_2^*=i(Q_{22})/K^2, A_3^*=(Q_{22})/K^2, A_4^*=(Q_{21})/K^2
\end{aligned} \tag{2.31}$$

Aeroelastic forces in time domain can be deduced as follows:

$$L_{ae}(t)=\frac{1}{2}\rho U^2 B\begin{pmatrix}\left(\left(A_0\right)_{11}+\left(F\right)_{11}\right)\dfrac{h}{B}+\left(A_1\right)_{11}\dfrac{\dot{h}}{U}\\ -\left(F\right)_{11}\dfrac{\lambda_L U}{B^2}\int_0^t e^{-\frac{U}{B}\lambda_L(t-\tau)}h(\tau)\,d\tau\\ +\left(\left(A_0\right)_{12}+\left(F\right)_{12}\right)\alpha+\left(A_1\right)_{12}\dfrac{B}{U}\dot{\alpha}\\ -\left(F\right)_{12}\dfrac{\lambda_L U}{B}\int_0^t e^{-\frac{U}{B}\lambda_L(t-\tau)}\alpha(\tau)\,d\tau\end{pmatrix} \tag{2.32}$$

$$M_{ae}(t)=\frac{1}{2}\rho U^2 B^2\begin{pmatrix}\left(\left(A_0\right)_{21}+\left(F\right)_{21}\right)\dfrac{h}{B}+\left(A_1\right)_{21}\dfrac{\dot{h}}{U}\\ -\left(F\right)_{21}\dfrac{\lambda_M U}{B^2}\int_0^t e^{-\frac{U}{B}\lambda_M(t-\tau)}h(\tau)\,d\tau\\ +\left(\left(A_0\right)_{22}+\left(F\right)_{22}\right)\alpha+\left(A_1\right)_{22}\dfrac{B}{U}\dot{\alpha}\\ -\left(F\right)_{22}\dfrac{\lambda_M U}{B}\int_0^t e^{-\frac{U}{B}\lambda_M(t-\tau)}\alpha(\tau)\,d\tau\end{pmatrix} \tag{2.33}$$

The equation above is phase lag independent which means the phase lag information is implicitly calculated.

In one DOF experiment, aeroelastic forces in matrix form can be written as:

$$\begin{bmatrix}L_{ae}^h & L_{ae}^\alpha\\ M_{ae}^h & M_{ae}^\alpha\end{bmatrix}=\begin{bmatrix}1/2\,\rho U^2 B & 0\\ 0 & 1/2\,\rho U^2 B^2\end{bmatrix}\begin{bmatrix}\left(A_0\right)_{11}+\left(A_1\right)_{11}p+\dfrac{\left(F_{11}\right)p}{p+\lambda_{L_1}} & \left(A_0\right)_{12}+\left(A_1\right)_{12}p+\dfrac{\left(F_{12}\right)p}{p+\lambda_{L_2}}\\ \left(A_0\right)_{21}+\left(A_1\right)_{21}p+\dfrac{\left(F_{21}\right)p}{p+\lambda_{M_1}} & \left(A_0\right)_{22}+\left(A_1\right)_{22}p+\dfrac{\left(F_{22}\right)p}{p+\lambda_{M_2}}\end{bmatrix}\begin{bmatrix}h/B & 0\\ 0 & \alpha\end{bmatrix} \tag{2.34}$$

Suppose the unknown parameter ψ_{ij} is defined as follows:

$$\begin{aligned}
&\psi_{11}=\lambda_{L_1}\left(A_0\right)_{11};\qquad &&\psi_{12}=\lambda_{L_2}\left(A_0\right)_{12};\\
&\psi_{21}=\left(A_0\right)_{11}+\lambda_{L_1}\left(A_1\right)_{11}+\left(F\right)_{11};\quad &&\psi_{22}=\left(A_0\right)_{12}+\lambda_{L_2}\left(A_1\right)_{12}+\left(F\right)_{12};\\
&\psi_{31}=\left(A_1\right)_{11};\qquad &&\psi_{32}=\left(A_1\right)_{12};\\
&\psi_{41}=\lambda_{M_1}\left(A_0\right)_{21};\qquad &&\psi_{42}=\lambda_{M_2}\left(A_0\right)_{22};\\
&\psi_{51}=\left(A_0\right)_{21}+\lambda_{M_1}\left(A_1\right)_{21}+F_{21};\quad &&\psi_{52}=\left(A_0\right)_{22}+\lambda_{M_2}\left(A_1\right)_{22}+\left(F\right)_{22};\\
&\psi_{61}=\left(A_1\right)_{21};\qquad &&\psi_{62}=\left(A_1\right)_{22}.
\end{aligned} \tag{2.35}$$

Each corresponding displacement and aeroelastic forces can be described in Laplace domain as follows:

$$
\begin{aligned}
&\dot{L}_{ae}^{h}+\lambda_{L_1}\frac{U}{B}L_{ae}^{h}=\frac{1}{2}\rho U^2 B\left(\left(\frac{U}{B}\right)\psi_{11}\left(h/B\right)+\psi_{21}\left(\dot{h}/B\right)+\left(\frac{B}{U}\right)\psi_{31}\left(\ddot{h}/B\right)\right)\\
&\dot{M}_{ae}^{h}+\lambda_{M_1}\frac{U}{B}M_{ae}^{h}=\frac{1}{2}\rho U^2 B^2\left(\left(\frac{U}{B}\right)\psi_{41}\left(h/B\right)+\psi_{51}\left(\dot{h}/B\right)+\left(\frac{B}{U}\right)\psi_{61}\left(\ddot{h}/B\right)\right)\\
&\dot{L}_{ae}^{\alpha}+\lambda_{L_2}\frac{U}{B}L_{ae}^{\alpha}=\frac{1}{2}\rho U^2 B\left(\left(\frac{U}{B}\right)\psi_{12}\left(\alpha\right)+\psi_{22}\left(\dot{\alpha}\right)+\left(\frac{B}{U}\right)\psi_{32}\left(\ddot{\alpha}\right)\right)\\
&\dot{M}_{ae}^{\alpha}+\lambda_{M_2}\frac{U}{B}M_{ae}^{\alpha}=\frac{1}{2}\rho U^2 B^2\left(\left(\frac{U}{B}\right)\psi_{42}\left(\alpha\right)+\psi_{52}\left(\dot{\alpha}\right)+\left(\frac{B}{U}\right)\psi_{62}\left(\ddot{\alpha}\right)\right)
\end{aligned}
\tag{2.36}
$$

Solving equation above by linear least square method, RFA coefficient can be obtained.

All the equation above is based on motivation that phase lag is implicitly calculated. Considering phase lag and amplitude of signal are calculated explicitly. For one DOF experiment, each component in aeroelastic force should be treated separately. i.e., each component in lift force associated with heaving time history and lift force associated with torsional time history are treated independently. In this part, only explain the derivation of the matrix Q_{11}. Recalling equation (2.13), (2.14) and (2.24). The formulation, which is including phase lag and amplitude information, can be rewritten as follows:

$$L_{ae}=L_0\sin\left(\omega_h t-\theta_L^h\right);\quad h=h_0\sin\left(\omega_h t\right)$$

$$\dot{L}_{ae}+\lambda_L\frac{U}{B}L_{ae}=\frac{1}{2}\rho U^2 B\left\{\left(\frac{U}{B}\right)\boldsymbol{\psi}_1\mathbf{q}+\boldsymbol{\psi}_2\dot{\mathbf{q}}+\left(\frac{B}{U}\right)\boldsymbol{\psi}_3\ddot{\mathbf{q}}\right\}$$

$$\omega_h L_0^h\cos\left(\omega_h t-\theta_L^h\right)+\lambda_L\frac{U}{B}L_0^h\sin\left(\omega_h t-\theta_L^h\right)=$$

$$\frac{1}{2}\rho U^2 B\left\{\left(\frac{U}{B}\right)\left(\boldsymbol{\psi}_1\right)_{11}\frac{h_0}{B}\sin\left(\omega_h t\right)+\left(\boldsymbol{\psi}_2\right)_{11}\frac{h_0}{B}\omega_h\cos\left(\omega_h t\right)-\left(\frac{B}{U}\right)\left(\boldsymbol{\psi}_3\right)_{11}\frac{h_0}{B}\left(\omega_h\right)^2\sin\left(\omega_h t\right)\right\}$$

$$\left[\omega_h B\sin\theta_L^h+\lambda_L U\cos\theta_L^h\right]\frac{L_0^h}{h_0}=\frac{1}{2}\rho U^2 B\left\{\left(\frac{U}{B}\right)\left(\boldsymbol{\psi}_1\right)_{11}-\left(\frac{B}{U}\right)\left(\boldsymbol{\psi}_3\right)_{11}\left(\omega_h\right)^2\right\}\ldots\ldots(a)$$

$$\left[\omega_h B\cos\theta_L^h-\lambda_L U\sin\theta_L^h\right]\frac{L_0^h}{h_0}=\frac{1}{2}\rho U^2 B\left\{\left(\boldsymbol{\psi}_2\right)_{11}\omega_h\right\}\qquad\ldots\ldots(b)$$

$$
\underbrace{\begin{bmatrix}\frac{1}{2}\rho U^3 & 0 & -\frac{1}{2}\rho UB^2\left(\omega_h\right)^2 & -U\frac{L_0^h}{h_0}\cos\theta_L^h\\ 0 & \frac{1}{2}\rho U^2 B\omega_h & 0 & U\frac{L_0^h}{h_0}\sin\theta_L^h\end{bmatrix}}_{\mathbf{X}_{L_1}}\underbrace{\begin{bmatrix}\left(\boldsymbol{\psi}_1\right)_{11}\\ \left(\boldsymbol{\psi}_2\right)_{11}\\ \left(\boldsymbol{\psi}_3\right)_{11}\\ \lambda_L\end{bmatrix}}_{\mathbf{A}_{L_1}}=\underbrace{\omega_h B\frac{L_0^h}{h_0}\begin{bmatrix}\sin\theta_L^h\\ \cos\theta_L^h\end{bmatrix}}_{\mathbf{b}_{L_1}}
\tag{2.37}
$$

And least square procedures can be done as follows:

$$\mathbf{A}_{L_1} = \left(\mathbf{X}_{L_1}{}^{T}{}_{(4x2)} \mathbf{X}_{L_1(2x4)} \right)^{-1} \left(\mathbf{X}_{L_1}{}^{T}{}_{(4x2)} \mathbf{b}_{L_1(1x2)} \right) \tag{2.38}$$

For two DOF experiment, There are some other expressions in which superposition is taken into account. Recalling equation (2.13), (2.14) and (2.24), superposition can be derived as follows:

$$\begin{aligned} L_{ae} &= L_{ae}^{h} + L_{ae}^{\alpha} \\ L_{ae} &= L_0^h \sin\left(\omega_h t - \theta_L^h\right) + L_0^\alpha \sin\left(\omega_\alpha t - \theta_L^\alpha\right) \\ \dot{L}_{ae} &= L_0^h \omega_h \cos\left(\omega_h t - \theta_L^h\right) + L_0^\alpha \omega_\alpha \cos\left(\omega_\alpha t - \theta_L^\alpha\right) \end{aligned} \tag{2.39}$$

Applying RFA extraction in inverse Laplace domain, we can obtain the equation as follows:

$$\begin{aligned} \dot{L}_{ae} + \lambda_L \frac{U}{B} L_{ae} &= \omega_h L_0^h \cos\left(\omega_h t - \theta_L^h\right) + \omega_\alpha L_0^\alpha \cos\left(\omega_\alpha t - \theta_L^\alpha\right) \\ &\quad + \lambda_L \frac{U}{B}\left(L_0^h \sin\left(\omega_h t - \theta_L^h\right) + L_0^\alpha \sin\left(\omega_\alpha t - \theta_L^\alpha\right)\right) \end{aligned} \tag{2.40}$$

Introducing $\mathbf{q}_s = \begin{bmatrix} \frac{h_0}{B} & \alpha_0 \end{bmatrix}^T$ and matching sin and cos function the final equation can be obtained as follows:

$$\begin{aligned} &\frac{1}{2}\rho U^3 \boldsymbol{\psi}_1 \mathbf{q}_s - \frac{1}{2}\rho U B^2 \omega^2 \boldsymbol{\psi}_3 \mathbf{q}_s - \lambda_L \frac{U}{B} L_0^h \sin\left(\theta_L^h\right) - \lambda_L \frac{U}{B} L_0^\alpha \sin\left(\theta_L^\alpha\right) \\ &= \omega\left(L_0^h \cos\left(\theta_L^h\right) + L_0^\alpha \cos\left(\theta_L^\alpha\right)\right) \ldots\ldots (a) \\ &\frac{1}{2}\rho U^2 B \omega \boldsymbol{\psi}_2 \mathbf{q}_s + \lambda_L \frac{U}{B}\left(L_0^h \sin\left(\theta_L^h\right) + L_0^\alpha \sin\left(\theta_L^\alpha\right)\right) \\ &= \omega\left(L_0^h \cos\left(\theta_L^h\right) + L_0^\alpha \cos\left(\theta_L^\alpha\right)\right) \ldots\ldots (b) \end{aligned} \tag{2.41}$$

$$\begin{bmatrix} \frac{1}{2}\rho U^3 \mathbf{q}_s & 0 & -\frac{1}{2}\rho U B^2 \omega^2 \mathbf{q}_s & -\frac{U}{B}\left(L_0^h \cos\left(\theta_L^h\right) + L_0^\alpha \cos\left(\theta_L^\alpha\right)\right) \\ 0 & \frac{1}{2}\rho U^2 B \omega \mathbf{q}_s & 0 & \frac{U}{B}\left(L_0^h \sin\left(\theta_L^h\right) + L_0^\alpha \sin\left(\theta_L^\alpha\right)\right) \end{bmatrix} \begin{bmatrix} \boldsymbol{\psi}_1 \\ \boldsymbol{\psi}_2 \\ \boldsymbol{\psi}_3 \\ \lambda_L \end{bmatrix} \tag{2.42}$$

$$= \begin{bmatrix} \omega\left(L_0^h \sin\left(\theta_L^h\right) + L_0^\alpha \sin\left(\theta_L^\alpha\right)\right) \\ \omega\left(L_0^h \cos\left(\theta_L^h\right) + L_0^\alpha \cos\left(\theta_L^\alpha\right)\right) \end{bmatrix}$$

a least square can be done as follows:

$$\mathbf{A}_L = \left(b_{L(1x2)}\mathbf{X}^T_{L(2x4)}\right)\left(\mathbf{X}_{L(4x2)}\mathbf{X}^T_{L(2x4)}\right)^{-1} \tag{2.43}$$

The least square method needs matrix inversion. Matrix inversion that contains zeros values will cause singularity and solving the equation by matching the equation is necessary.

In literature [21]–[23], lag term plays a role, and flutter derivatives must be obtained before calculating RFA. Increasing lag terms, the number of unknowns becomes increases and consequently time-consuming. The detailed RFA formulation in higher order lag terms is explained in the appendix.

2.5 Flutter analysis

Flutter speed can be determined by performing the equation of motion in a state-space form. for a typical complex conjugate pair of eigenvalue can be derived as:

$$s_i = -\omega_i\xi_i \pm j\omega_i\sqrt{1-\xi_i} \quad ; j = \sqrt{-1} \tag{2.44}$$

The corresponding frequency of oscillation and the logarithmic decrement can be derived from following:

$$\omega_i = \sqrt{\left\{\mathrm{Re}\left(s_i\right)\right\}^2 + \left\{\mathrm{Im}\left(s_i\right)\right\}^2} \tag{2.45}$$

$$\delta_i = \frac{-2\pi\,\mathrm{Re}\left(s_i\right)}{\sqrt{\left\{\mathrm{Re}\left(s_i\right)\right\}^2 + \left\{\mathrm{Im}\left(s_i\right)\right\}^2}} \tag{2.46}$$

Chapter 3. Numerical Simulation for Direct Extraction of RFA

This chapter is a baseline study in this research. Numerical simulation is conducted by using secondary data of flutter derivatives at the angle of attack being zero degrees. Different deck types such as a twin deck from the spindle bridge, a truss deck from the Akashi Kaikyo Bridge, an edge girder deck from the Suramadu Bridge are used for simulation. As verification for the extraction algorithm, airfoil will be used in the simulation. Displacement time histories defined as $h(t)=\sin(2\pi f_h t)$ and $a(t)=\sin(2\pi f_\alpha t)$ for heaving and torsional, respectively. Using those time histories and tabular data of flutter derivatives, aeroelastic force using (2.7) can be generated. Applying the procedure in chapter 3, RFA coefficients can be extracted. Flutter derivatives are used as the experimental results.

To quantitatively assess the discrepancy between obtained extracted and experimental flutter derivatives, the following percentage error function is given as:

$$Error=\frac{\sum_{j=1}^{N_{fd}}\left\{\sqrt{\sum_{i=1}^{N}\left(X_i^{(j)}-X_i^{0(j)}\right)^2}\Big/\sqrt{\sum_{i=1}^{N}\left(X_i^{0(j)}\right)^2}\right\}}{N_{fd}}\times 100\ \% \tag{3.1}$$

where $X_i^{(j)}$ is the *j*-th flutter derivative from extraction. $X_i^{0(j)}$ is the corresponding flutter derivative of experimental data at *i*-th wind speed. N is the number of wind speed involved in the calculation. N_{fd} is the number of types of flutter derivative. The procedure of numerical analysis can be shown in the figure below. The allowable error is not defined because the purpose is only to assess the accuracy of RFA extraction against all the flutter derivatives. If the allowable error is a primary concern, a weighting factor must be applied. For example, an edge girder which is susceptible to pure torsional flutter (A_2^*) should have more priority than other flutter derivatives. In this simulation, some parameters such phase lag and pre-set amplitude are neglected. Tabular data of flutter derivatives from experiment directly used for simulation of aeroelastic forces.

Extraction of flutter derivatives with RFA will use two and three wind speed. Each case has its combination as presented in Table 1. Each simulation will have eleven wind speeds which are varied in each bridge deck type. Therefore, there are eleven indices. For example, the combination '1-10' in case 9 means that simulation will carry out two wind speed at 1 and 10 indices. A Higher case number means a wider range of wind speed

combination. Furthermore, a higher combination number means a combination with higher wind speed. Case number also shows the increment of wind speed for each wind speed combination, case 1 means in three wind speed combinations means that there are three wind speeds that have a discrepancy of only 1 m/s.

In the numerical simulation algorithm, the inverse matrix can cause numerical instability and a small magnitude of time histories must be added to avoid matrix singularity during inverse matrix process.

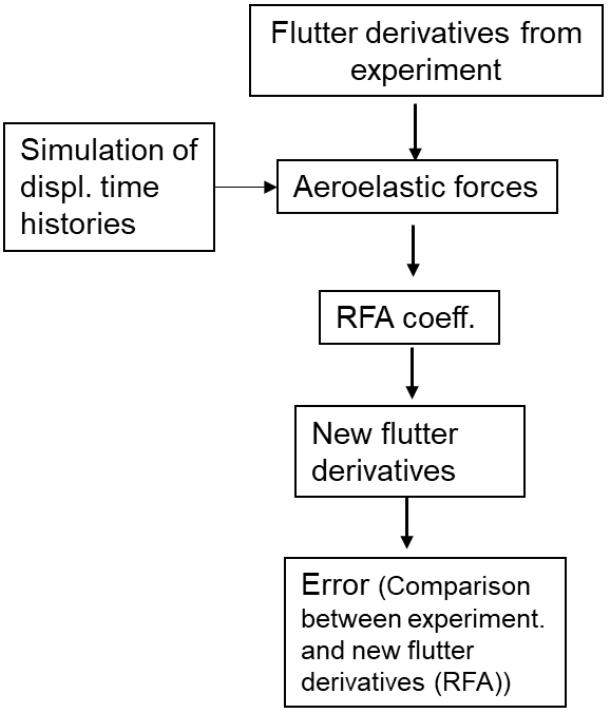

Fig. 3 Numerical simulation procedure.

Table 1 Wind speed combination for simulation.

Number of wind speed combination	Wind speed index combination (combination number)	Case
2 wind speed	1-2 (1), 2-3 (2), 3-4 (3), 4-5 (4), 5-6 (5), 6-7 (6), 7-8 (7), 8-9 (8), 9-10 (9), 10-11 (10)	case 1
	1-3 (2), 2-4 (3), 3-5 (4), 4-6 (5), 5-7 (6), 6-8 (7), 7-9 (8), 8-10 (9), 9-11 (10)	case 2
	1-4 (3), 2-5 (4), 3-6 (5), 4-7 (6), 5-8 (7), 6-9 (8), 7-10 (9), 8-11 (10)	case 3
	1-5 (4), 2-6 (5), 3-7 (6), 4-8 (7), 5-9 (8), 6-10 (9), 7-11 (10)	case 4
	1-6 (5), 2-7 (6), 3-8 (7), 4-9 (8), 5-10 (9), 6-11 (10)	case 5
	1-7 (6), 2-8 (7), 3-9 (8), 4-10 (9), 5-11 (10)	case 6
	1-8 (7), 2-9 (8), 3-10 (9), 4-11 (10)	case 7
	1-9 (8), 2-10 (9), 3-11 (10)	case 8
	1-10 (9), 2-11 (10)	case 9
	1-11 (10)	case 10
3 wind speed	1-2-3 (1), 2-3-4 (2), 3-4-5 (3), 4-5-6 (4), 5-6-7 (5), 6-7-8 (6), 7-8-9 (7), 8-9-10 (8), 9-10-11 (9)	case 1
	1-3-5 (3), 2-4-6 (4), 3-5-7 (5), 4-6-8 (6), 5-7-9 (7), 6-8-10 (8), 7-9-11 (9)	case 2
	1-4-7 (5), 2-5-8 (6), 3-6-9 (7), 4-7-10 (8), 5-8-11 (9)	case 3
	1-5-9 (7), 2-6-10 (8), 3-7-11 (9)	case 4
	1-6-11 (9)	case 5

4 wind speed	1-2-3-4 (1), 2-3-4-5 (2), 3-4-5-6 (3), 4-5-6-7 (4), 5-6-7-8 (5), 6-7-8-9 (6), 7-8-9-10 (7), 8-9-10-11(8)	case 1
	1-3-5-7 (4), 2-4-6-8 (5), 3-5-7-9 (6), 4-6-8-10 (7), 5-7-9-11 (8)	case 2
	1-4-7-10 (7), 2-5-8-11 (8)	case 3

3.1 Airfoil

3.1.1 Wind speed combination

Assuming the frequency response of a structure for lift and moment is defined as 1 Hz and 2 Hz, respectively and deck width is 0.35 meters. Wind speed that are used for simulation are 3 m/s, 4 m/s, 5 m/s, 6 m/s, 7 m/s, 8 m/s, 9 m/s, 10 m/s, 11 m/s, 12 m/s and 13 m/s. Applying equation (2.6) flutter derivatives can be obtained and have a trend in second-order polynomial as shown in the graph below.

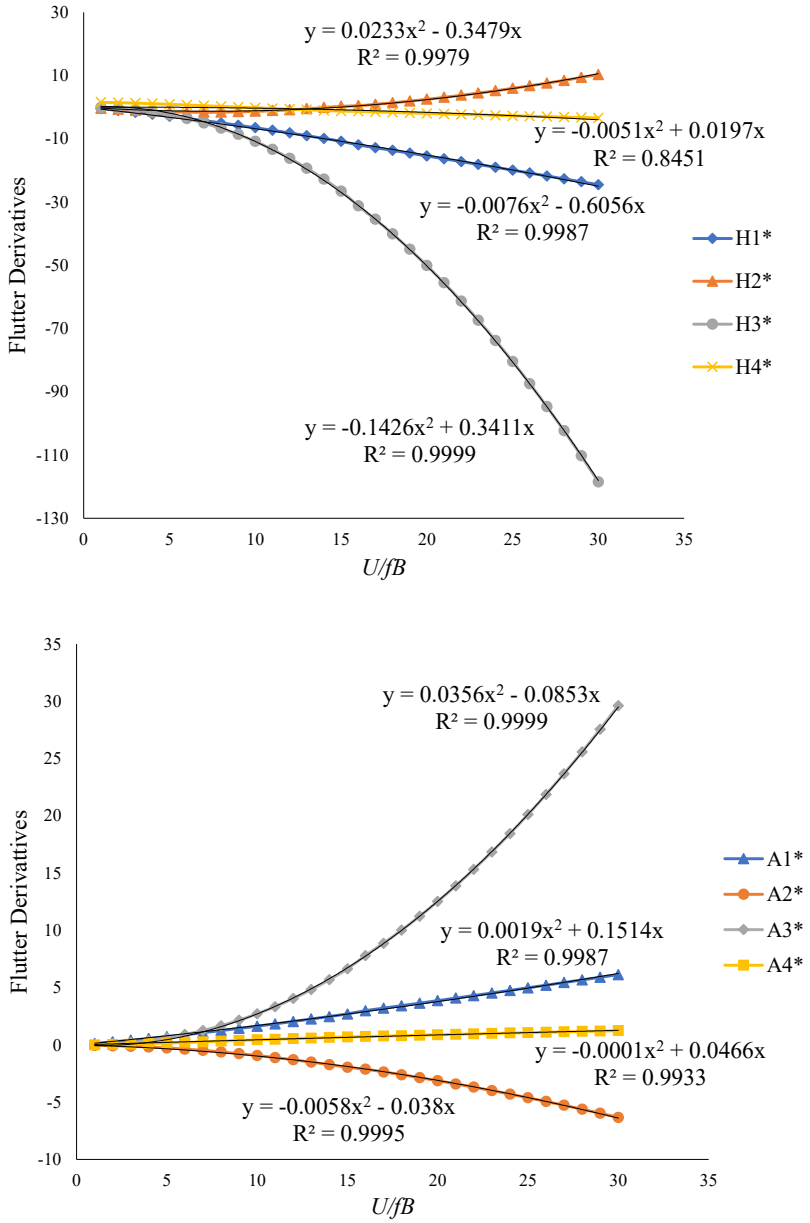

Fig. 4. Flutter derivatives of airfoil.

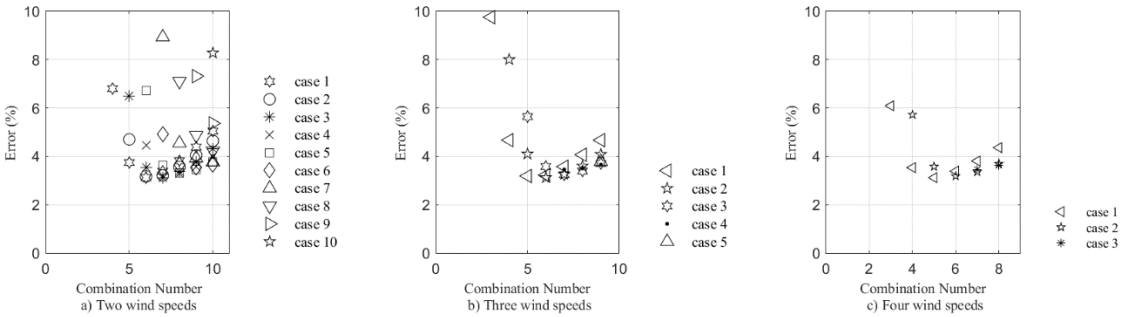

Fig. 5. Error comparison of flutter derivatives extraction at various combinations.

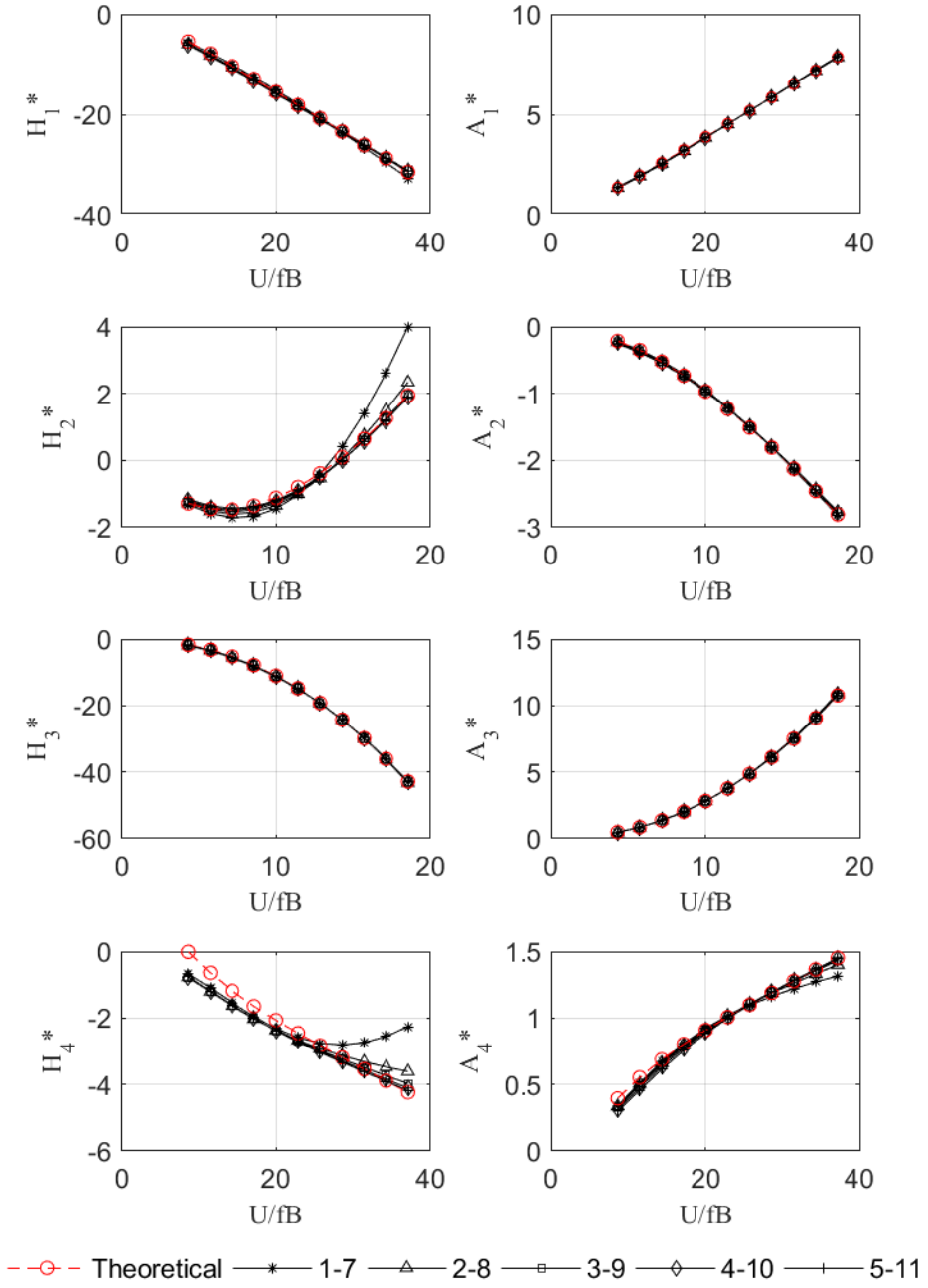

Fig. 6 Comparison of flutter derivatives of airfoil in case 6 using one lag term.

Fig. 5 presents an error comparison of flutter derivatives extraction from two, three and four wind speed combinations. The minimum error at two wind speed is around 3 %. In this case, case 6 gives a stable result with an average error of about 4 % except for combination one. Using three wind speeds does not reduce the error significantly. A comparison of each flutter derivative between the theoretical and simulation result is presented in Fig. 6. All derivatives cases show similar results between theoretical and extraction from RFA. From this result, it can be concluded that the RFA extraction algorithm is correct.

3.1.2 Lag terms effect

Numerical analysis is analyzed with one, two and three lag terms. Airfoil theory is used to facilitate discussion. In the figure below, we can see that the increasing number lag term does not decrease the number of errors. Additionally, with the same lag term, increasing the number of wind speed, the error will not reduce.

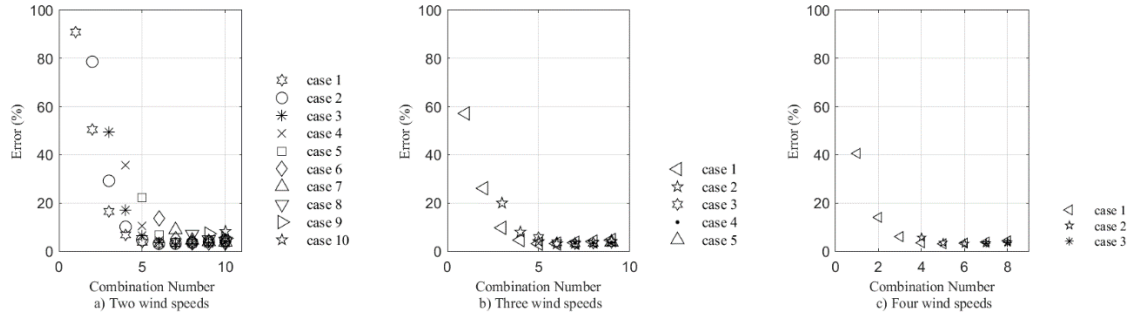

Fig. 7 Wind speed combination using one lag term.

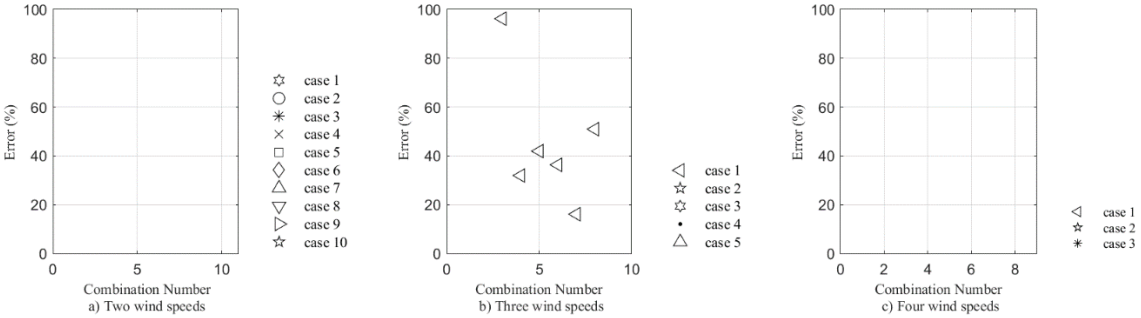

Fig. 8 Wind speed combination using two lag terms.

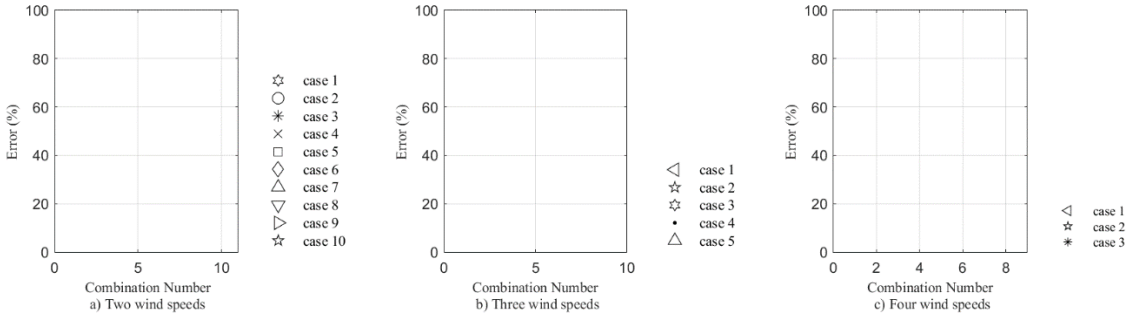

Fig. 9 Wind speed combination using three lag terms.

Error result that shown in the figure above for two and three lag terms are out of range. In more detailed explanation can be shown in the figure below. As we can see here, there are some discrepancies that come from other flutter derivatives. Increasing the number of lag terms will increase the unknown number of parameters, and the result becomes redundant.

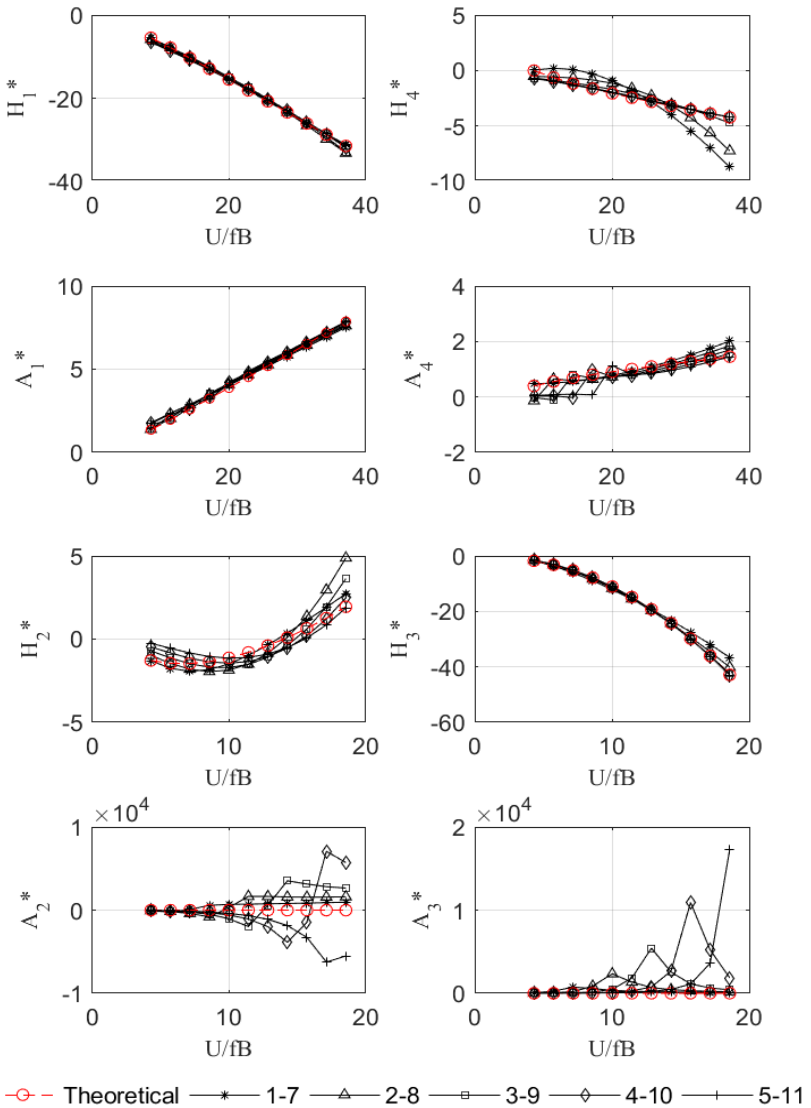

Fig. 10 Comparison of flutter derivatives based on airfoil in case 6 using two lag terms.

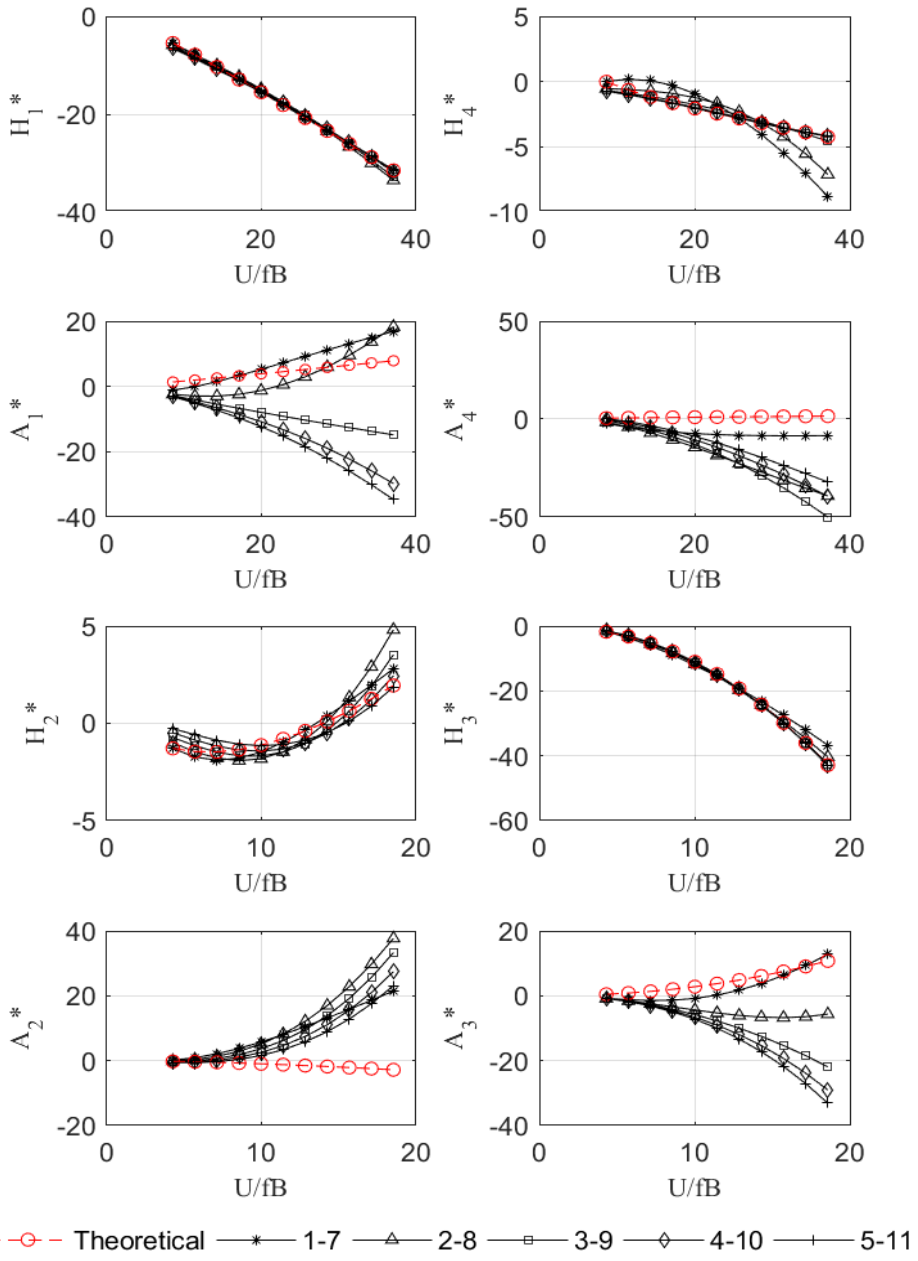

Fig. 11 Comparison of flutter derivatives based on airfoil in case 6 using three lag terms.

The concept of RFA extraction here is different from the previous publication. [21], [32] where lag term plays an important role. λ is should be identified first and optimized until discrepancies between experimental and approximation become minimum. In time domain, it really quite hard to understand if multi lag terms is applied.

3.2 Twin deck

A spindle bridge is a bridge that has separated traffic lanes in the main span and merged near to pylon to overcome the unsteady aerodynamic force because the center deck has an essential role in the occurrence of the flutter [33]. For this purpose, the spindle bridge uses a twin deck. The simulation frequency of the deck for lift and moment is 1.5 Hz and 4.43 Hz, respectively. Deck width is 0.35 m. Wind speed that are used for simulation are 6.08 m/s, 6.87 m/s, 7.71 m/s, 8.42 m/s, 9.28 m/s, 10.14 m/s, 10.64 m/s, 11.08 m/s, 13.24 m/s, 14.99 m/s and 17.53 m/s. The trend of flutter derivatives of twin-deck can be shown below.

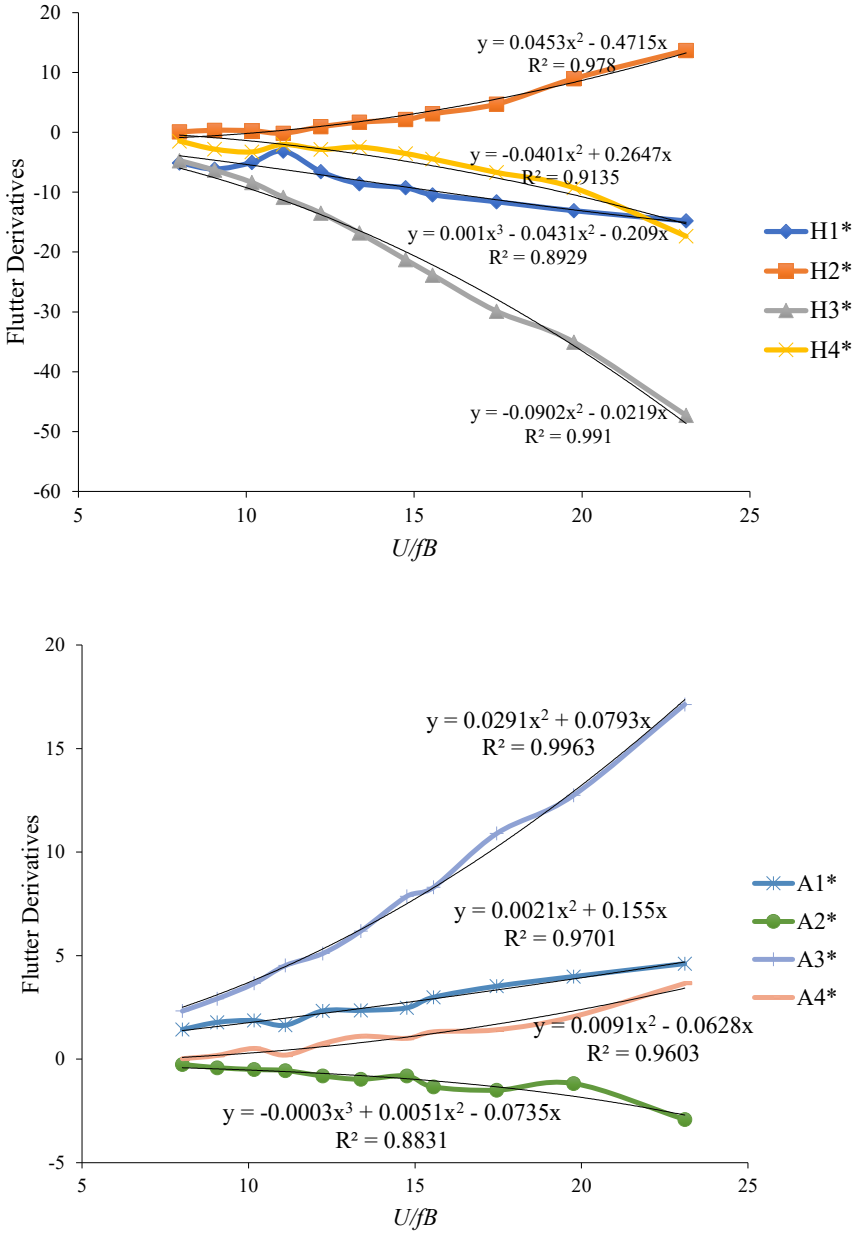

Fig. 12 Flutter derivatives of twin decks.

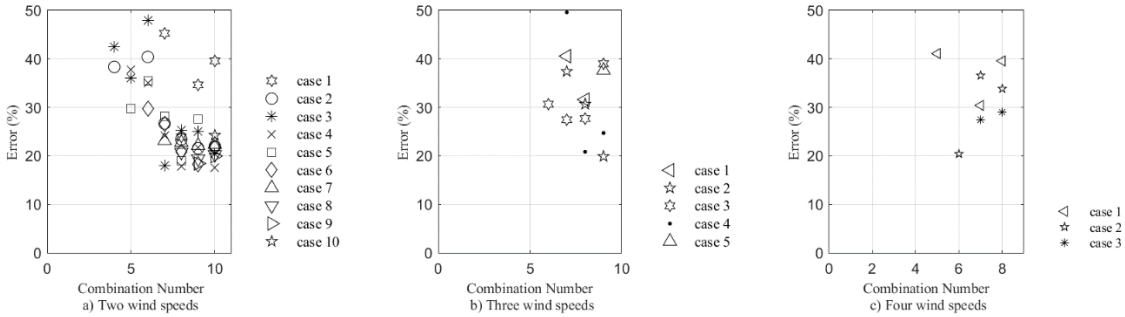

Fig. 13 Error comparison of flutter derivatives extraction at various combinations.

.

Fig 13 shows an error comparison of flutter derivatives extraction using two and three and four wind combinations. Fig. 14 shows the comparison of each flutter derivative between experimental data and RFA extraction in case 6. Generally, all derivatives between experimental and extraction give the same trend. The discrepancy occurs due to the experimental data have third order polynomial in H_1^* and A_2^*.

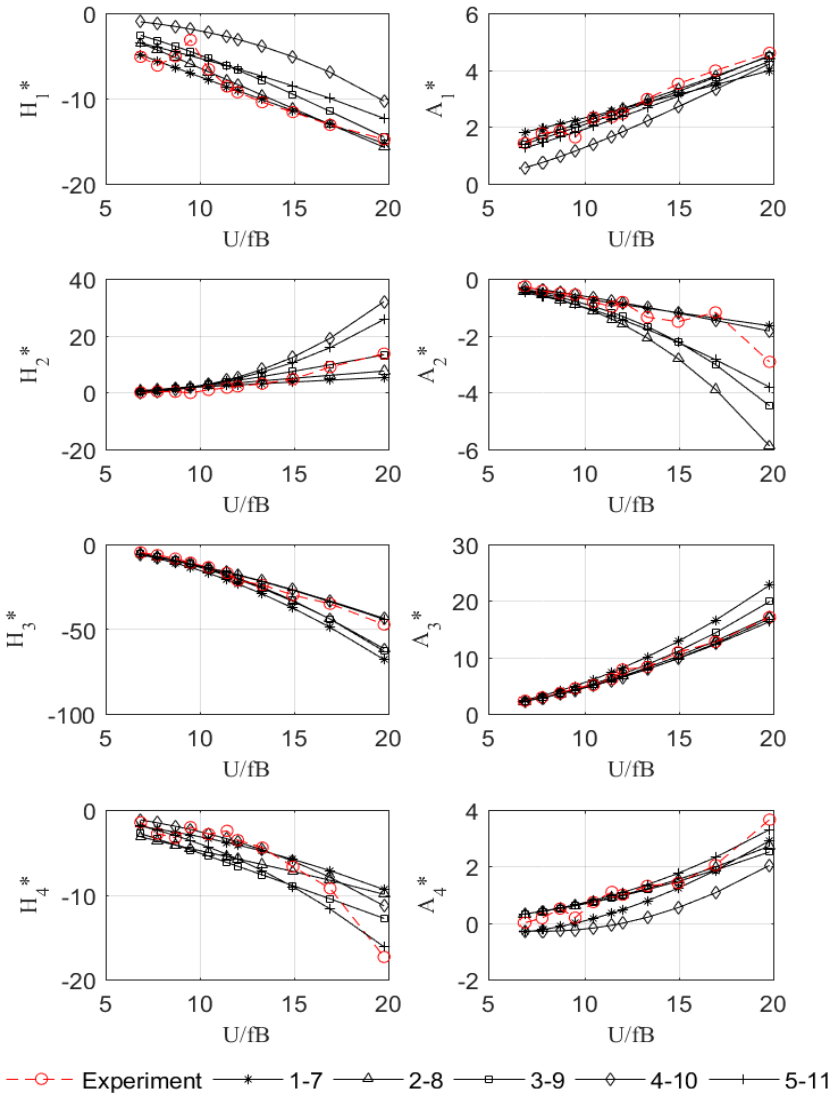

Fig. 14 Comparison of flutter derivatives of spindle bridge in case 6.

3.3 Truss deck

A truss deck of Akashi Kaikyo bridge deck is selected for the simulation. Flutter derivatives were obtained by the Honshu Shikoku Bridge Authority [34] that contained 12 types of flutter derivatives data. RFA extraction algorithm is extended into 3 DOF. Assuming that the frequency response of lift and moment of the bridge deck is 1.5 Hz. Wind speed that is used for the simulation are 4.79 m/s, 5.64 m/s, 6.55 m/s, 7.53 m/s, 8.46 m/s, 9.38 m/s, 10.37 m/s, 11.27 m/s, 12.23 m/s, 13.08 m/s, and 14.04 m/s. The deck has characteristic coupled flutter and trend of graphs in third-order polynomial in A_2*.

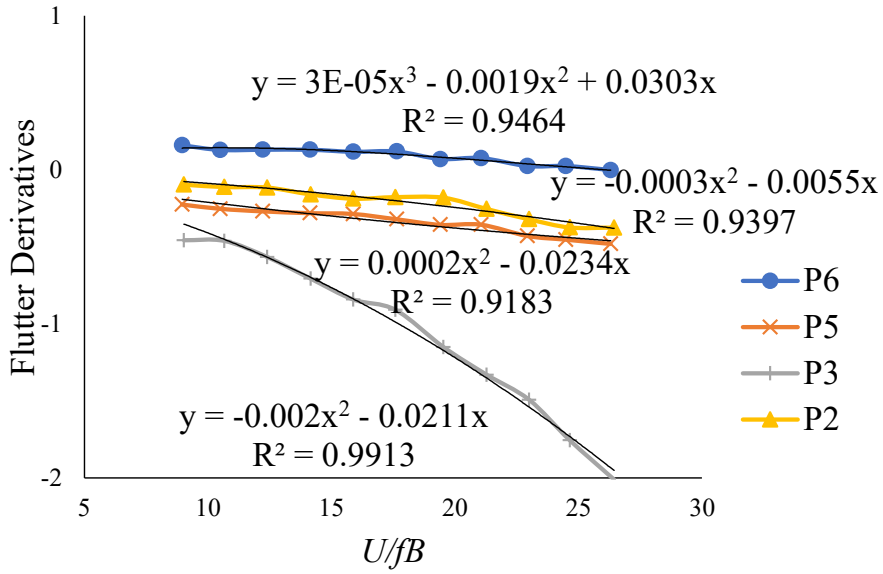

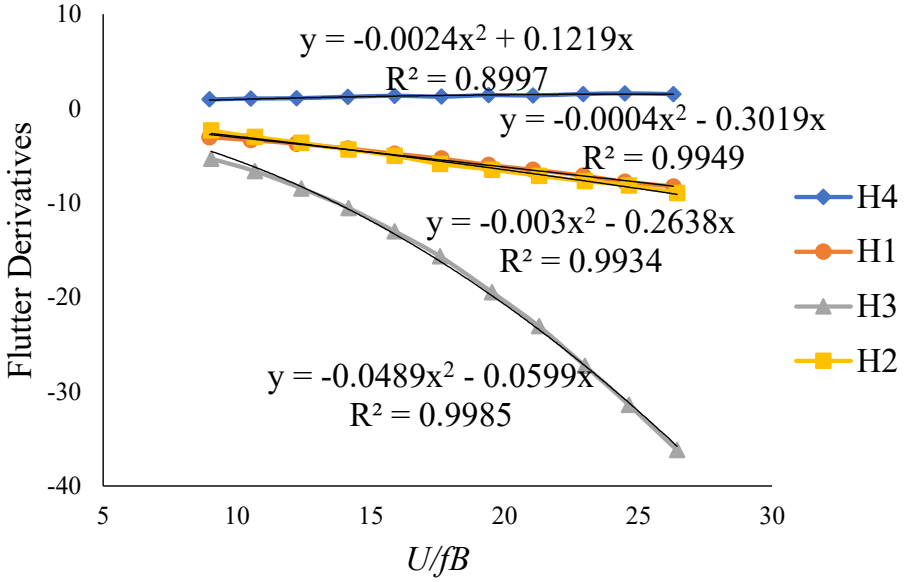

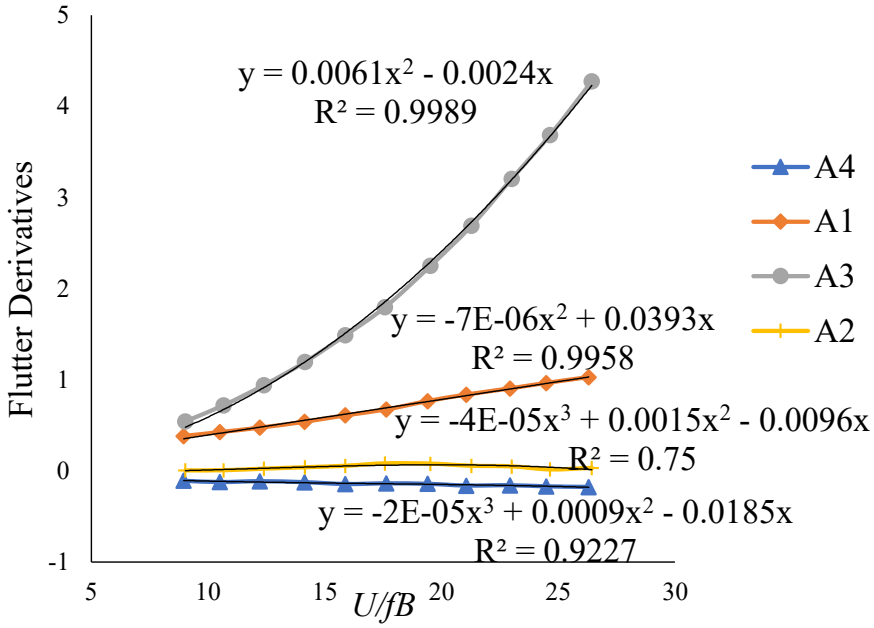

Fig. 15 Flutter derivatives of Akashi Kaikyo at 0^0.

RFa extraction for 12 Flutter derivatives can be obtained as the following formulation, the formulation in the equation (2.24) can be extended as

$$\begin{aligned}
\dot{L}_{ae} + \lambda_L \frac{U}{B} L_{ae} &= \frac{1}{2}\rho U^2 B\left(\left(\frac{U}{B}\right)\psi_1 q + \psi_2 \dot{q} + \left(\frac{B}{U}\right)\psi_3 \ddot{q}\right) \\
\dot{D}_{ae} + \lambda_D \frac{U}{B} D_{ae} &= \frac{1}{2}\rho U^2 B\left(\left(\frac{U}{B}\right)\psi_4 q + \psi_5 \dot{q} + \left(\frac{B}{U}\right)\psi_6 \ddot{q}\right) \\
\dot{M}_{ae} + \lambda_M \frac{U}{B} M_{ae} &= \frac{1}{2}\rho U^2 B^2\left(\left(\frac{U}{B}\right)\psi_7 q + \psi_8 \dot{q} + \left(\frac{B}{U}\right)\psi_9 \ddot{q}\right)
\end{aligned} \tag{3.2}$$

Applying the least square method and following the procedure as described in chapter 2, we can obtain 12 flutter derivatives.

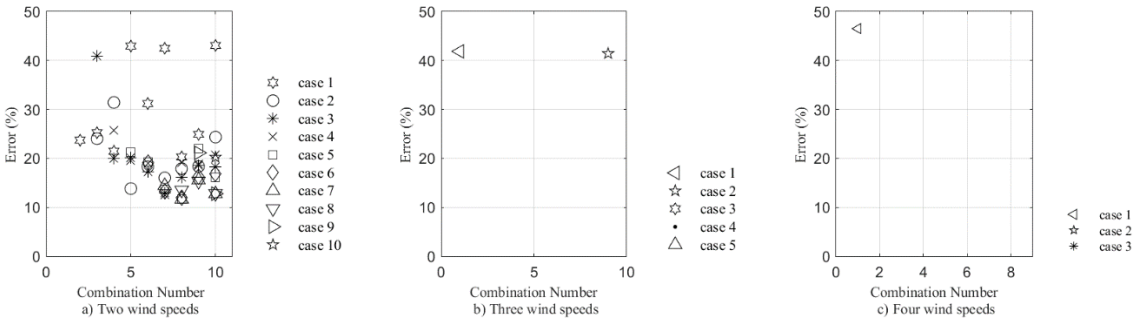

Fig. 16 Error comparison of flutter derivatives extraction at various combinations.

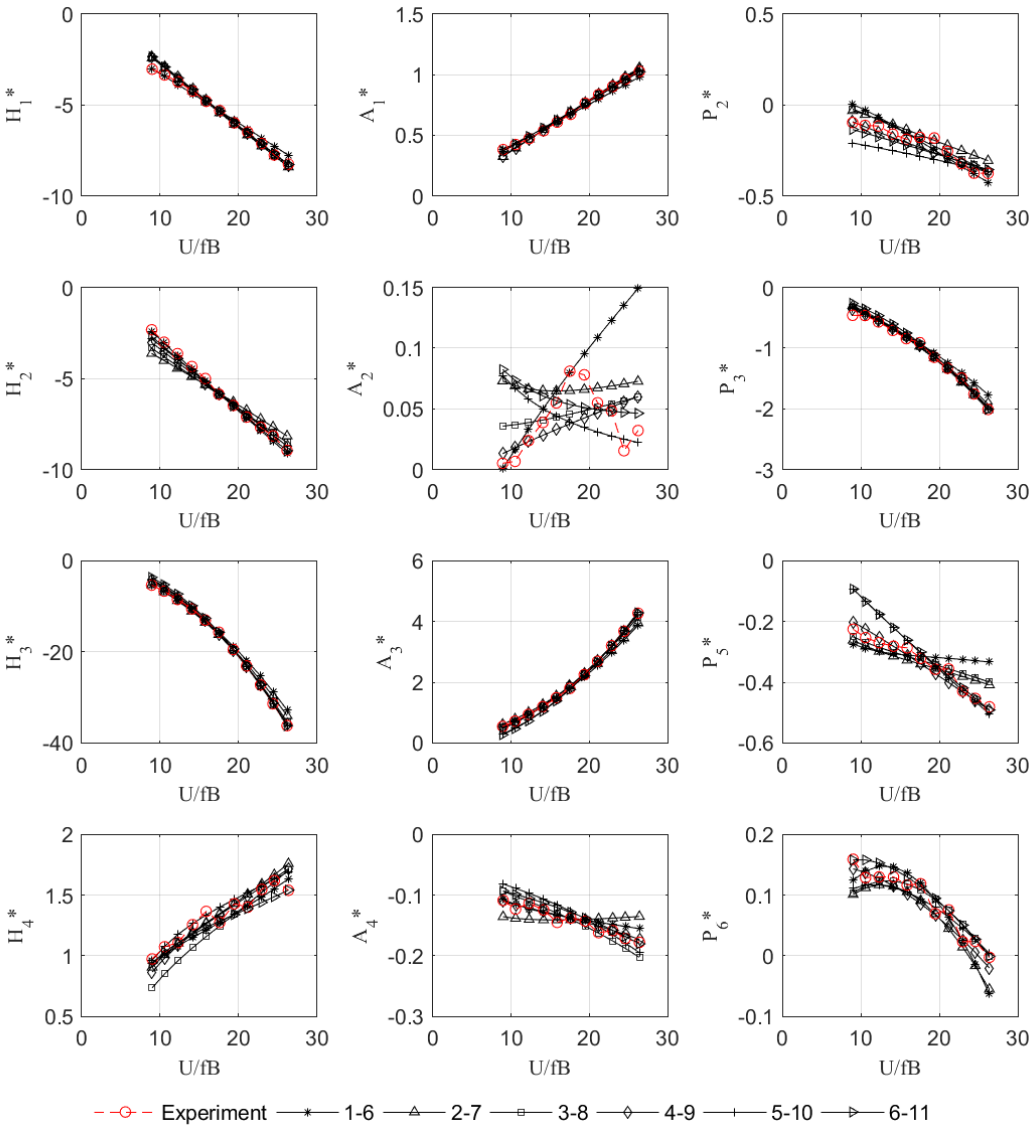

Fig. 17 Comparison of flutter derivatives of Akashi Kaikyo Bridge deck in case 6.

Fig. 16 shows an error comparison of flutter derivatives extraction using various wind speed combinations where the increase of wind speed does not reduce the discrepancy.

Fig. 17 shows the comparison of each flutter derivative between experimental data and RFA extraction in case 6. Flutter derivatives of A_2* change in a complex manner with higher polynomial while extraction from RFA changes quadratically.

3.4 Edge girder deck

Suramadu Bridge is the longest cable-stayed bridge in Indonesia. The main span length is 434 meters, and the deck width is 30 meters with edge girder deck type. The experiment with a section model in one DOF was conducted at Tongji University [35] by

free vibration method. Frequency simulation for lift and moment are 1.61 and 3.76 *Hz*, respectively. In this case, frequency simulation is the same as the frequency of the deck model. Wind speed that is used for the simulation are 3.98 m/s, 4.98 m/s, 6.00 m/s, 7.01 m/s, 8.07 m/s, 9.16 m/s, 10.22 m/s, 11.32 m/s, 12.39 m/s, 12.93 m/s, and 13.54 m/s. This deck type has the characteristic in torsional divergent where A_2^* tends to become positive. In heaving excitation, the data change in a complex manner.

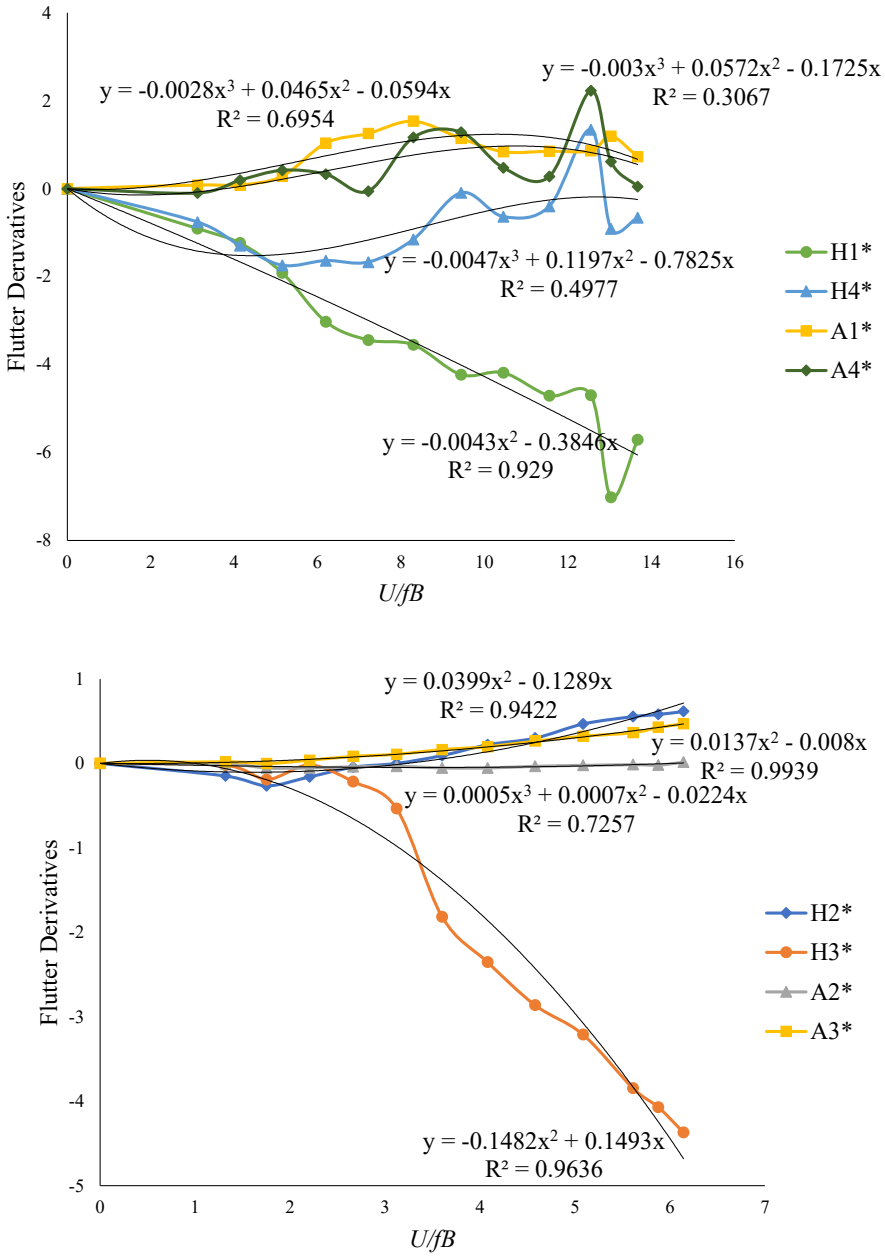

Fig. 18 Flutter derivatives of Suramadu Bridge at 0^0.

Fig.19 shows the error using various wind speed step combinations. The trend is nearly the same as the previous case, where the increase of wind speed does not reduce

the discrepancy. Fig. 20 shows the comparison of each flutter derivative between experimental data and RFA extraction in case 6.

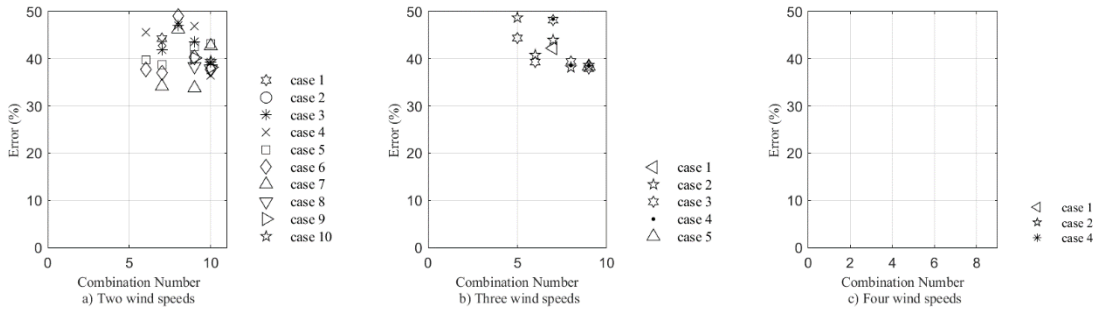

Fig. 19 Error comparison of flutter derivatives extraction at various combinations.

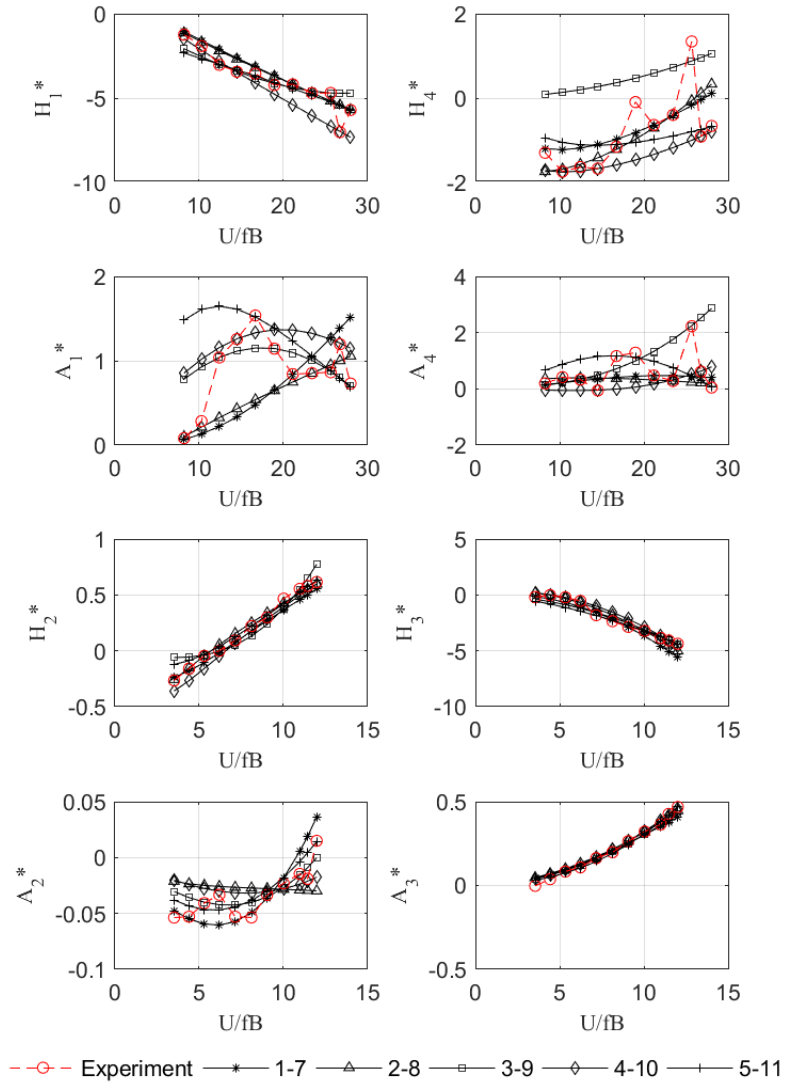

Fig. 20 Comparison of flutter derivatives of Suramadu Bridge deck in case 6.

As seen in the figure above, there are some discrepancies in flutter derivatives for moment force that come from a complex manner of experimental data. Torsional

excitation derivatives the data is smooth while heaving excitation is not smooth. This condition will affect the accuracy of RFA extraction.

3.5 Summary

In this chapter, using secondary data of flutter derivatives in frequency domain using simulated sinusoidal displacement time histories, direct extraction of the RFA coefficients has been successfully presented. This chapter aims to verify the accuracy of RFA extraction against various trends of flutter derivatives. Some points can be summarized as follows:

1. In the airfoil theory case, it shows that the RFA extraction program is correct.
2. As a numerical simulation result, an increasing number of wind speed combinations and lag terms will not reduce the discrepancy. Increasing lag terms will increase unknown parameters and cause the result to become redundant.
3. Two wind speed combinations with one lag term give optimum results for RFA extraction. From numerical simulation for two wind speed combinations, cases 5,6 and 7 give optimum discrepancy between simulation and experiments. Cases 5,6 and 7 are wind speed combinations between wid range and higher wind speed.
4. Some variations in second-order polynomial can be diminished by averaging of wind speed combination. However, in third-order polynomial such A_2^* in Akashi kaikyo bridge and some derivatives in Suramadu bridge, the discrepancies can be reduced to some extent.
5. Many parameters did not consider simulation, such as phase lag between displacement time histories and white noise gaussian.

Chapter 4. Wind Tunnel Experiment

4.1 Experimental setup

A bluff body bridge deck model was tested in a closed-circuit wind tunnel at Yokohama National University. The working section is 1.8 m wide and 1.8 m high. The maximum wind velocity that can be generated by the propeller is equivalent to 35 m/s. The wooden model has a width B of 0.37 m and a height H of 0.04 m. The side ratio B/D (the ratio of width B to depth D) is 9.25:1. The measured vertical and natural frequency of the model are f_h = 2.382 Hz f_α = 5.883 Hz, respectively. The mass of the bridge model per unit length is 4.166 kg/m, and the mass moment of inertia in the torsional direction is 6.368 x 10^{-2} kg m^2/m. Mechanical damping ratios are ζ_h= 2.3% for the heaving motion and ζ_α= 1.41% for the torsional motion. The section model was attached to a shaft system and supported at each corner by a linear spring. The test was conducted with an angle of attack being 0^o.

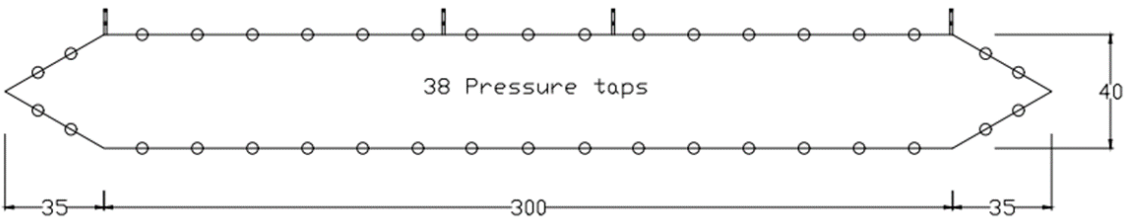

Fig. 21 Deck section.

The section model is attached to a rigid frame and suspended across the wind tunnel by eight helical springs with stiffness *k*. Piano wires were used to restrain the desired degree of freedom. Displacement time histories are measured by a laser transducer.

4.2 Experimental procedures

The experimental procedures[36], [37] briefly can be described as follows:

1. Wind flow is generated by propeller-driven with the desired RPM. A pitot tube is placed under the section model and connected to a manometer, and relative pressure will be displayed. The velocity of wind speed can be calculated from pressure by the calculation

$$U = \sqrt{\frac{2\Delta p}{\rho}} \tag{4.1}$$

The vertical and torsional displacement time history can be obtained through laser device measurement at a specific location. The time histories for vertical *h* (heaving) and torsional (pitching) α responses can be calculated as:

$$h = \frac{h_1 + h_2}{2}$$
$$\alpha = \tan^{-1}\left(\frac{h_1 - h_2}{2}\right) \tag{4.2}$$

Where h_1 and h_2 are the displacement time histories that are measured by laser 1 and laser 2, respectively.

2. The measurement data need to convert from volt to SI unit by calibration factor which derived from zero wind speed measurement

4.2.1 Determination of vertical frequency and mass

The mechanical properties of the section model can be determined by adding additional mass to the deck. The natural frequency of the deck model can be described as:

$$\omega = \sqrt{\frac{K}{m}} \tag{4.3}$$

If the additional mass is located in the center of the deck, the natural frequency in the vertical direction can be written as:

$$\omega_i = \sqrt{\frac{K}{m + \triangle m_i}} \tag{4.4}$$

By adding mass, we can obtain linear regression of additional mass and frequency in the vertical direction. An additional parameter is known as deck mass.

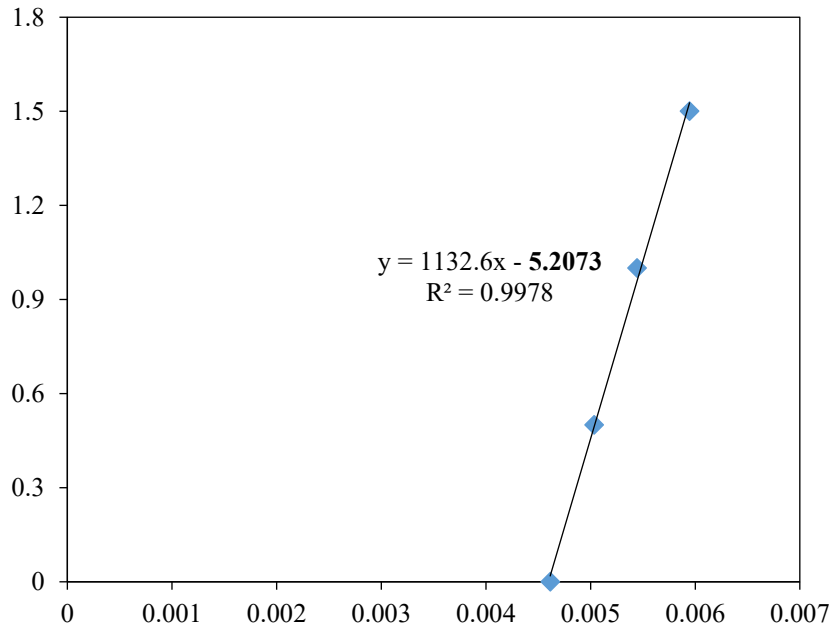

Fig. 22 Mass calibration.

4.2.2 Torsional frequency and moment of inertia of deck model

Determining torsional frequency and moment of inertial of deck model is similar to vertical frequency. The difference is the mass location located at the edge of the mid-chord of the deck section. The moment of inertia of the additional mass can be defined as:

$$\Delta I_i = d_i^2 \Delta m_i \tag{4.5}$$

and torsional frequency is defined as

$$\omega = \sqrt{\frac{K}{I}} \tag{4.6}$$

4.2.3 Determination of mechanical damping

From free vibration of the bridge deck, the logarithmic decrement can be calculated as follows:

$$\delta = \ln \frac{x_n}{x_{n+1}} = \frac{1}{j} \ln \frac{x_n}{x_{n+j}} \tag{4.7}$$

Where x_n and x_{n+j} are amplitudes of a response corresponding to the time

$$\xi = \frac{\delta}{\sqrt{(2\pi)^2 + \delta^2}} \cong \frac{\delta}{2\pi}$$

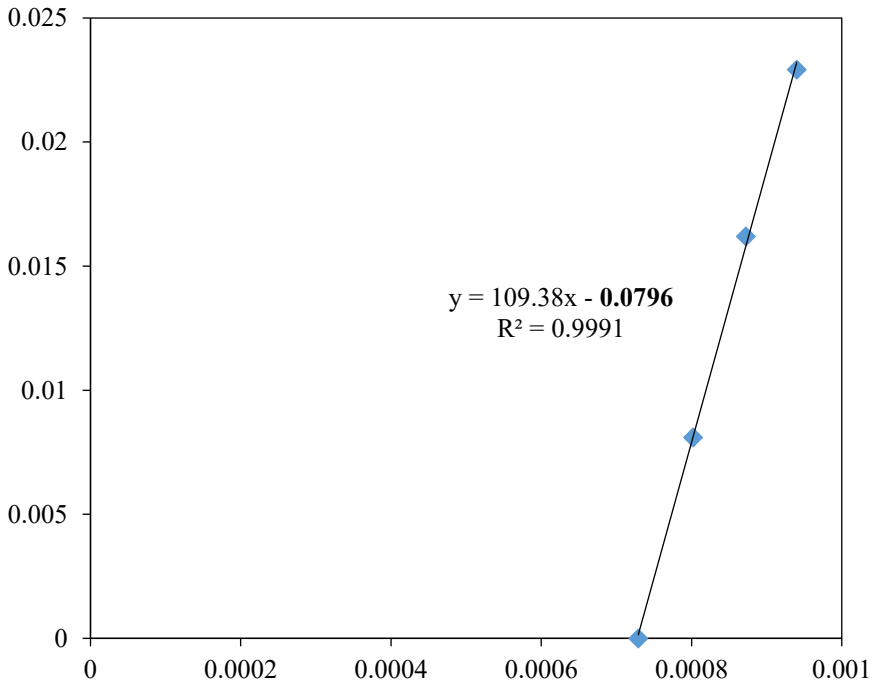

Fig. 23 Moment of inertia calibration.

4.2.4 Pre-set amplitude calibration (forced vibration case)

In case of heaving amplitude, 1 kg a mass is put in the center is equal to *b*/100 where *b* is the deck's width. For the heaving signal, the amplitude of the heaving signal = 0.3076 Volt.

Calibration factor = $\frac{3.7\text{mm}}{0.3076\text{volt}} = 12.03\,\text{mm/volt}$ for *b*/100.

In case of torsional amplitude additional 1 kg, a mass is put in the edge of the deck, which is equal to 1 degree, the amplitude of torsional signal = 0.2899 volts.

Calibration factor = $\frac{1^0}{0.2899\text{ volt}} = 3.45\,^0/\text{volt} = 3.45\frac{\pi}{180} = 0.0602\,\text{rad/volt}$ for 1 degree,

4.3 Free vibration method

The test was conducted in one DOF, heaving mode, and torsional mode. The sampling frequency was set at 200 Hz. There was some lock-in phenomenon in the heaving mode that occurred in wind speed from 1.93 m/s to 2.21 m/s. Keyence wave logger NR-500 program was used for data acquisition.

4.4 Forced vibration method

The motion was generated by two exciters. The high-strength thin wires were used to connect the exciters to the end of the shafts, which enable vertical and torsional oscillation of the deck section. The test was forced oscillated in one DOF, heaving mode, and torsional mode and two DOF. A wave factory WF 1946 2 channel was used to produce an oscillation of heaving and torsion. In the torsional case of one DOF, the phase difference was set on 0^{o} and 90^{o} for each exciter, respectively.

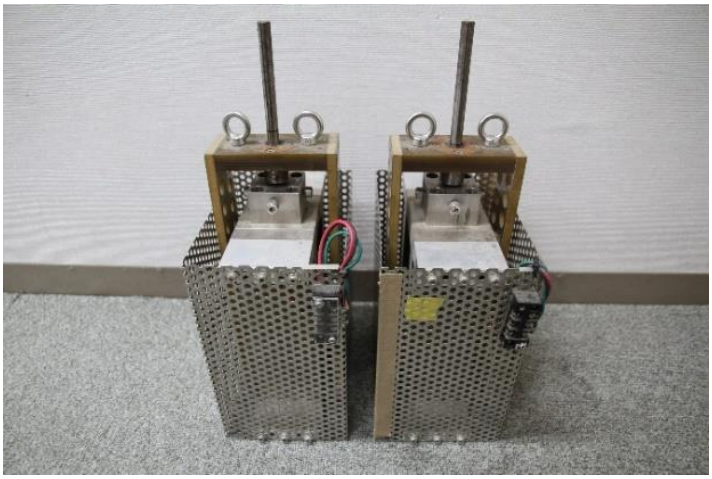

(a) Exciters

(b) Pressure acquisition system

(c) Graphtec Thermal Arracycorder WR300.

(d) Wave Factory WF 1946 2 Channel.

Fig. 24 Equipment devices for forced vibration method.

There are 38 surface pressure taps used in the section model, which are arranged around the cross-section in the middle of the span. The sampling rate and the total sampling time were set at 200 Hz and 60 seconds for time history displacement and surface pressure measurement, respectively. The measurement used the acquisition system of the model MT-MP-32-R1-R±1250 Pa Melon Technos multi-point pressure measurement system with 64 tube connectors to measure the fluctuating surface pressure. Displacement time histories and pressure signals were connected to National Instruments CDAQ-9174. The deck model is forced to vibrate controlled by wave factory WF 1946 2 channel.

Wind tunnel tests were performed from 1 m/s to 15 m/s with 1 m/s increment, which was controlled by propeller speed and total pressure. The amplitude was always monitored by Graphtec Thermal Arraycorder WR300 during data acquisition.

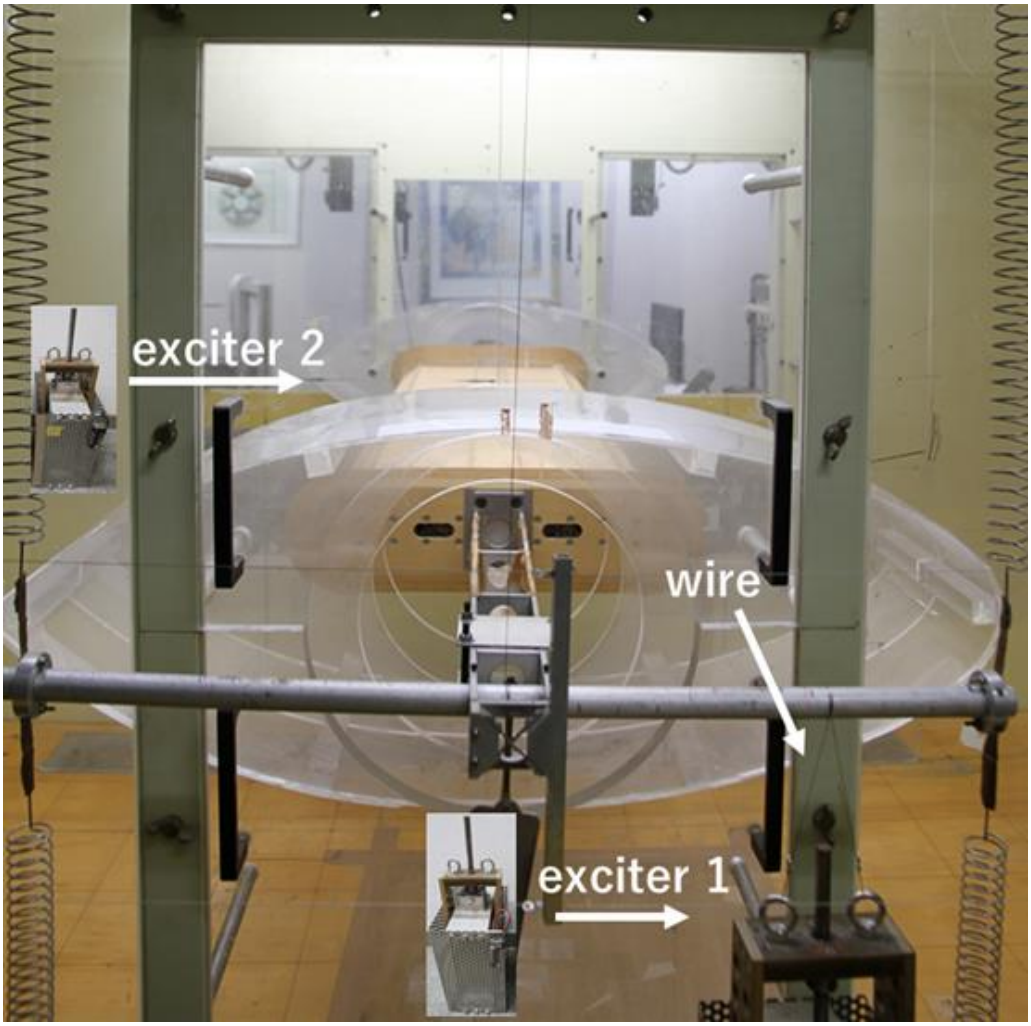

Fig. 25 Experimental setup for one DOF.

The system above can be excited in one DOF heaving mode and torsional mode. The frequency of excitation was set at 1.5 Hz, 2 Hz, and 2.5 Hz for heaving and torsional oscillation, respectively. There are three cases of pre-set amplitude of heaving and torsional mode for the amplitude-dependent case, namely B/100 and $\alpha=1^{o}$, B/50 and $\alpha=0.5^{o}$, and B/200 and $\alpha=2^{o}$, respectively.

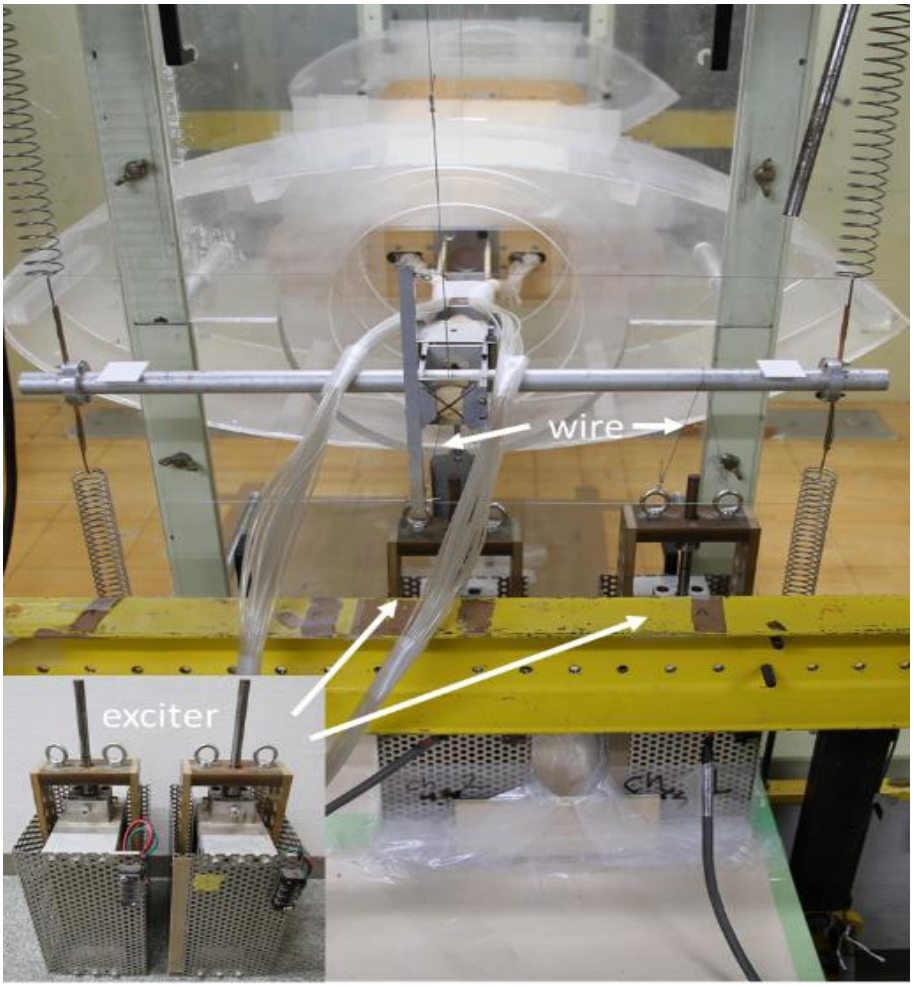

Fig. 26 Experimental setup for two DOF.

In two DOF case, only pre-set amplitude B/100 and 1° will be tested. In two DOF experiments, excitation frequency was tuned to maintain amplitude. Considering vortices in lower wind speed, the sampling frequency was set at 500 Hz. The exciter was set on the center of rotation and at the outer end as the figure above.

4.5 Result and discussion

A program based on MATLAB was developed for RFA extraction. The result of the displacement time histories measurement was reduced by means of displacement time histories in order to set them in the coordinate x-y axis. Aeroelastic forces were generated by the integration of unsteady surface pressure using a rectangular rule. A center of the deck is defined as a mid-chord.

4.5.1 Free vibration method

Free decay signals are obtained at a sampling frequency 200 Hz. The example of free decay response can be shown as below:

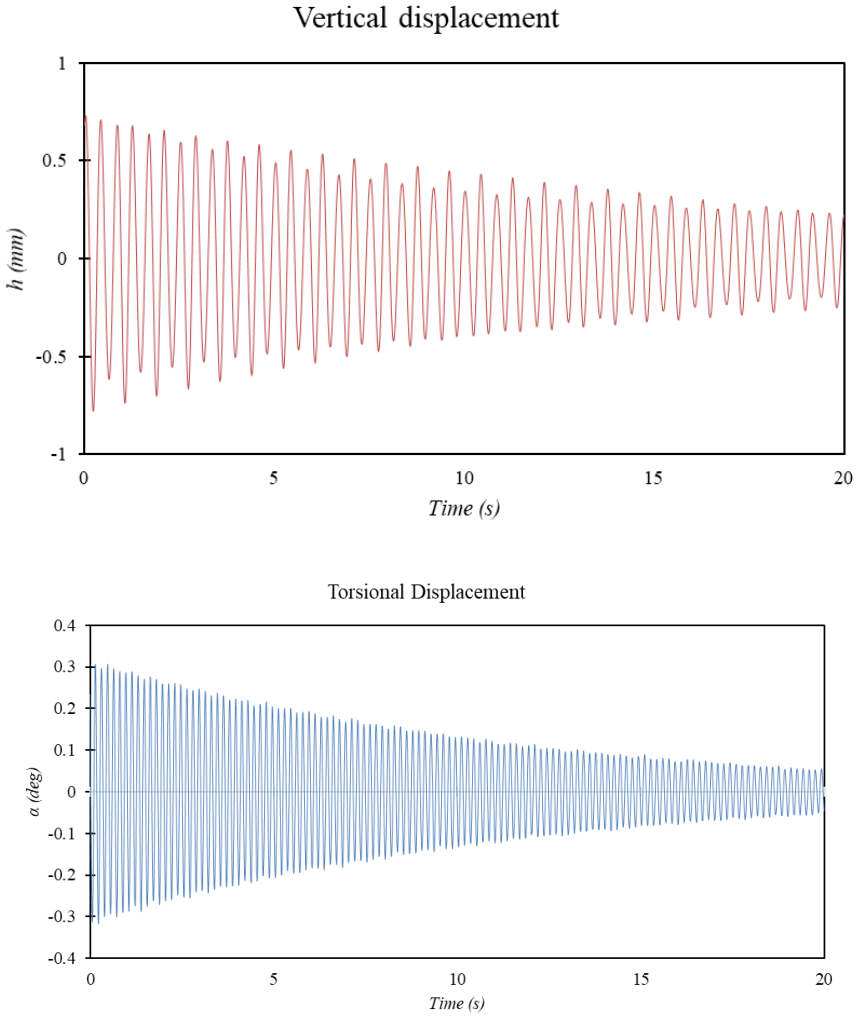

Fig. 27 Free decay response at 0 m/s.

4.5.2 Forced vibration method in one DOF experiment

In a forced vibration test, aeroelastic forces were calculated by the integration of unsteady surface pressure using the rectangular rule. Phase lags can be calculated as a time delay associated with the peak in the cross-correlation [38], [39] function. In this method, sampling frequency choice is an important thing to determine an accurate phase lag. In this work, phase lags were obtained by cross power spectrum between displacement time histories and aeroelastic forces. The bandpass filter with low filter order was used to eliminate white Gaussian noise of fluctuating surface pressures.

In using the bandpass filter, filter order and cut-off frequencies need to be identified. Compared to Chebyshev type I and Elliptic filtering, Butterworth gives better

peak amplitude in the filtering process. It is worth noting that filtering will affect the analytical result. In this dissertation, the bandpass filter with low order was used to eliminate the noise of resultant forces of surface pressure.

The figure below shows the effect of filter order and cut-off frequencies for excitation frequency 2.5 Hz for heaving and torsional, respectively.

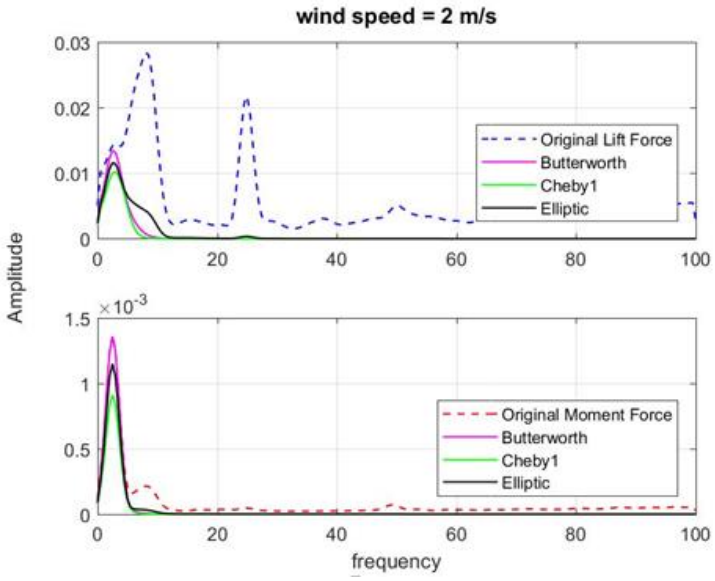

(a) Cut-off frequency 0.5-4.5 Hz

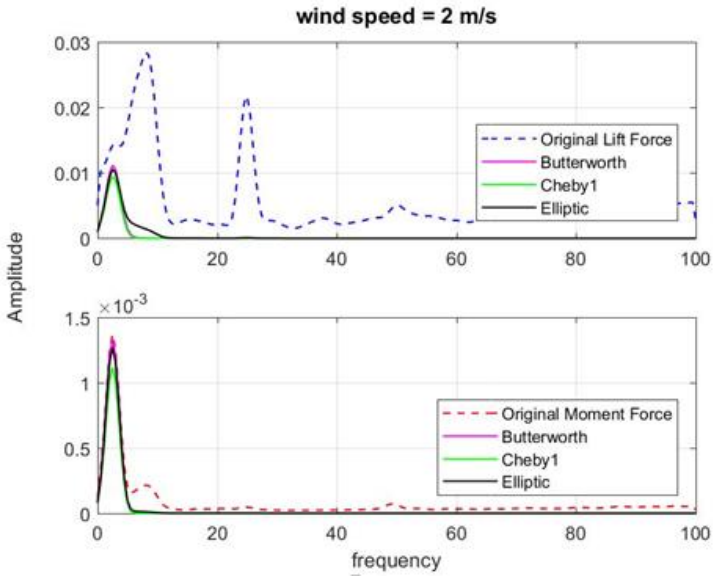

(b) Cut-off frequency 1.5 -3.5 Hz

Fig. 28 Cut-off effect in filtering.

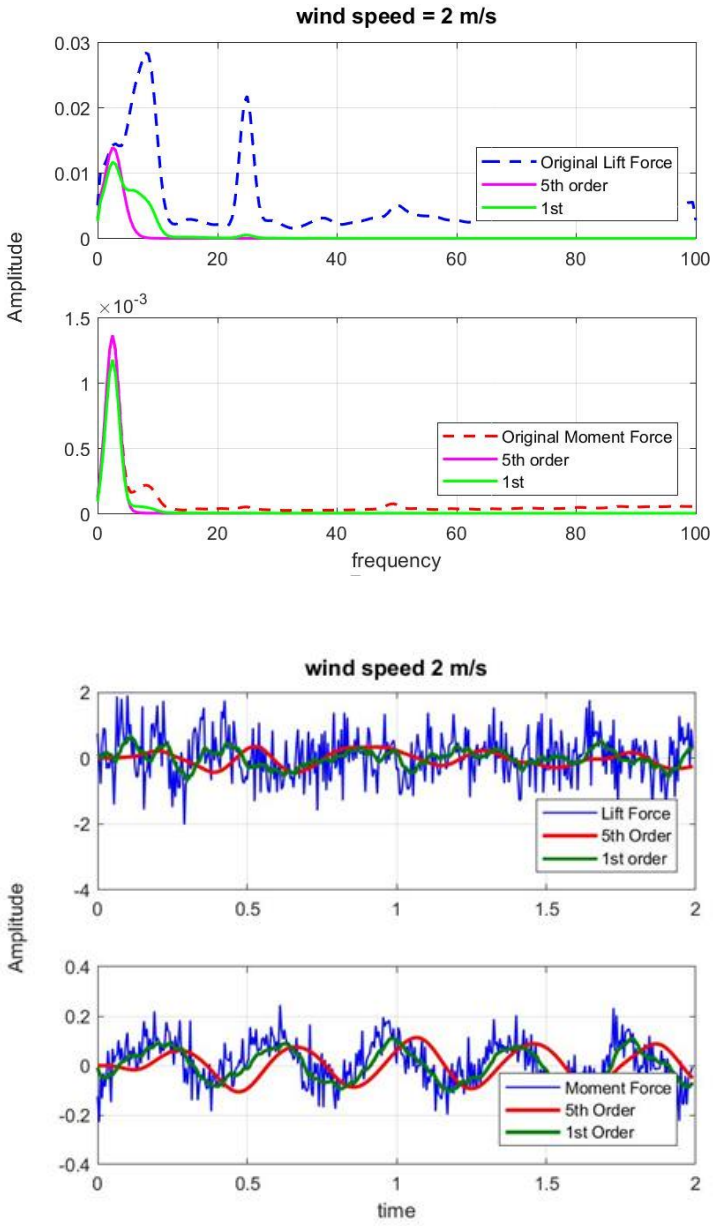

Fig. 29 Transfer function order effect in filtering.

Bandpass filter in range +/- 0.5 Hz of excitation frequency is used as cut-off frequency because it will not affect much of time history amplitude. Increasing the order of transfer function will not affect the amplitude but phase lag between displacement time history and resultant force will be changed. Vice versa, a low order of transfer function will decrease the amplitude and do not change phase lag between displacement time history and resultant force. In the RFA extraction algorithm, the first-order forward finite difference method was employed to differentiate displacement time histories and aeroelastic force. It is interesting to note that between first-order and second-order give the same result. The experiment was conducted several times in one DOF for the heaving

and torsional case. Some combination of the result has been observed, and a good combination is presenting in this dissertation.

Phase lag is negative when a displacement time history leads self-excited force component. The vertical motion in the downward direction and torsional motions in the clockwise direction are defined as positive.

4.5.2.1 Direct extraction of forced vibration

A free vibration test has the advantage that the instability phenomenon can be directly observed. On the other hand, aerodynamic derivative estimation in forced vibration test is straightforward, and phase lag plays a role in the accuracy of flutter derivatives identification.

The coupled derivatives H_2^* and H_3^* describe the aerodynamic coupling between fluctuating lift and torsional excitation. The coupled derivatives A_1^* and A_4^* describe the aerodynamic coupling between fluctuating moment and vertical excitation. The negative value of the uncoupled derivatives H_1^* and H_4^* indicate increasing aerodynamic damping and stiffness for heaving motion as a function of reduced wind speed. The positive or negative value of the uncoupled derivative A_2^* indicates negative or positive damping for torsional motion.

Fig. 30 a), in the heaving oscillation of forced vibration method, H_1^* and A_1^* change slightly, while there is no effect on another two aerodynamics derivatives (H_4^* and A_4^*). An anomaly trend of A_4^* that might be explained by the difficulties of observing in lower wind speed with large damping of structure. In the torsional oscillation, torsional amplitude is strongly affected H_2^* and A_2^* because of the movement of the reattaching point of separation flow [40]. In this experiment, the effect of torsional amplitude emerges in H_2^* of case A. Because the graphs are plotted in reduced frequency and plotted free vibration result depends on natural frequency on the deck, it makes the result seem no proportional to forced vibration result. Additionally, system identification of the Kalman filter will identify the derivatives that have the same frequency. In this manner, torsional frequency is more dominant.

Fig. 30 b) presents the effect of excitation frequency against flutter derivates extraction with case B pre-set amplitude. There is a slight discrepancy in derivatives H_2^* and A_2^*at higher reduced wind speed. It seems that higher excitation frequency will induce the movement of the reattaching point of separation flow.

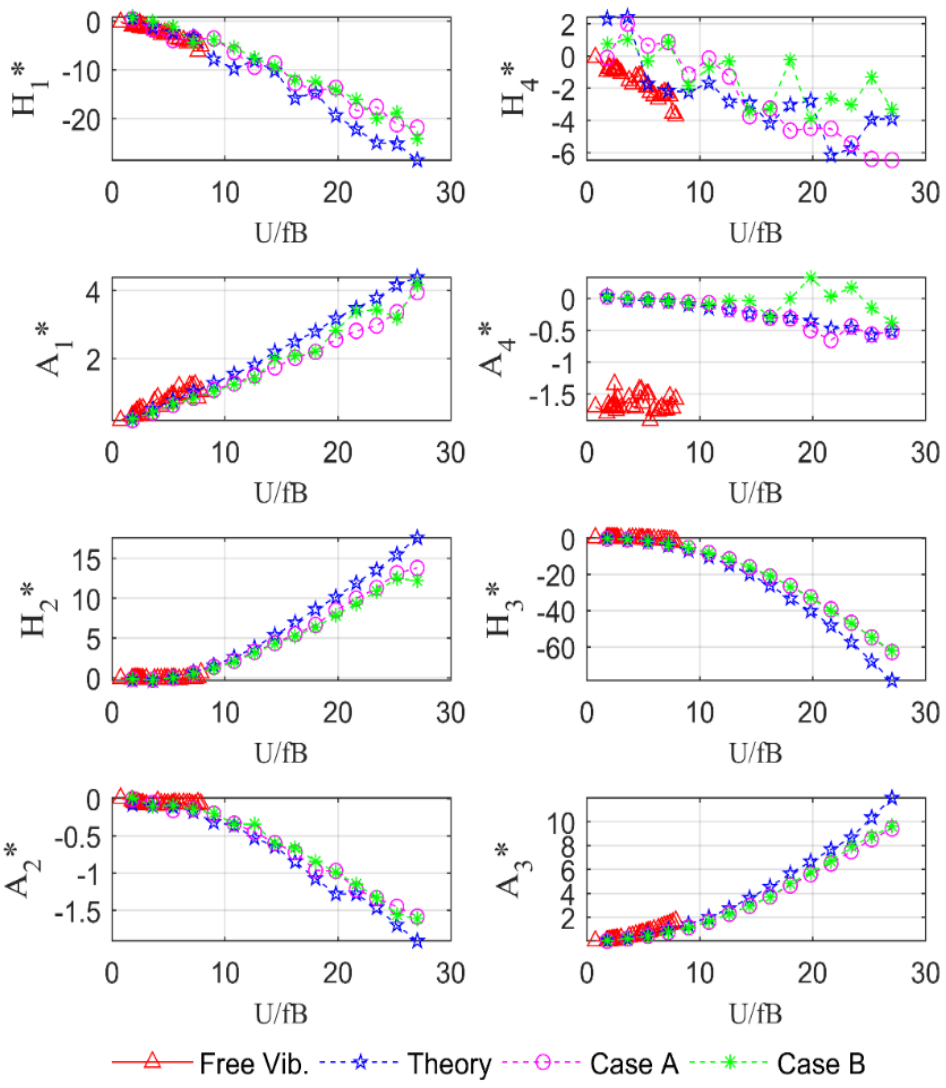

a) Pre-set amplitude effect.

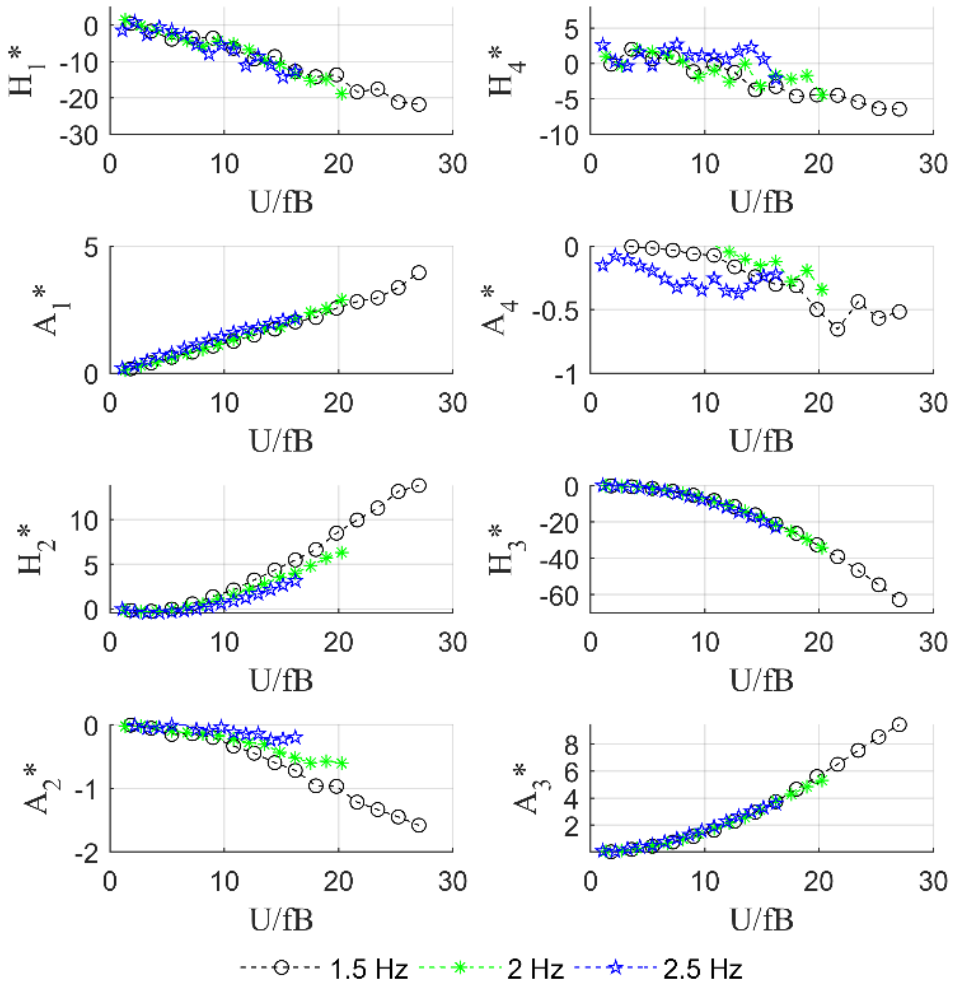

b) Frequency excitation effect.

Fig. 30 Flutter derivatives extraction from forced vibration method.

4.5.2.2 RFA extraction

In RFA extraction algorithm, the displacement time histories and aeroelastic force need to be numerically differentiated and phase lag is an independent parameter. There are many ways to do numerical differentiation, such as first-order forward and second-order central finite difference method. Recorded the fluctuating surface pressures are contaminated with Gaussian white noise [3] and will be eliminated by a digital filter.

In this deck type, H_1^* indicates heaving instability (i.e., galloping) will never occur and the trend typically remains negative. A_2^* usually positive as reduced wind speed increases. Fluctuating surface pressure contains noise and consequently, integration of surface pressures and their derivatives do not become nearly harmonic oscillation. Additionally, a least square of two wind speeds means solely complement each other. Previous studies[5], [7] were based on two DOF forced vibration mechanism where phase

lag sign that might be unnoticed. We encountered some challenges for conversion from RFA coefficient to flutter derivatives due to the phase lag issued and sign convention solves this problem.

In the numerical simulation in chapter 3, we use flutter derivatives data which represent intercorrelation between heaving and torsional oscillation. Aeroelastic forces are generated as coupled aeroelastic forces. However, in the experiment, we treated aeroelastic forces separately as an equation (2.34) because classical approach is also treated as well. The result can be shown in the figure below.

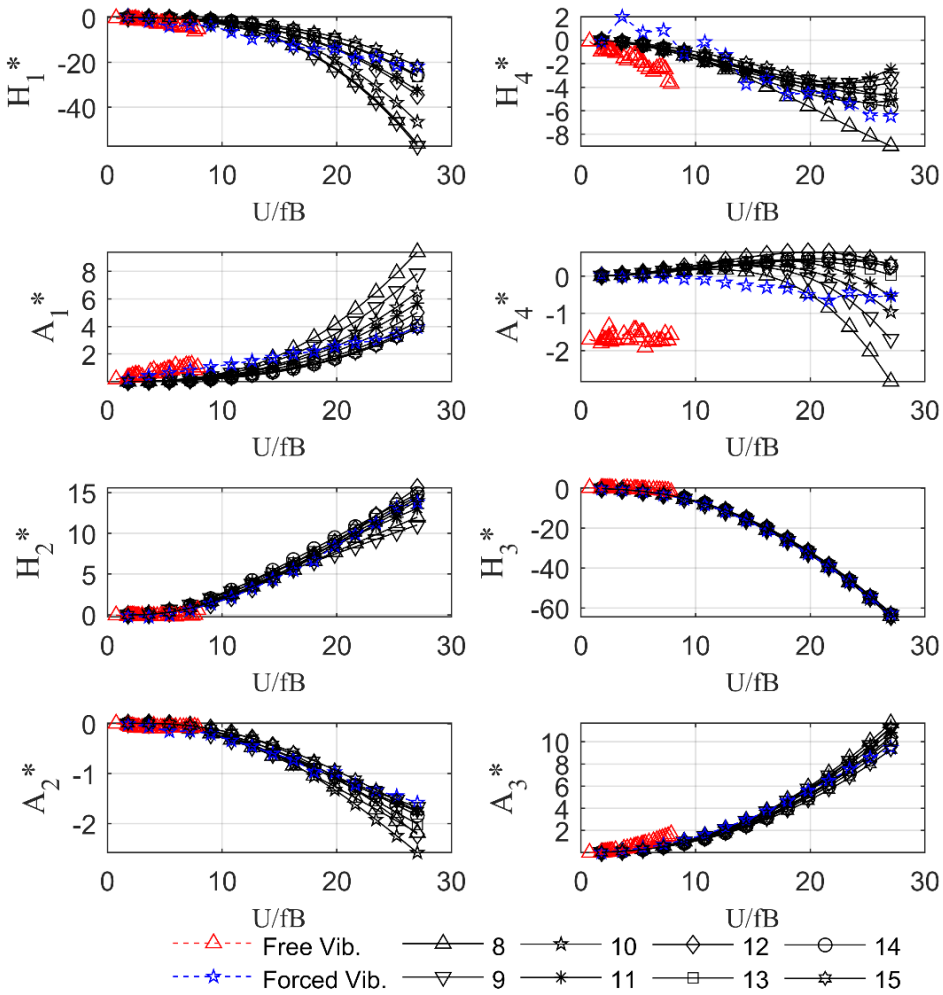

a) One wind speed

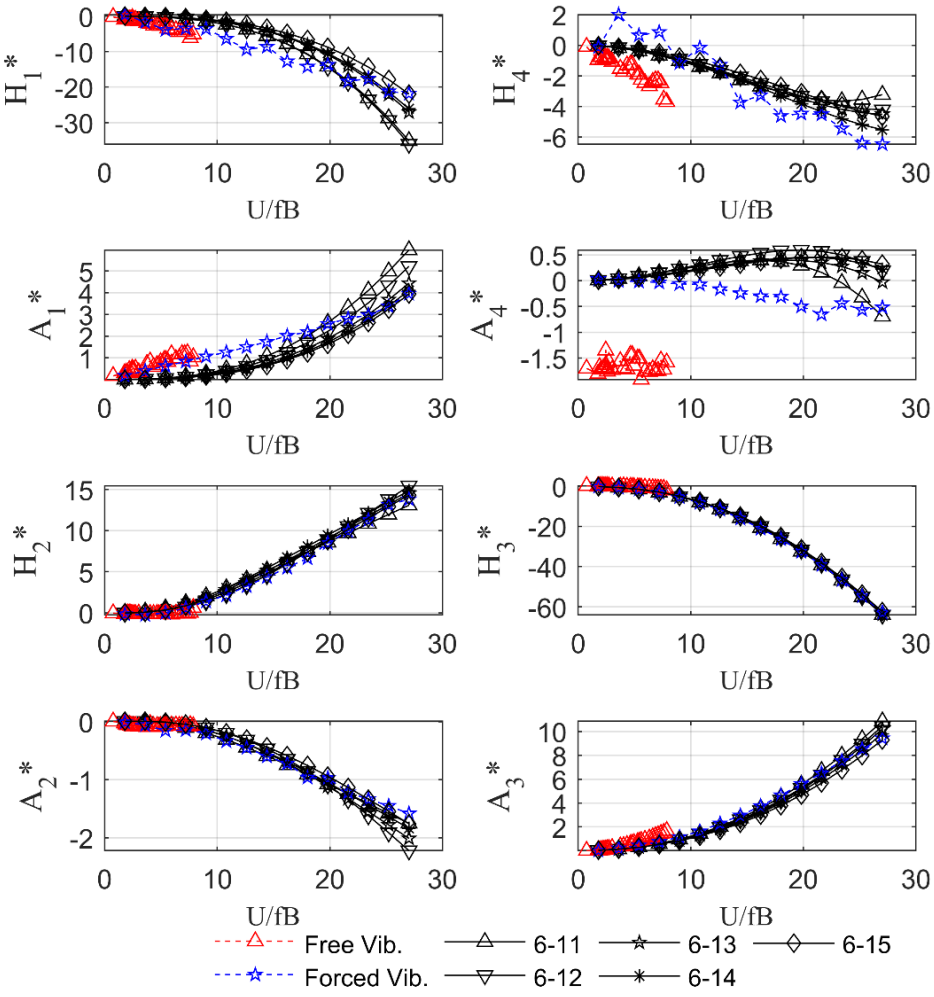

b) two wind speed combination

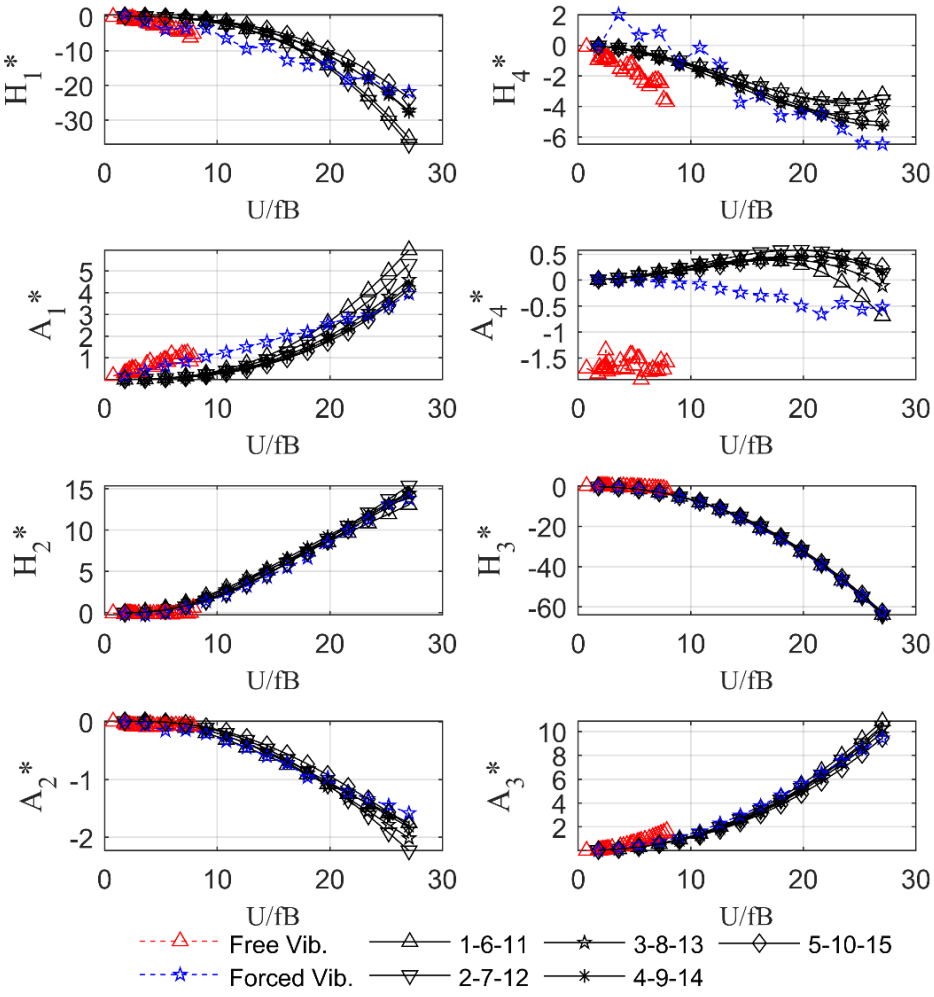

c) Three wind speed combination

Fig. 31 RFA extraction with various wind speed combinations.

The figures above show that various wind speed combinations show a good agreement between forced vibration and RFA extraction methods for different kinds of wind speed combinations, especially in one wind speed. It is hard to understand why one wind speed can cover a wider range of reduced frequency. To understand this phenomenon, we conducted numerical simulation as the procedure in chapter 3.

4.5.2.3 Numerical simulation

In figures below show the trend of direct extraction of forced vibration method is in a quadratic polynomial.

One DOF experiment has the advantage that each heaving and torsional excitation contribution to aeroelastic forces is well quantified and separated at every wind speed. In RFA extraction experiment, that separation must be treated by decoupling aeroelastic forces and solve the extraction for each force. However, in numerical simulation, aeroelastic forces must be constructed as coupled aeroelastic forces.

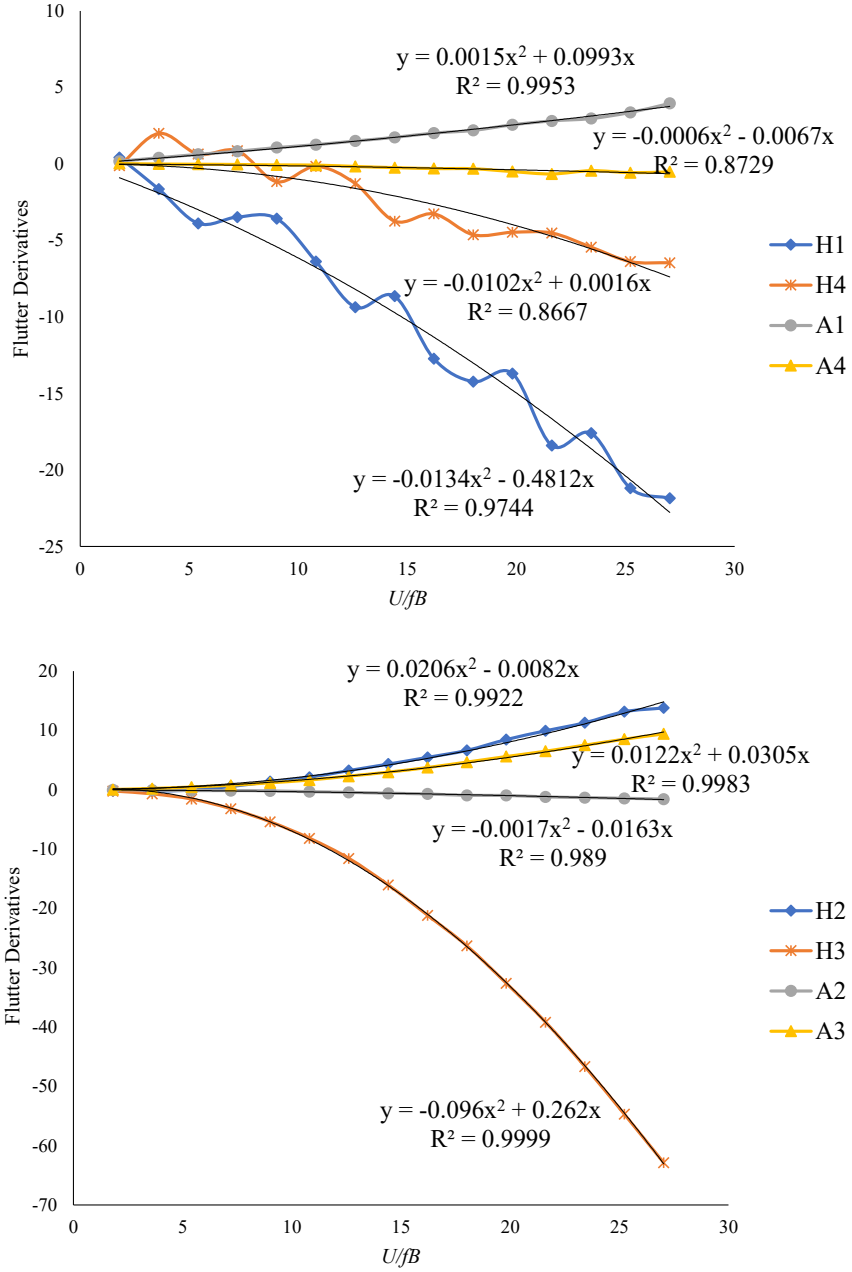

Fig. 32 Polynomial order of flutter derivatives of 1 DOF experiment at B/100-1^0.

Numerical simulation will be done with various wind speed combinations as described in chapter 3 with simulation case as the table 2 below. In this case, aeroelastic force is generated with the fitting curve of flutter derivatives. The purpose of curve fitting is to minimize the error due to fluctuated phase lag in other to have a smooth graph. The figure below shows that between simulation and experimental has a good agreement among all derivatives, which confirms that the program is correct.

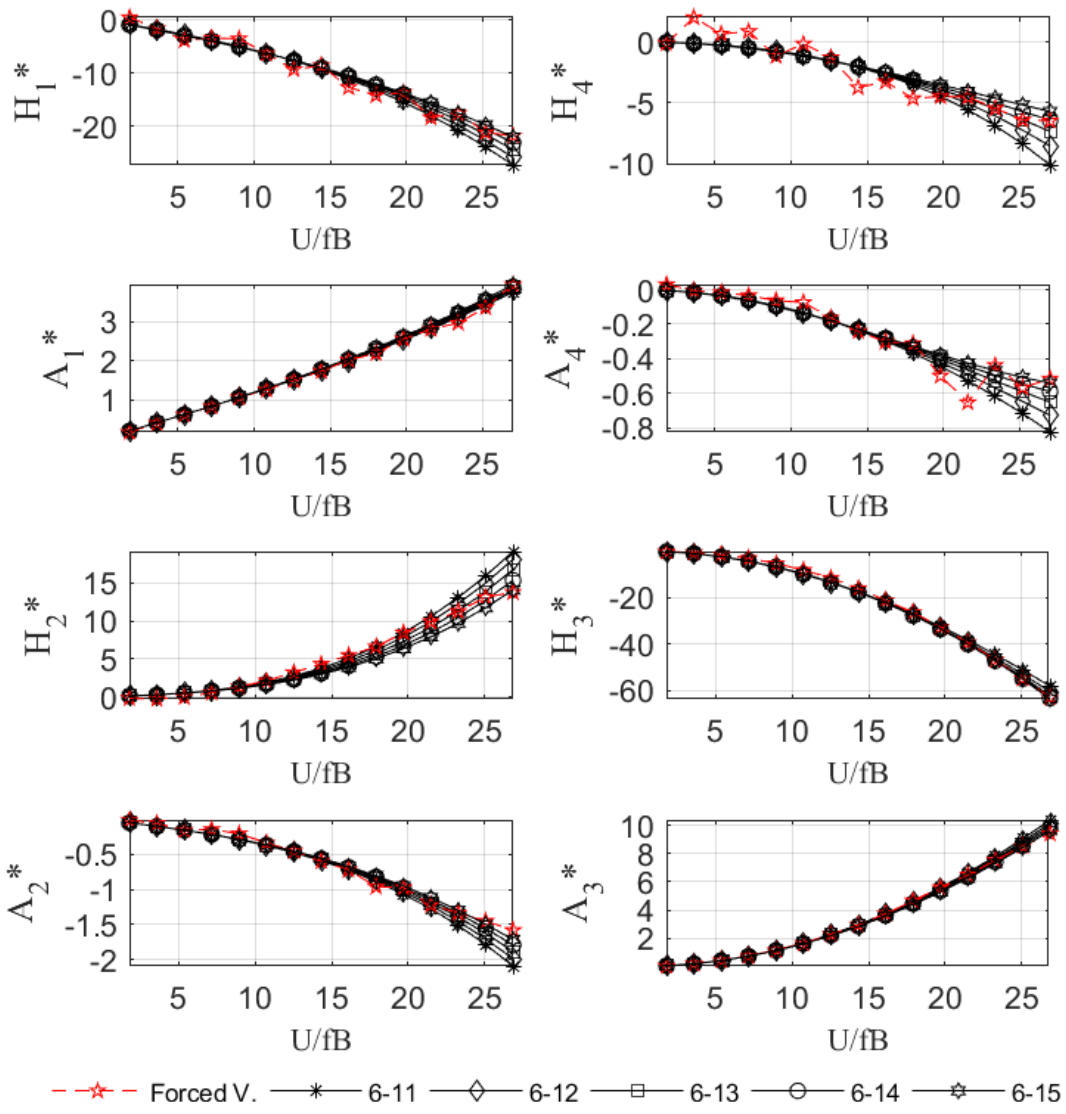

Fig. 33 Simulation of RFA extraction in 1 DOF at B/100-1^0.

Another wind speed combination such as 3 and 4 wind speed combination is also observed.

Table 2 Wind speed combination for experimental simulation.

Number of wind speed combination	Wind speed index combination (combination number)	Case
2 wind speed	1-2 (1), 2-3 (2), 3-4 (3), 4-5 (4), 5-6 (5), 6-7 (6), 7-8 (7), 8-9 (8), 9-10 (9), 10-11 (10), 11-12 (11), 12-13 (12),13-14 (13), 14-15 (14)	case 1
	1-3 (2), 2-4 (3), 3-5 (4), 4-6 (5), 5-7 (6), 6-8 (7), 7-9 (8), 8-10 (9), 9-11 (10), 10-12 (11),11-13 (12),12-14 (13),13-15 (14)	case 2
	1-4 (3), 2-5 (4), 3-6 (5), 4-7 (6), 5-8 (7), 6-9 (8), 7-10 (9), 8-11 (10), 9-12 (11), 10-13 (12), 11-14 (13), 12-15 (14)	case 3
	1-5 (4), 2-6 (5), 3-7 (6), 4-8 (7), 5-9 (8), 6-10 (9), 7-11 (10), 8-12 (11) , 9-13 (12), 10-14 (13), 11-15 (14)	case 4
	1-6 (5), 2-7 (6), 3-8 (7), 4-9 (8), 5-10 (9), 6-11 (10), 7-12 (11), 8-13 (12), 9-14 (13), 10-15 (14)	case 5
	1-7 (6), 2-8 (7), 3-9 (8), 4-10 (9), 5-11 (10), 6-12 (11), 7-13 (12), 8-14 (13), 9-15 (14)	case 6
	1-8 (7), 2-9 (8), 3-10 (9), 4-11 (10), 5-12 (11), 6-13 (12), 7-14 (13), 8-15 (14)	case 7
	1-9 (8), 2-10 (9), 3-11 (10), 4-12 (11), 5-13 (12), 6-14 (13), 7-15 (14)	case 8
	1-10 (9), 2-11 (10), 3-12 (11), 4-13 (12), 5-14 (13), 6-15 (14)	case 9
	1-11 (10), 2-12 (11), 3-13 (12), 4-14 (13), 5-15 (14)	case 10
	1-12 (11), 2-13 (12), 3-14 (13), 4-15 (14)	case 11
	1-13 (12), 2-14 (13), 3-15 (14)	case 12
	1-14 (13), 2-15 (14)	case 13
	1-15 (14)	case 14
3 wind speed	1-2-3 (1), 2-3-4 (2), 3-4-5 (3), 4-5-6 (4), 5-6-7 (5), 6-7-8 (6), 7-8-9 (7), 8-9-10 (8), 9-10-11 (9), 10-11-12 (10), 11-12-13 (11), 12-13-14 (12), 13-14-15 (13)	case 1
	1-3-5 (3), 2-4-6 (4), 3-5-7 (5), 4-6-8 (6), 5-7-9 (7), 6-8-10 (8), 7-9-11 (9), 8-10-12 (10), 9-11-13 (11), 10-12-14 (12), 11-13-15 (13)	case 2
	1-4-7 (5), 2-5-8 (6), 3-6-9 (7), 4-7-10 (8), 5-8-11 (9), 6-9-12 (10), 7-10-13 (11), 8-11-14 (12), 9-12-15 (13)	case 3
	1-5-9 (7), 2-6-10 (8), 3-7-11 (9), 4-8-12 (10), 5-9-13 (11), 6-10-14 (12), 7-11-15 (13)	case 4
	1-6-11 (9), 2-7-12 (10), 3-8-13 (11), 4-9-14 (12), 5-10-15 (13)	case 5
	1-7-13 (11), 2-8-14(12), 3-9-15 (13)	case 6
	1-8-15 (13)	case 7
4 wind speed	1-2-3-4 (1), 2-3-4-5 (2), 3-4-5-6 (3), 4-5-6-7 (4), 5-6-7-8 (5), 6-7-8-9 (6), 7-8-9-10 (7), 8-9-10-11 (8), 9-10-11-12 (9), 10-11-12-13 (10), 11-12-13-14 (11), 12-13-14-15 (12)	case 1
	1-3-5-7 (4), 2-4-6-8 (5), 3-5-7-9 (6), 4-6-8-10 (7), 5-7-9-11 (8),6-8-10-12 (9), 7-9-11-13 (10), 8-10-12-14 (11), 9-11-13-15 (12)	case 2
	1-4-7-10 (7), 2-5-8-11 (8), 3-6-9-11 (9), 4-7-10-13 (10), 5-8-11-14(11), 6-9-12-15 (12)	case 3
	1-5-9-13 (10), 2-6-10-14 (11), 3-7-11-15 (12)	case 4

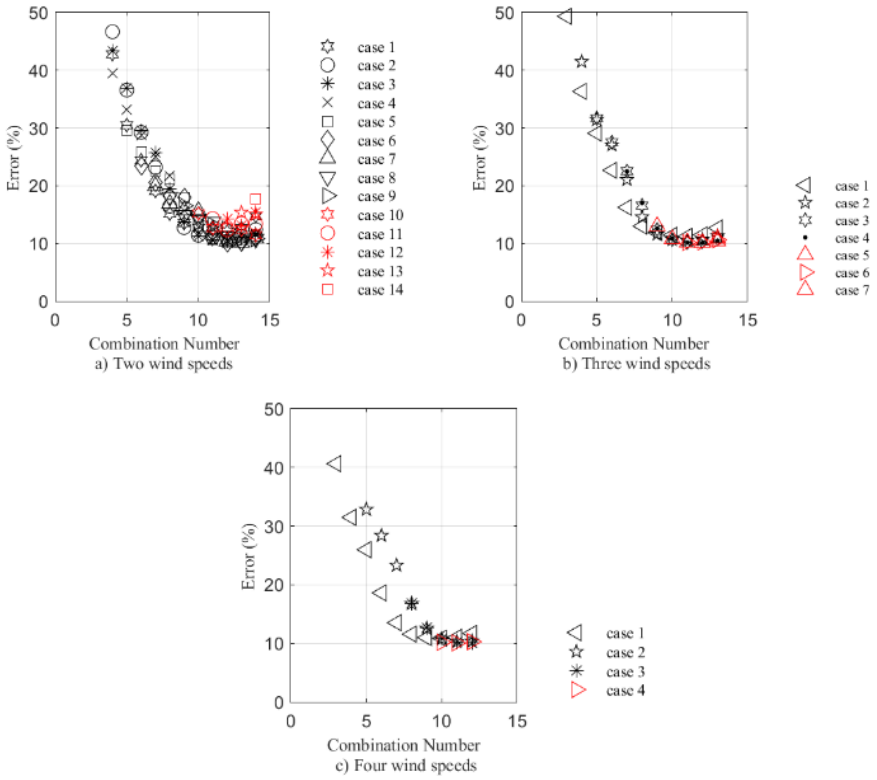

Fig. 34 Error comparison of flutter derivatives extraction at various combinations.

The figure above shows the error comparison of flutter derivatives at various combinations of wind speed combinations. The error seems around 10 % for all wind speed combinations. Direct extraction result gives fluctuated phase lag and it may contribute to the discrepancy. The figure above shows that the combination in mid-range and higher wind speed will give minimum discrepancies. The largest range will not give the best option. It can be understood since in lower wind speed, the resultant force is too small for RFA extraction. For the sake of simplicity, combination 6-13 m/s is chosen the next analysis.

4.5.2.4 Data length effect

RFA extraction is conducted in time domain, and the data length is an important thing to observe. Experiment data from case B pre-set Amplitude is used to extract RFA coefficients. Since reference results are described in aeroelastic coefficients, extraction of RFA coefficients will be converted to flutter derivatives and then compared with EKWGI and classical approach of case B pre-set amplitude. Due to high-quality experimental data, the results presented here have been obtained from wind speed combinations 6 m/s and 13 m/s. In the measurement, the total sampling time was set on 60 seconds and the sampling rate is 200 Hz which means that there is a 12000 array dimension of data length. Smaller

data length will speed up the calculation and it is interesting to investigate RFA extractions against data length. Fig. 35 illustrates that flutter derivatives from RFA extractions generally compare well. There is no much difference between 60 seconds and 10 seconds of data length.

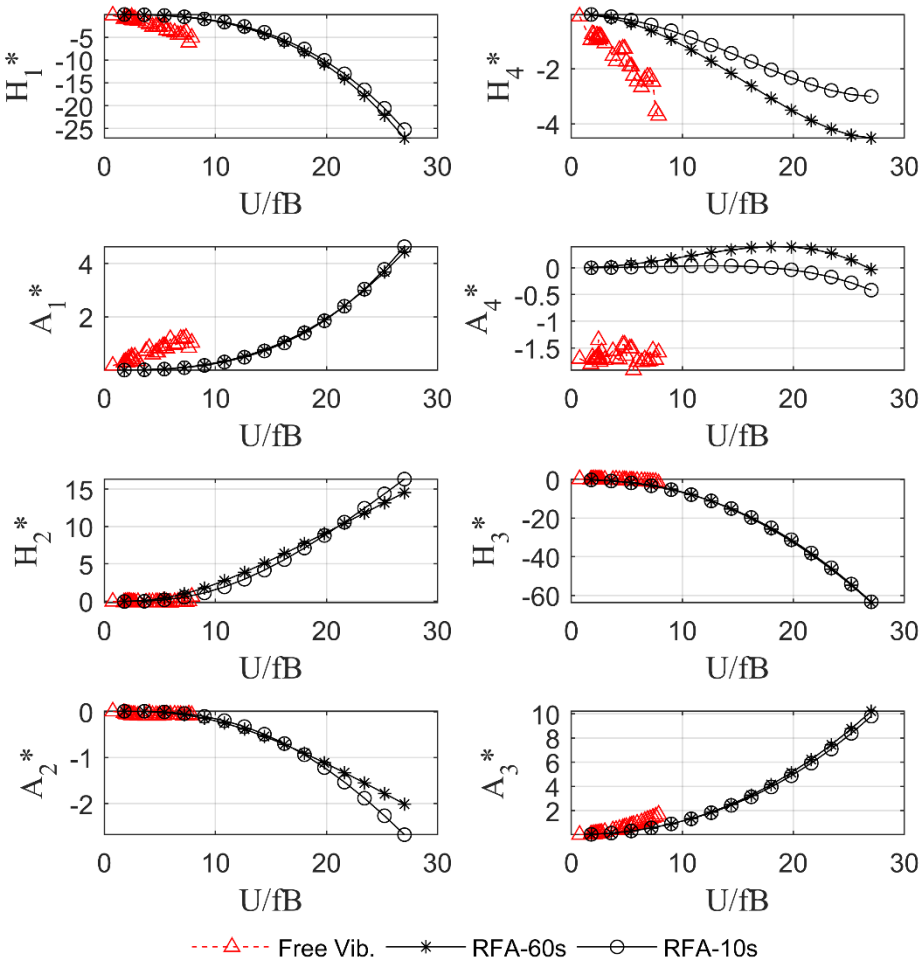

Fig. 35 RFA extraction considering data length effect.

4.5.2.5 Pre-set amplitude effect

In the same manner in the direct extraction, Fig. 36 depicts the effect of pre-set amplitude on RFA extraction with 60 seconds of data length. Generally, they have the same trend as in the direct extraction approach. However, there are anomaly trends in case C pre-set amplitude that is the largest amplitude case.

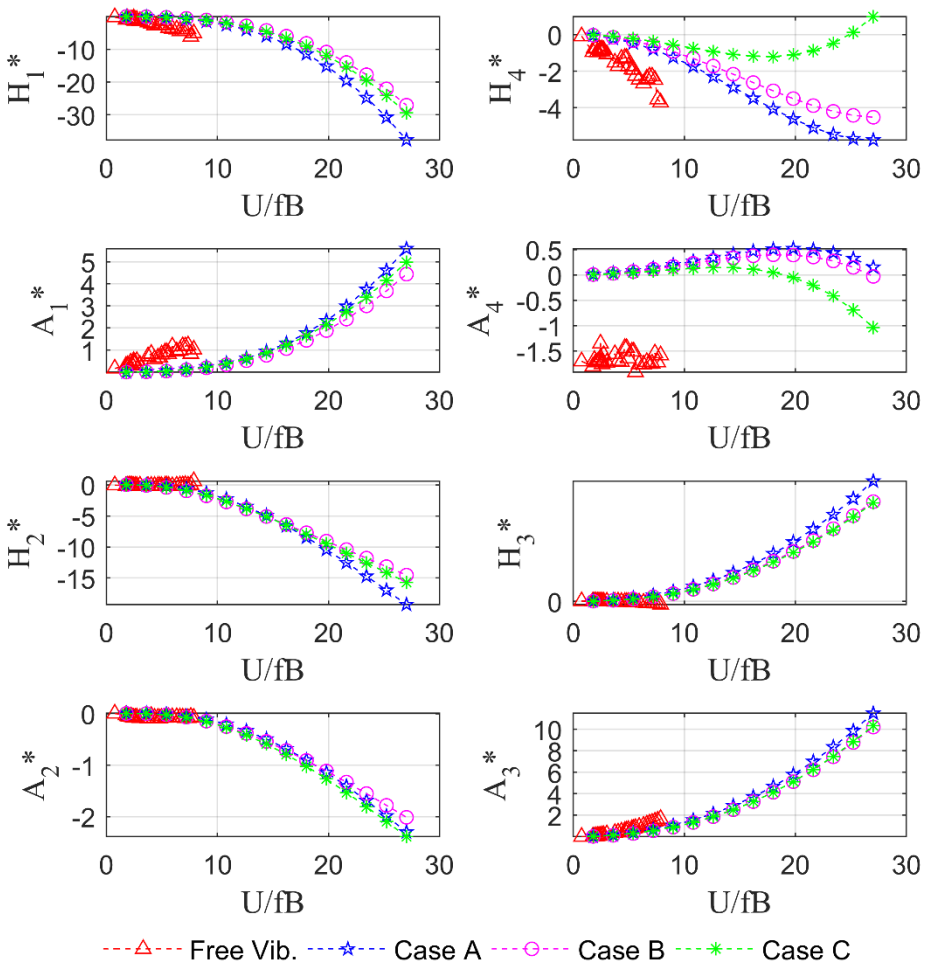

Fig. 36 RFA extraction considering pre-set amplitude effect.

4.5.2.6 Flutter analysis

In order to investigate the effect on pre-set amplitude, two DOF flutter analyses were conducted for cases A-C of the RFA extraction as well as forced vibration case B, as shown in Fig. 37. A discrepancy in coupled derivatives is the reason for flutter instability in case of RFA extraction. However, it was recognized that some other derivative components also affect the flutter speed sensitively.

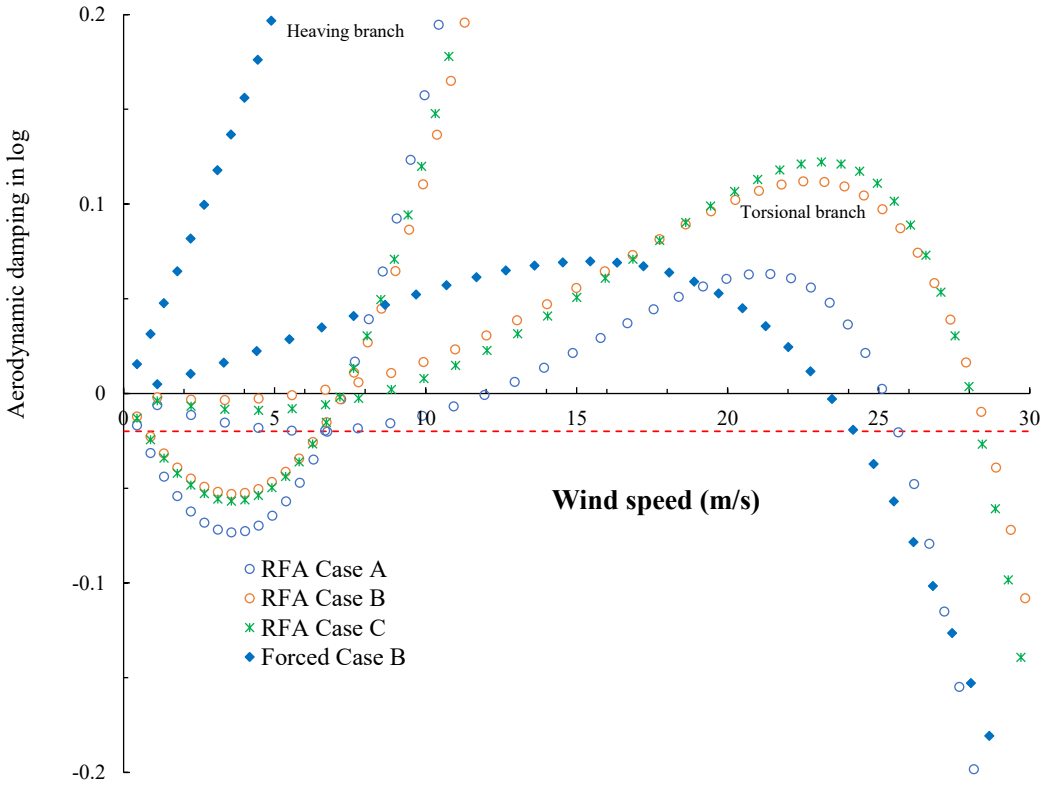

Fig. 37 Two modes flutter analysis.

4.5.3 Forced vibration method in two DOF experiment.

4.5.3.1 Direct extraction of forced vibration

Experimental setup either in one DOF or in two DOF has a different system. In one DOF, a harmonic motion will contribute to each vertical and modal branch, the purpose that couple terms of derivatives can be accurately quantified. The reduced wind speed can be unified by setting the same excitation frequency. On the other hand, two DOF experiment is more precisely to measure a couple of aeroelastic forces. However, in two DOF experiment, phase lag must be maintained in order to produce designated coupled vibration. Nevertheless, due to the experiment device, in this thesis, excitation frequency was tuned to maintain pre-set amplitude. The figure below shows the direct extraction of flutter derivatives with pre-set amplitude with B/100 and 1°. Compared to one DOF experiment H_1^* and H_2^* have the trend in third-order polynomial.

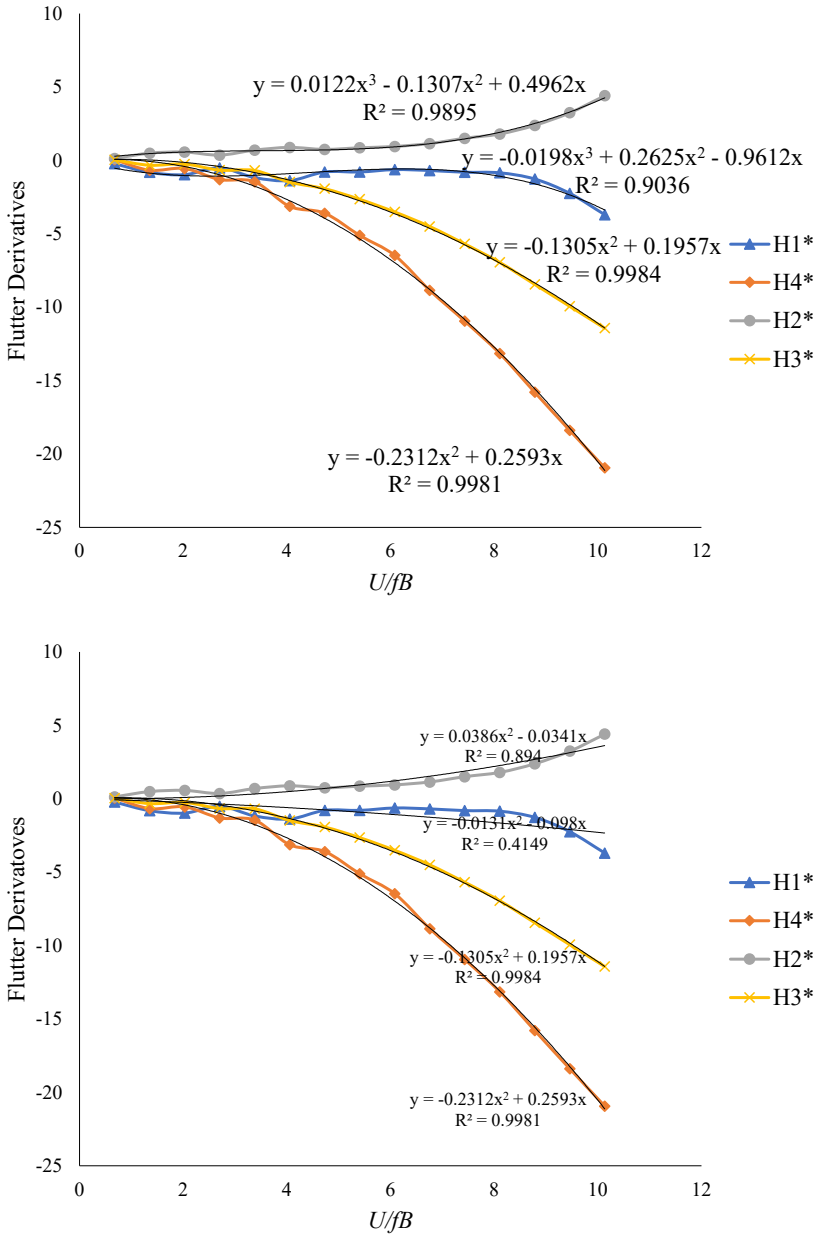

Fig. 38 Direct extraction of flutter derivatives in two DOF experiment.

4.5.3.2 RFA extraction

Since RFA coefficient extraction can be extracted at every wind speed, the similarity between resultant forces and force simulation as well as the comparison of flutter derivatives are necessary. Two parameters are used to measure aeroelastic forces similarity, namely, correlation coefficient and coefficient of determination. The correlation coefficient (ρ_{xy}) and coefficient of determination (R^2) between the measurement of resultant force (x_i) and simulation (y_i) within n-step signals can be calculated using the following equation:

$$\rho_{xy} = \frac{\sum_{i=1}^{n} x_i y_i}{\sigma_x \sigma_y n} \tag{4.8}$$

$$R^2 = 1 - \frac{\sum_{i=1}^{n} (x_i - y_i)^2}{\sum_{i=1}^{n} x_i^2} \tag{4.9}$$

Because it is the spring-mass system, a wind tunnel experiment was conducted with the frequency of excitation the same as deck's natural frequency to verify the calculation. The figures below show the RFA extraction in one DOF experiment. Results show there is no effect among wind speed combinations. Some discrepancies occur due to phase lag fluctuation for every wind speed.

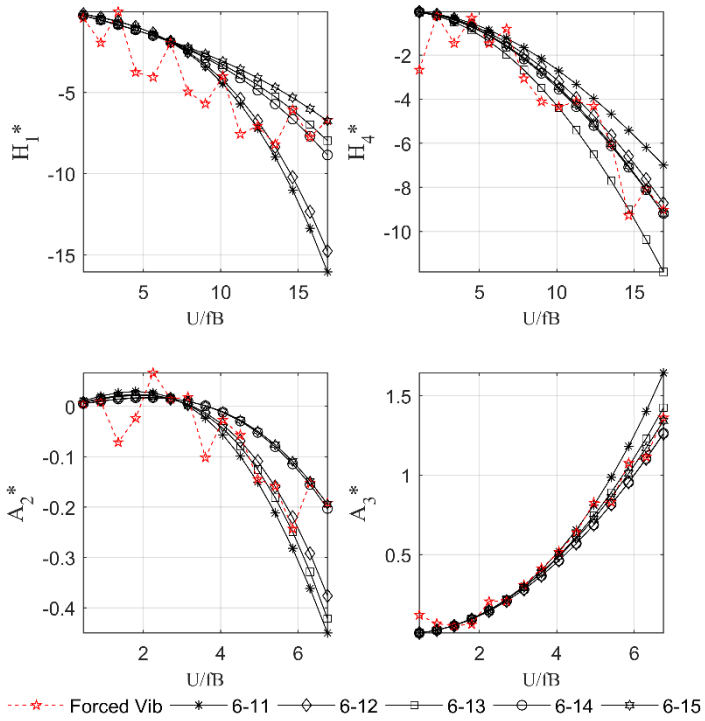

Fig. 39 RFA extraction in one DOF experiment by two DOF system.

Fig. 40 below show the flutter derivatives extraction in two DOF excitation. Wind speed combination for the extraction was selected at wind speed 6 m/s with various higher wind speed from 11 to 15 m/s. Considering A_2^*, wind speed combination 6 – 12 m/s and 6 – 13 m/s have a good agreement with forced vibration result. Nevertheless, the RFA coefficients need to be investigated to find a reasonable reason why flutter derivatives have a large discrepancy in the small range of wind speed combination.

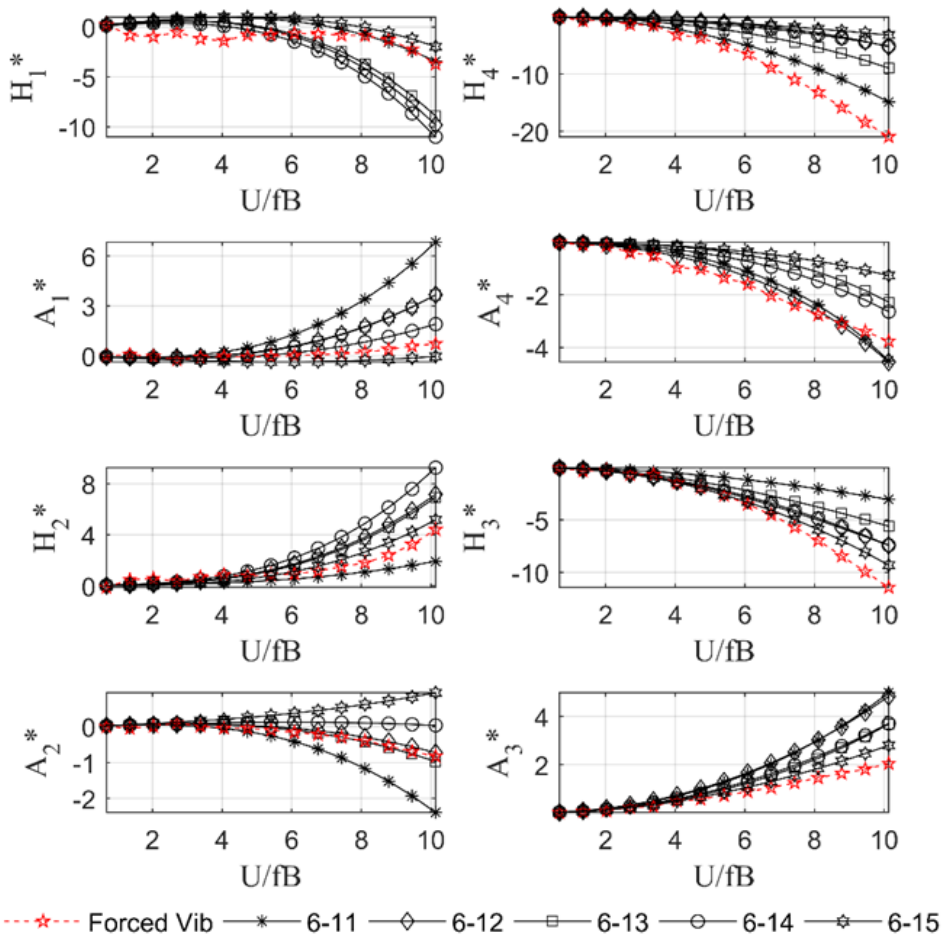

Fig. 40 RFA extraction in two DOF experiment.

Table 4 shows a summary of aeroelastic force comparison between measurement and simulation. Correlation coefficients and coefficients of determination are over 90 %, except for the 6 – 15 m/s combination case. Therefore, it is essential to emphasize that the coefficients tell that the identification algorithm and program are correct. The discrepancy which occurred indicates that direct extraction of RFA requires enhancement in the advanced model due to higher-order polynomial.

Considering flutter derivatives result and similarity between measurement and simulation, combination 6 – 13 m/s is the best option for direct extraction of RFA. There is some error in combination 6 – 15 m/s in Fig. 41 g) that can be explained in table 4.

Table 3 Correlation coefficient (ρ_{xy}) and coefficient of determination (R^2) between measurement and simulation by RFA method with various 6 m/s combinations.

Wind speed combination (m/s)	Wind Speed simulation (m/s)	Lift force (Nm)		Moment force (Nm/m)	
		ρ_{xy}	R^2	ρ_{xy}	R^2
6-11	15	0.967	0.935	0.976	0.938
	10	0.997	0.993	0.995	0.986
	6	0.998	0.996	0.997	0.992
6-12	15	0.981	0.961	0.989	0.968
	10	0.995	0.987	0.995	0.986
	6	0.998	0.994	0.997	0.991
6-13	15	0.990	0.979	0.993	0.985
	10	0.992	0.979	0.995	0.986
	6	0.998	0.994	0.997	0.988
6-14	15	0.996	0.993	0.995	0.989
	10	0.988	0.967	0.995	0.987
	6	0.998	0.994	0.997	0.986
6-15	15	0.010	-	0.997	0.993
	10	-	-	0.996	0.989
	6	0.010	-	0.997	0.977

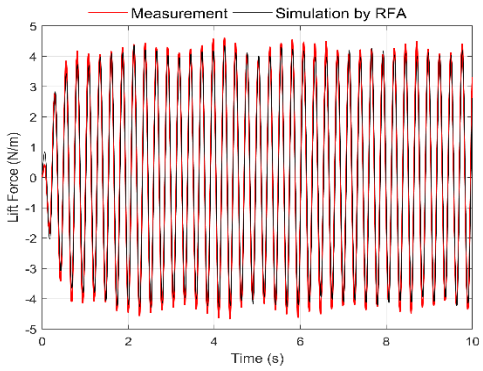

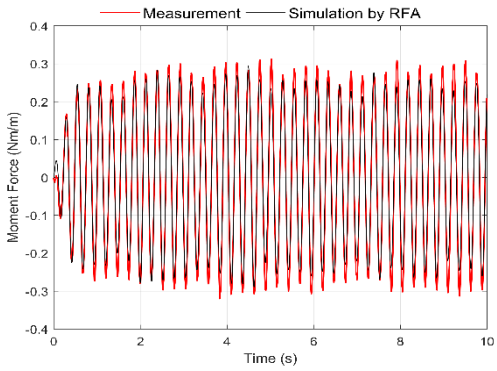

a) Lift force time history by 6 - 12 m/s combination. ›) Moment time history by 6 - 12 m/s combination.

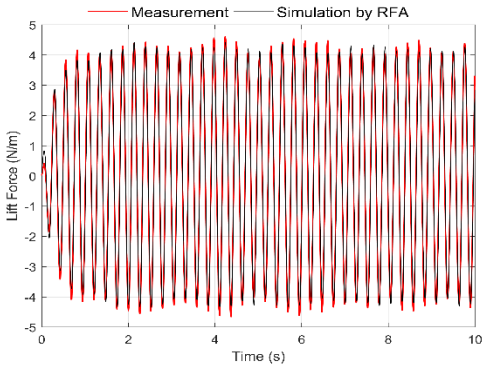

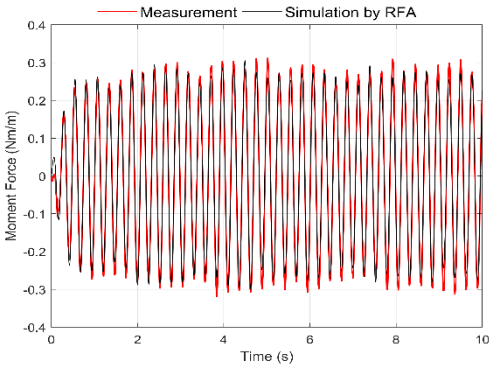

c) Lift force time history by 6 - 13m/s combination. d) Moment time history by 6 - 13 m/s combination.

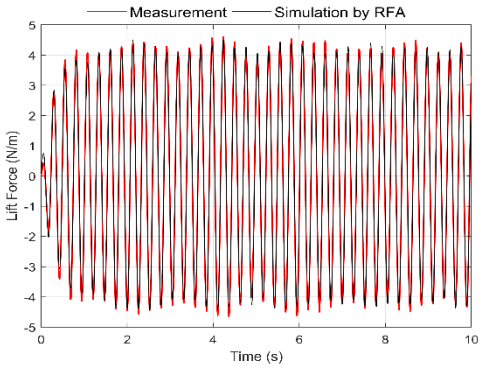

e) Lift force time history by 6 - 14 m/s combination.

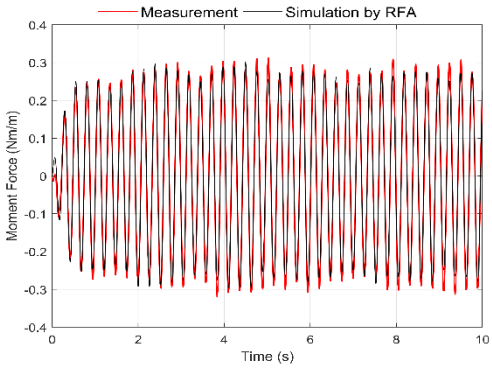

f) Moment time history by 6 - 14 m/s combination.

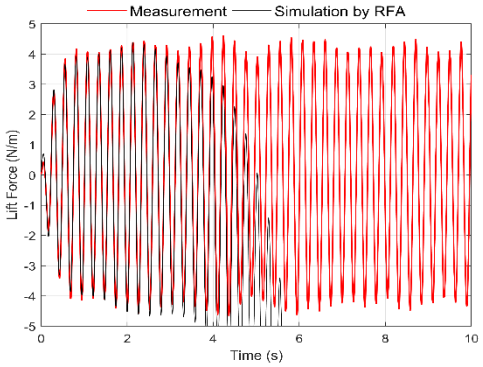

g) Lift force time history by 6 - 15 m/s combination.

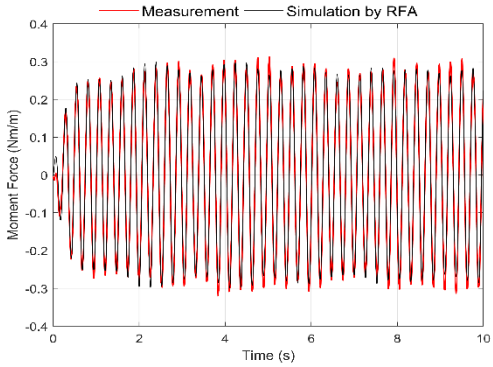

h) Moment time history by 6 - 15 m/s combination.

Fig. 41 Comparison of aeroelastic forces between measurement and simulation by RFA at wind speed 15 m/s.

The RFA coefficients extracted from various wind combinations are shown in Table 4. One interesting point is that λ parameter should be genuinely considered. In Table 4, there is a negative value of λ in the wind speed combination 6 and 15 m/s. A negative value of λ will make the predicted aeroelastic force infinity. Some literature [21], [41] pointed out that λ should be greater or equal to zero. Parameter λ associate with the transfer function in which output lags behind the inputs and permits an approximation of the delays by the positive value of λ. The error comes from a numerical manner since during wind tunnel experiment divergent was never occur. Many factors can contribute, such as phase lag which could not be controlled during the experiment.

Table 4 RFA coefficient extraction from various 6 m/s combinations.

Wind speed combination (m/s)	A_0		A_1		F		λ_L	λ_M
6 - 11	-16.837	-1.404	-2.222	0.182	11.771	2.725	0.150	0.184
	11.449	5.440	0.430	0.210	-10.581	-3.837		
6 - 12	-30.701	-12.041	-2.031	0.226	29.585	15.357	0.109	0.208
	6.698	3.048	0.408	0.196	-5.510	-1.325		
6 - 13	-39.421	-17.747	-1.979	0.152	36.590	20.233	0.080	0.206
	5.961	2.926	0.459	0.208	-5.647	-1.679		
6 - 14	-109.408	-67.371	-1.505	0.302	107.697	70.383	0.030	0.238
	3.638	1.699	0.440	0.190	-3.010	-0.313		
6 - 15	43.873	47.821	-2.057	0.002	-45.186	-44.328	-0.028	0.276
	1.297	0.614	0.602	0.250	-0.970	0.552		

4.5.3.3 Numerical simulation

To understand the mechanism of RFA extraction in two DOF experiment and why within in small different wind speed gives a different result. Numerical simulation is conducted following the procedure in chapter 3.

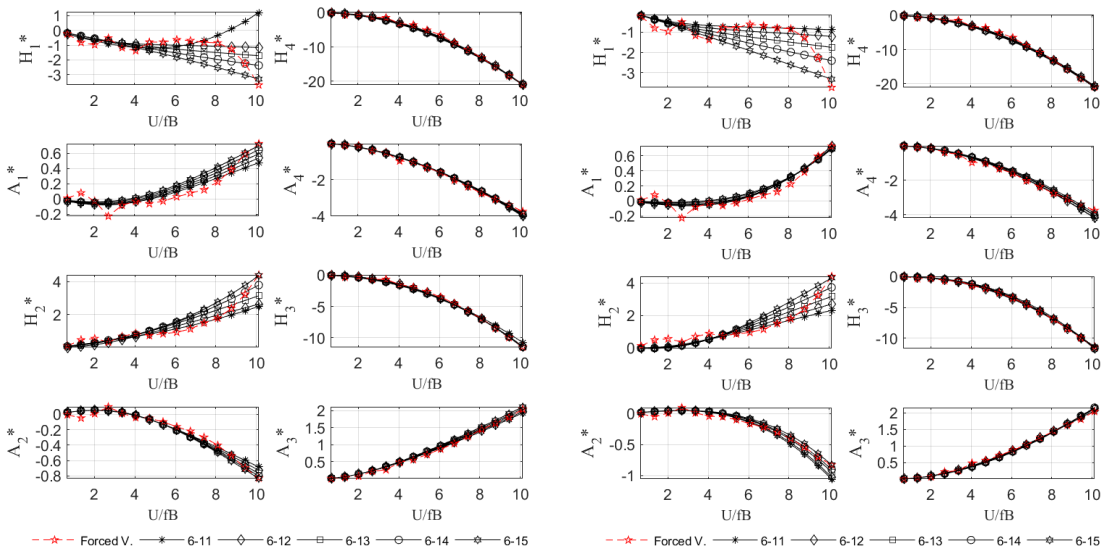

a) b)

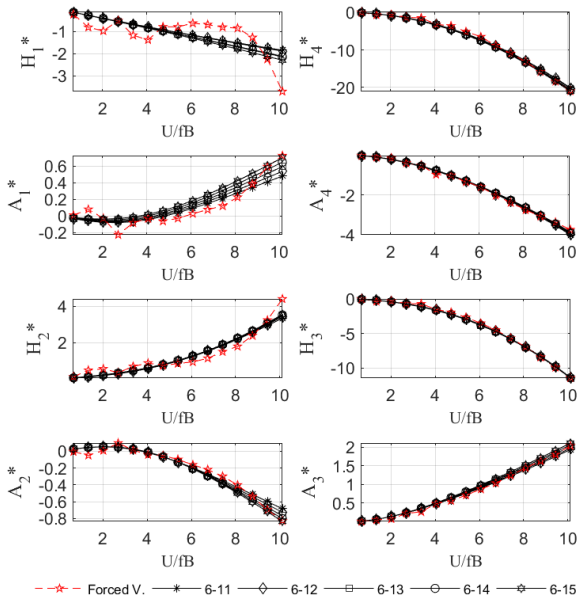

c)

Fig. 42 Simulation of RFA extraction in two DOF experiment

In Fig. 42 a) shows RFA extraction with conditions $H_1^*$and H_2^* are approximated with third-order polynomial and phase lag between displacement time histories are included. Fig. 42 b) shows RFA extraction with conditions $H_1^*$and H_2^* are approximated with third-order polynomial and phase lag between displacement time histories are neglected. Fig. 42 c) shows RFA extraction with conditions $H_1^*$and H_2^* are approximated with second-order polynomial and phase lag between displacement time histories are neglected. From the graph above, it can be concluded that the trend of aeroelastic forces which is represented by flutter derivatives, gives many contributions to RFA extraction. Since the experimental phase lag cannot be controlled and from the Fig. 42 (a) and (b) show that phase lag gives a small contribution to RFA extraction that can be ignored. Nevertheless, phase lag will contribute to a flutter derivatives trend.

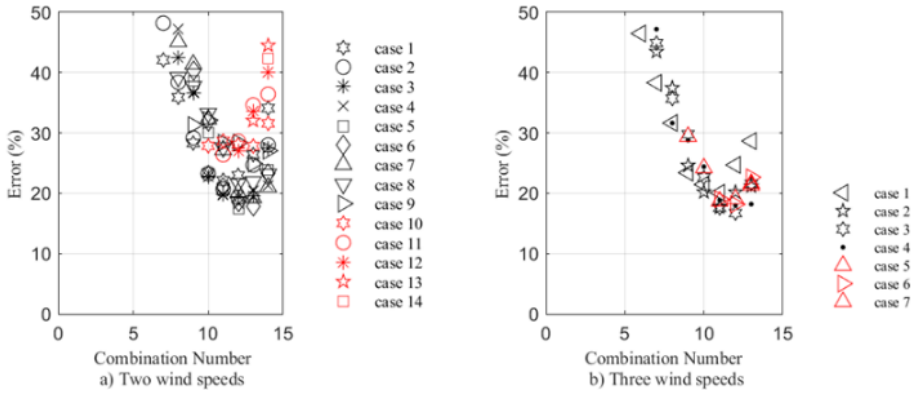

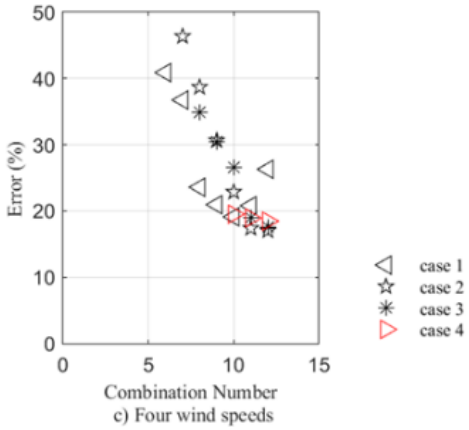

Fig. 43 Error comparison of flutter derivatives extraction at various combinations of experimental simulation using third-order polynomial.

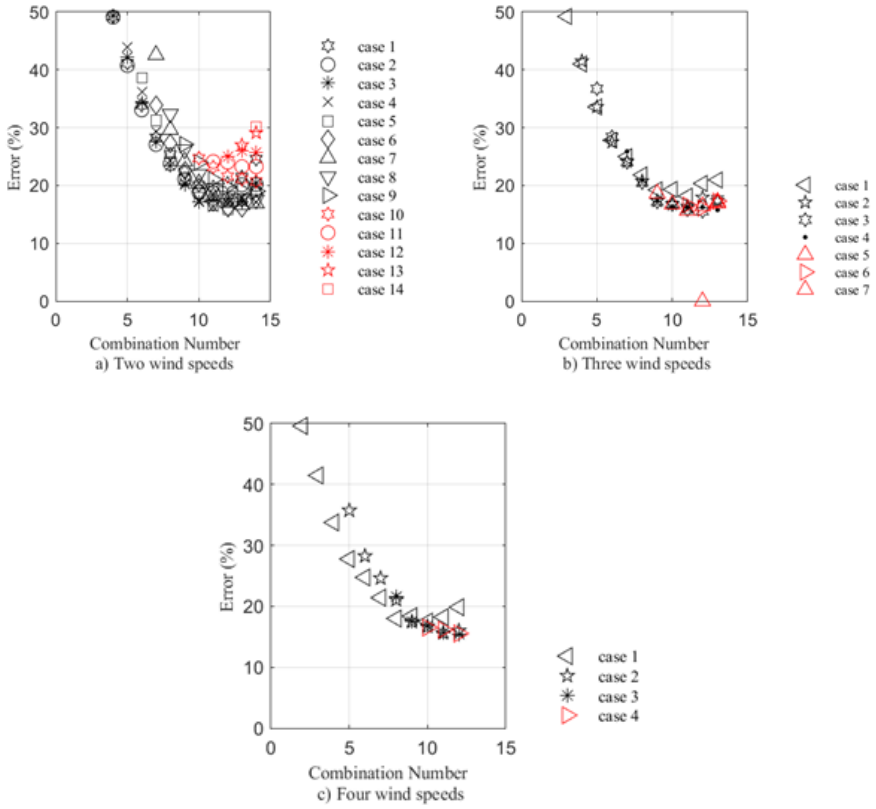

Fig. 44 Error comparison of flutter derivatives extraction at various combinations of experimental simulation using second-order polynomial.

In Fig. 43 and Fig 44 show error comparison using various combinations, third-order polynomial will give an average error of 25 % and second-order polynomial give an average error of 15%.

4.6 Summary

The conclusions from this chapter are summarized as follows:

1. The flutter derivatives obtained by the free and forced vibration (direct extraction) test generally compare well.
2. In the direct extraction, excitation frequency and pre-set amplitudes will affect $A_2^*$and H_2^*. Some literature points out that those discrepancies caused by separation flow the movement of the reattaching point of separation flow which needs further investigation.
3. The direct extraction approach requires the amplitude and phase lag parameters to extract flutter derivatives. On the other hand, the RFA extraction requires time histories and a proper data measurement is necessary because aeroelastic forces contain noise that will amplify after taking the numerical derivative.
4. In RFA extraction, the data length of time history will not influence RFA extraction results and 10 seconds of data length is sufficient for RFA extraction.
5. In the pre-set amplitude case, it seems that the RFA algorithm does not affect much. An anomaly trend occurs in case C pre-set amplitude that might come from data processing.
6. One DOF experiment has the advantage that each heaving and torsional excitation contribution to aeroelastic forces is well quantified and separated at every wind speed. Direct excitation can approximate it. In experimental, RFA extraction can approximate well in heaving and torsional excitation very well.
7. The simulation of RFA extraction was conducted with the superposition of aeroelastic forces and showed a good agreement with all components of derivatives.
8. Based on experimental result, one DOF experiment gives derivatives in second-order polynomial while two DOF experiment gives a result of derivatives in third-order polynomial. The trend of derivatives provides a different result within a small range wind speed combination. Simulation of RFA extraction in two DOF experiments clearly shows that trend derivatives will affect the extraction and fluctuating phase lag will not contribute to RFA extraction result.

Chapter 5. Conclusion and Future Research

5.1 Conclusion

Direct extraction of flutter derivatives in time domain requires less wind speed than in frequency domain. Previous study stated that two wind speed combination is sufficient to extract flutter derivatives. The identification process caused ambiguity in the flutter derivatives extraction principle because the aerodynamic damping did not always change monotonically and must be extracted in every wind speed. However, what condition of wind speed is chosen to extract a full set of RFA coefficients such as time length, polynomial order of derivatives was not yet fully explained. This thesis aims to find the applicability and mechanism of direct extraction of RFA. On the basis of the numerical and experimental study, the following conclusion is established.

1. Direct extraction of RFA required one lag term with a minimum of two wind speed combination. The increasing number of wind speed in the combination will not improve the result significantly as well as the increasing number of lag terms.
2. Increasing the number of lag terms will cause redundant results due to increasing unknown parameter numbers. This technique is quite different from indirect extraction, in which lag terms play an important role in approximation.
3. There are some discrepancies in obtaining flutter derivatives between free and forced vibrations methods that might be caused by airflow state.
4. In one DOF of direct extraction, excitation frequencies and pre-set amplitude will affect derivative associated with torsional oscillation due to state flow issue, and previous publication confirmed that issue.
5. In one DOF of direct extraction of RFA, there is no effect on data length and discrepancies occur in case pre-set amplitude solely due to data processing.
6. Based on simulation and experimental results, The trend of derivatives influence of RFA extraction, RFA extraction can only approximate derivative in second-order polynomial.
7. In a third-order polynomial case, the error can be minimized by averaging the result to some extent.

5.2 Future Research

Some suggestion for future research can be described as follows:

1. A more advanced wind tunnel setup is required to extract flutter derivatives in forced vibration method where phase lag between aeroelastic forces and time histories can be controlled in order to study coupled vibration effect with different phase lag.
2. The results from free vibration, one and two DOF of forced vibration give different values. Further investigation in wind flow by using Particle Image Velocimetry (PIV) and validated pressure field by numerical simulation is strongly suggested.

Bibliography

[1] R. H. Scanlan, “The action of flexible bridges under wind, I: Flutter theory,” *J. Sound Vib.*, vol. 60, no. 2, pp. 187–199, 1978.

[2] R. H. Scanlan and J. J. Tomko, “Airfoil and Bridge Deck Flutter Derivatives,” *Airfoil Bridg. Deck Flutter Deriv.*, vol. 97, pp. 1717–1733, Jan. 1971.

[3] A. G. Chowdhury and P. P. Sarkar, “Experimental identification of rational function coefficients for time-domain flutter analysis,” *Eng. Struct.*, vol. 27, no. 9, pp. 1349–1364, Aug. 2005.

[4] B. Cao and P. P. Sarkar, “Identification of Rational Functions by Forced Vibration Method for Time-Domain Analysis of Flexible Structures,” in *Proceedings of The Fifth International Symposium on Computational Wind Engineering*, 2010.

[5] B. Cao and P. P. Sarkar, “Identification of Rational Functions using two-degree-of-freedom model by forced vibration method,” *Eng. Struct.*, vol. 43, pp. 21–30, Oct. 2012.

[6] H. Scot Sauder and P. Sarkar, “A 3-DOF forced vibration system for time-domain aeroelastic parameter identification,” *Wind Struct. An Int. J.*, vol. 24, pp. 481–500, May 2017.

[7] B. Siedziako and O. Øiseth, “An enhanced identification procedure to determine the rational functions and aerodynamic derivatives of bridge decks,” *J. Wind Eng. Ind. Aerodyn.*, vol. 176, pp. 131–142, May 2018.

[8] H. Yamada, T. Miyata, and H. Ichikawa, “Measurement of Aerodynamic Coefficients by System identification methods,” *J. Wind Eng. Ind. Aerodyn.*, vol. 42, no. 1–3, pp. 1255–1263, Oct. 1992.

[9] M. Hoshiya and E. Saito, “Structural Identification by Extended Kalman Filter,” *J. Eng. Mech.*, vol. 110, no. 12, pp. 1757–1770, 1984.

[10] A. G. Chowdhury and P. P. Sarkar, “A new technique for identification of eighteen flutter derivatives using a three-degree-of-freedom section model,” *Eng. Struct.*, vol. 25, no. 14, pp. 1763–1772, Dec. 2003.

[11] M. Gu, R. Zhang, and H. Xiang, “Identification of flutter derivatives of bridge decks,” *J. Wind Eng. Ind. Aerodyn.*, vol. 84, no. 2, pp. 151–162, Jan. 2000.

[12] J. BogunovićJakobsen and E. Hjorth-Hansen, “Determination of the aerodynamic derivatives by a system identification method,” *J. Wind Eng. Ind. Aerodyn.*, vol. 57, no. 2–3, pp. 295–305, Jul. 1995.

[13] H. T. Lam, H. Katsuchi, and H. Yamada, “Investigation of Turbulence Effects on the Aeroelastic Properties of a Truss Bridge Deck Section,” *Engineering*, vol. 3, no. 6, pp. 845–853, Dec. 2017.

[14] V. Boonyapinyo and T. Janesupasaeree, “Data-driven stochastic subspace identification of flutter derivatives of bridge decks,” *J. Wind Eng. Ind. Aerodyn.*, vol. 98, no. 12, pp. 784–799, Dec. 2010.

[15] Roger and K. L., “Airplane Math Modeling Methods for Active Control Design,” *AGARD-CP-228*, pp. 4.1-4.11, 1977.

[16] M. Karpel, “Design for Active Flutter Suppression and Gust Alleviation Using State-Space Aeroelastic Modeling,” *J. Aircr.*, vol. 19, no. 3, pp. 221–227, Mar. 1982.

[17] S. H. Tiffany and W. M. Adams, “Nonlinear Programming Extensions to Rational Function Approximation Methods for Unsteady Aerodynamic Forces,” Virginia, 1988.

[18] W. Eversman and A. Tewari, “Consistent rational-function approximation for unsteady aerodynamics,” *J. Aircr.*, vol. 28, no. 9, pp. 545–552, 1991.

[19] E. H. Dowell, “A Simple Method for Converting Frequency-Domain Aerodynamics to the Time Domain,” Virginia.

[20] C. R. Marqui, D. D. Bueno, L. C. S. Goes, and P. J. P. Gonçalves, “A reduced order state space model for aeroelastic analysis in time domain,” *J. Fluids Struct.*, vol. 69, pp. 428–440, Feb. 2017.

[21] K. Wilde, Y. Fujino, and J. Masukawa, “Time domain modelling of bridge deck flutter, Journal of Structural Enginnering and Earthquake Engineering,” *Japan Soc. Civ. Eng.*, vol. 13, pp. 93–104, Jan. 1996.

[22] N. Danh Thang, H. Katsuchi, H. Yamada, and E. Sasaki, “Effects of approximation of self-excited forces by rational function on wind-induced response of a long-span bridge,” *J. Struct. Eng. A*, vol. 54A, pp. 420–428, 2008.

[23] V. Boonyapinyo, T. Miyata, and H. Yamada, “Advanced Aerodynamic Analysis of Suspension Bridges by State-Space Approach,” *J. Struct. Eng.*, vol. 125, no. 12, pp. 1357–1366, 1999.

[24] X. Chen, M. Matsumoto, and A. Kareem, “Time Domain Flutter and Buffeting Response Analysis of Bridges,” *J. Eng. Mech.*, vol. 126, no. 1, pp. 7–16, 2002.

[25] K. K. Bera and N. K. Chandiramani, “Time Domain Flutter Speed Analysis of Cable Stayed Bridge,” *Procedia Eng.*, vol. 144, pp. 917–927, Jan. 2016.

[26] H. Katsuchi, H. Yamada, and S. Kusuhara, “Analysis of Wind-Induced Response of Long-Span Suspension Bridges with Rational Function Approximation of Flutter Derivatives,” *Proc. Wind Eng. Symp.*, vol. 19, pp. 441–446, 2006.

[27] H. Irpanni, H. Katsuchi, and H. Yamada, “Numerical Simulation for Direct Extraction of Flutter Derivatives with Rational Function Approximation,” in *The 15th International Conference on Wind Engineering*, 2019.

[28] T. Theodorsen, *Mechanism of flutter : a theoretical and experimental investigation of the flutter problem*. Washington D.C.: U.S. Government Printing Office, 1940.

[29] Y. C. Fung, *An introduction to the theory of aeroelasticity,*. New York: Wiley, 1955.

[30] E. Simiu and R. H. Scanlan, *Wind effects on structures: fundamentals and applications to design*. Dover Publications, Incorporated, 2013.

[31] S. S. Mishra, K. Kumar, and P. Krishna, “Multimode flutter of long-span cable-stayed bridge based on 18 experimental aeroelastic derivatives,” *J. Wind Eng. Ind. Aerodyn.*, vol. 96, no. 1, pp. 83–102, Jan. 2008.

[32] S. H. Tiffany and W. M. Adams, *Nonlinear Programming - Extensions to Rational Function Approximation Methods for Unsteady Aerodynamic Forces Nonlinear Programming Extensions to Rational Function Approximation Methods for Unsteady Aerodynamic Forces*, no. Accessed from https://nla.gov.au/nla.cat-vn4021383. [Washington, DC] : [Springfield, Va: National Aeronautics and Space Administration, Scientific and Technical Information Division ; For sale by the National Technical Information Service], 1988.

[33] T. Miyata, N. (Nobumitsu) Fujisawa, H. Yamada, and J. ISBAP ’98 (1998 : Kobe-shi, *Long-span bridges and aerodynamics*. Springer, 1999.

[34] T. Miyata, H. Sato, R. Toriumi, M. Kitagawa, and H. Katsuchi, “Full Model Wind Tunnel Study of the Akashi Kaikyo Bridge,” in *Full Model Wind Tunnel Study of the Akashi Kaikyo Bridge*, 1995, pp. 793–802.

[35] Consortium of China Contractor, “Wind Tunnel Study on Wind-resistant Performance of Suramadu Bridge in Indonesia,” State Key Laboratory for Disaster Reduction in Civil Engineering, Tongji University, Shanghai, China, 2005.

[36] F. A. Ismail, “Problematic Discussions on Application of Aerodynamic Parameter Identification to the Compound Wind Induced Vibration,” Yokohama National University, 1997.

[37] H. T. Lam, H. Katsuchi, and H. Yamada, “Identification of flutter derivatives of

truss deck from gust response," Yokohama National University, 2017.

[38] P. P. Sarkar, L. Caracoglia, F. L. Haan, H. Sato, and J. Murakoshi, "Comparative and sensitivity study of flutter derivatives of selected bridge deck sections, Part 1: Analysis of inter-laboratory experimental data," *Eng. Struct.*, vol. 31, no. 1, pp. 158–169, Jan. 2009.

[39] F. L. Haan, "The effects of turbulence on the aerodynamics of long-span bridges.," University of Notre Dame, 2000.

[40] M. Noda, H. Utsunomiya, F. Nagao, M. Kanda, and N. Shiraishi, "Effects of oscillation amplitude on aerodynamic derivatives," *J. Wind Eng. Ind. Aerodyn.*, vol. 91, no. 1–2, pp. 101–111, Jan. 2003.

Appendix 1. Lag terms coefficient formulation

a) One lag term

$$\mathbf{Q}(p) = \mathbf{A}_0 + \mathbf{A}_1 p + \begin{bmatrix} D_{11} \\ D_{21} \end{bmatrix} \frac{p}{p+\lambda_l} \begin{bmatrix} E_{11} & E_{12} \end{bmatrix}$$

$$\mathbf{Q}(p) = \mathbf{A}_0 + \mathbf{A}_1 p + \frac{p}{p+\lambda_l} \begin{bmatrix} D_{11}E_{11} & D_{11}E_{12} \\ D_{21}E_{11} & D_{21}E_{12} \end{bmatrix}$$

$$\mathbf{Q}(p) = \mathbf{A}_0 + \mathbf{A}_1 p + \frac{\mathbf{F}p}{p+\lambda_l}$$

$$\mathbf{Q}(p) = \begin{bmatrix} (A_0)_{11} + (A_1)_{11} + \dfrac{pF_{11}}{p+\lambda_l} & (A_0)_{12} + (A_1)_{12} + \dfrac{pF_{12}}{p+\lambda_l} \\ (A_0)_{21} + (A_1)_{21} + \dfrac{pF_{21}}{p+\lambda_l} & (A_0)_{22} + (A_1)_{22} + \dfrac{pF_{22}}{p+\lambda_l} \end{bmatrix}$$

Inverse Laplace domain of aeroelastic for one lag term can be written as follows:

$$\dot{L}_{ae} + \lambda_L \frac{U}{B} L_{ae} = \frac{1}{2}\rho U^2 B \left\{ \left(\frac{U}{B}\right) \boldsymbol{\psi}_1 \mathbf{q} + \boldsymbol{\psi}_2 \dot{\mathbf{q}} + \left(\frac{B}{U}\right) \boldsymbol{\psi}_3 \ddot{\mathbf{q}} \right\}$$

$$\dot{M}_{ae} + \lambda_L \frac{U}{B} M_{ae} = \frac{1}{2}\rho U^2 B^2 \left\{ \left(\frac{U}{B}\right) \boldsymbol{\psi}_4 \mathbf{q} + \boldsymbol{\psi}_5 \dot{\mathbf{q}} + \left(\frac{B}{U}\right) \boldsymbol{\psi}_6 \ddot{\mathbf{q}} \right\}$$

$$\boldsymbol{\psi}_1 = \begin{bmatrix} \lambda_L (A_0)_{11} & \lambda_L (A_0)_{12} \end{bmatrix};$$

$$\boldsymbol{\psi}_2 = \begin{bmatrix} (A_0)_{11} + \lambda_L (A_1)_{11} + (F)_{11} & (A_0)_{12} + \lambda_L (A_1)_{12} + (F)_{12} \end{bmatrix}$$

$$\boldsymbol{\psi}_3 = \begin{bmatrix} (A_1)_{11} & (A_1)_{12} \end{bmatrix};$$

$$\boldsymbol{\psi}_4 = \begin{bmatrix} \lambda_M (A_0)_{21} & \lambda_M (A_0)_{22} \end{bmatrix}$$

$$\boldsymbol{\psi}_5 = \begin{bmatrix} (A_0)_{21} + \lambda_M (A_1)_{21} + (F)_{21} & (A_0)_{22} + \lambda_M (A_1)_{22} + (F)_{22} \end{bmatrix};$$

$$\boldsymbol{\psi}_6 = \begin{bmatrix} (A_1)_{21} & (A_1)_{22} \end{bmatrix}$$

b) Two lag terms

$$\mathbf{Q}(p)=\mathbf{A}_0+\mathbf{A}_1 p+\begin{bmatrix} D_{11} & D_{12} \\ D_{21} & D_{22} \end{bmatrix}\begin{bmatrix} \dfrac{p}{p+\lambda_1} & 0 \\ 0 & \dfrac{p}{p+\lambda_2} \end{bmatrix}\begin{bmatrix} E_{11} & E_{12} \\ E_{21} & E_{22} \end{bmatrix}$$

$$\mathbf{Q}(p)=\mathbf{A}_0+\mathbf{A}_1 p+p\begin{bmatrix} \dfrac{D_{11}E_{11}}{p+\lambda_1}+\dfrac{D_{12}E_{21}}{p+\lambda_2} & \dfrac{D_{11}E_{12}}{p+\lambda_1}+\dfrac{D_{12}E_{22}}{p+\lambda_2} \\ \dfrac{D_{21}E_{11}}{p+\lambda_1}+\dfrac{D_{22}E_{21}}{p+\lambda_2} & \dfrac{D_{21}E_{12}}{p+\lambda_1}+\dfrac{D_{22}E_{22}}{p+\lambda_2} \end{bmatrix}$$

$$\mathbf{Q}(p)=\mathbf{A}_0+\mathbf{A}_1 p+\frac{p\mathbf{F}}{p+\lambda_1}+\frac{p\mathbf{G}}{p+\lambda_2}$$

$$\mathbf{Q}(p)=\mathbf{A}_0+\mathbf{A}_1 p+\frac{\mathbf{F}p\left(p+\lambda_2\right)+\mathbf{G}p\left(p+\lambda_1\right)}{\left(p+\lambda_1\right)\left(p+\lambda_2\right)}$$

$$\mathbf{Q}(p)=\mathbf{A}_0+\mathbf{A}_1 p+\frac{p^2(\mathbf{F}+\mathbf{G})+p\left(\mathbf{G}\lambda_1+\mathbf{F}\lambda_2\right)}{p^2+p\left(\lambda_1+\lambda_2\right)+\lambda_1\lambda_2}$$

Inverse Laplace domain of aeroelastic for two lag terms can be written as follows:

$$\ddot{L}_{ae}+\left(\lambda_{L1}+\lambda_{L2}\right)\left(\frac{U}{B}\right)\dot{L}_{ae}+\left(\lambda_{L1}\lambda_{L2}\right)\left(\frac{U}{B}\right)^2 L_{ae}=\frac{1}{2}\rho U^2 B\left(\left(\frac{U}{B}\right)^2\boldsymbol{\psi}_1\mathbf{q}+\left(\frac{U}{B}\right)\boldsymbol{\psi}_2\dot{\mathbf{q}}+\boldsymbol{\psi}_3\ddot{\mathbf{q}}+\left(\frac{B}{U}\right)\boldsymbol{\psi}_4\ddot{\mathbf{q}}\right)$$

$$\ddot{M}_{ae}+\left(\lambda_{M1}+\lambda_{M2}\right)\left(\frac{U}{B}\right)\dot{M}_{ae}+\left(\lambda_{M1}\lambda_{M2}\right)\left(\frac{U}{B}\right)^2 M_{ae}=\frac{1}{2}\rho U^2 B^2\left(\left(\frac{U}{B}\right)^2\boldsymbol{\psi}_5\mathbf{q}+\left(\frac{U}{B}\right)\boldsymbol{\psi}_6\dot{\mathbf{q}}+\boldsymbol{\psi}_7\ddot{\mathbf{q}}+\left(\frac{B}{U}\right)\boldsymbol{\psi}_8\ddot{\mathbf{q}}\right)$$

$$\boldsymbol{\psi}_1=\begin{bmatrix}\lambda_{L1}\lambda_{L2}\left(A_0\right)_{11} & \lambda_{L1}\lambda_{L2}\left(A_0\right)_{12}\end{bmatrix}$$

$$\boldsymbol{\psi}_2=\begin{bmatrix}\left(\lambda_{L1}+\lambda_{L2}\right)\left(A_0\right)_{11}+\left(\lambda_{L1}\lambda_{L2}\right)\left(A_1\right)_{11}+\lambda_{L2}\left(F\right)_{11}+\lambda_{L1}\left(G\right)_{11} \\ \left(\lambda_{L1}+\lambda_{L2}\right)\left(A_0\right)_{12}+\left(\lambda_{L1}\lambda_{L2}\right)\left(A_1\right)_{12}+\lambda_{L2}\left(F\right)_{12}+\lambda_{L2}\left(G\right)_{12}\end{bmatrix}^T$$

$$\boldsymbol{\psi}_3=\begin{bmatrix}\left(A_0\right)_{11}+\left(\lambda_{L1}+\lambda_{L2}\right)\left(A_1\right)_{11}+\left(F\right)_{11}+\left(G\right)_{11} & \left(A_0\right)_{11}+\left(\lambda_{L1}+\lambda_{L2}\right)\left(A_1\right)_{11}+\left(F\right)_{11}+\left(G\right)_{11}\end{bmatrix}$$

$$\boldsymbol{\psi}_4=\begin{bmatrix}\left(A_1\right)_{11} & \left(A_1\right)_{12}\end{bmatrix}$$

$$\boldsymbol{\psi}_5=\begin{bmatrix}\lambda_{M1}\lambda_{M2}\left(A_0\right)_{21} & \lambda_{M1}\lambda_{M2}\left(A_0\right)_{22}\end{bmatrix}$$

$$\boldsymbol{\psi}_6=\begin{bmatrix}\left(\lambda_{M1}+\lambda_{M2}\right)\left(A_0\right)_{21}+\left(\lambda_{M1}\lambda_{M2}\right)\left(A_1\right)_{21}+\lambda_{M2}\left(F\right)_{21}+\lambda_{M1}\left(G\right)_{11} \\ \left(\lambda_{M1}+\lambda_{M2}\right)\left(A_0\right)_{12}+\left(\lambda_{M1}\lambda_{M2}\right)\left(A_1\right)_{12}+\lambda_{M2}\left(F\right)_{12}+\lambda_{M2}\left(G\right)_{12}\end{bmatrix}^T$$

$$\boldsymbol{\psi}_7=\begin{bmatrix}\left(A_0\right)_{21}+\left(\lambda_{L1}+\lambda_{L2}\right)\left(A_1\right)_{21}+\left(F\right)_{21}+\left(G\right)_{21} & \left(A_0\right)_{22}+\left(\lambda_{L1}+\lambda_{L2}\right)\left(A_1\right)_{22}+\left(F\right)_{22}+\left(G\right)_{22}\end{bmatrix}$$

$$\boldsymbol{\psi}_8=\begin{bmatrix}\left(A_1\right)_{21} & \left(A_1\right)_{22}\end{bmatrix}$$

c) Three lag terms

$$\mathbf{Q}(p)=\mathbf{A}_0+\mathbf{A}_1 p+\begin{bmatrix} D_{11} & D_{12} & D_{13} \\ D_{21} & D_{22} & D_{23} \end{bmatrix}\begin{bmatrix} \frac{p}{p+\lambda_1} & 0 & 0 \\ 0 & \frac{p}{p+\lambda_2} & 0 \\ 0 & 0 & \frac{p}{p+\lambda_3} \end{bmatrix}\begin{bmatrix} E_{11} & E_{12} \\ E_{21} & E_{22} \\ E_{31} & E_{32} \end{bmatrix}$$

$$\mathbf{Q}(p)=\mathbf{A}_0+\mathbf{A}_1 p+p\begin{bmatrix} \frac{D_{11}E_{11}}{p+\lambda_1}+\frac{D_{12}E_{21}}{p+\lambda_2}+\frac{D_{13}E_{31}}{p+\lambda_3} & \frac{D_{11}E_{12}}{p+\lambda_1}+\frac{D_{12}E_{22}}{p+\lambda_2}+\frac{D_{13}E_{32}}{p+\lambda_3} \\ \frac{D_{21}E_{11}}{p+\lambda_1}+\frac{D_{22}E_{21}}{p+\lambda_2}+\frac{D_{23}E_{31}}{p+\lambda_3} & \frac{D_{21}E_{12}}{p+\lambda_1}+\frac{D_{22}E_{22}}{p+\lambda_2}+\frac{D_{23}E_{32}}{p+\lambda_3} \end{bmatrix}$$

$$\mathbf{Q}(p)=\mathbf{A}_0+\mathbf{A}_1 p+\frac{\mathbf{F}}{p+\lambda_1}p+\frac{\mathbf{G}}{p+\lambda_2}p+\frac{\mathbf{H}}{p+\lambda_3}p$$

$$\mathbf{Q}(p)=\mathbf{A}_0+\mathbf{A}_1 p+\frac{p\left(p^2(\mathbf{F}+\mathbf{G}+\mathbf{H})+p\left((\lambda_2+\lambda_3)\mathbf{F}+(\lambda_1+\lambda_3)\mathbf{G}+(\lambda_1+\lambda_2)\mathbf{H}\right)+\left(\mathbf{G}\lambda_1\lambda_3+\mathbf{H}\lambda_1\lambda_2+\mathbf{F}\lambda_2\lambda_3\right)\right)}{(p+\lambda_1)(p+\lambda_2)(p+\lambda_3)}$$

$$\mathbf{Q}(p)=\mathbf{A}_0+\mathbf{A}_1 p+\frac{p^3(\mathbf{F}+\mathbf{G}+\mathbf{H})+p^2\left((\lambda_2+\lambda_3)\mathbf{F}+(\lambda_1+\lambda_3)\mathbf{G}+(\lambda_1+\lambda_2)\mathbf{H}\right)+p\left(\mathbf{G}\lambda_1\lambda_3+\mathbf{H}\lambda_1\lambda_2+\mathbf{F}\lambda_2\lambda_3\right)}{p^3+p^2(\lambda_1+\lambda_2+\lambda_3)+p(\lambda_1\lambda_2+\lambda_1\lambda_3+\lambda_2\lambda_3)+\lambda_1\lambda_2\lambda_3}$$

Inverse Laplace domain of aeroelastic for three lag terms can be written as follows:

$$\ddot{L}_{ae}+(\lambda_{L1}+\lambda_{L2}+\lambda_{L3})\left(\frac{U}{B}\right)\ddot{L}_{ae}+(\lambda_{L1}\lambda_{L2}+\lambda_{L1}\lambda_{L3}+\lambda_{L2}\lambda_{L3})\left(\frac{U}{B}\right)^2\dot{L}_{ae}+(\lambda_{L1}\lambda_{L2}\lambda_{L3})\left(\frac{U}{B}\right)^3 L_{ae}=$$

$$\frac{1}{2}\rho U^2 B\left(\left(\frac{U}{B}\right)^3\boldsymbol{\psi}_1\mathbf{q}+\left(\frac{U}{B}\right)^2\boldsymbol{\psi}_2\mathbf{q}+\left(\frac{U}{B}\right)\boldsymbol{\psi}_3\dot{\mathbf{q}}+\boldsymbol{\psi}_4\ddot{\mathbf{q}}+\left(\frac{B}{U}\right)\boldsymbol{\psi}_5\ddot{\dot{\mathbf{q}}}\right)$$

$$\ddot{M}_{ae}+(\lambda_{M1}+\lambda_{M2}+\lambda_{M3})\left(\frac{U}{B}\right)\ddot{M}_{ae}+(\lambda_{M1}\lambda_{M2}+\lambda_{M1}\lambda_{M3}+\lambda_{M2}\lambda_{M3})\left(\frac{U}{B}\right)^2\dot{M}_{ae}+(\lambda_{M1}\lambda_{M2}\lambda_{M3})\left(\frac{U}{B}\right)^3 M_{ae}=$$

$$\frac{1}{2}\rho U^2 B^2\left(\left(\frac{U}{B}\right)^3\boldsymbol{\psi}_6\mathbf{q}+\left(\frac{U}{B}\right)^2\boldsymbol{\psi}_7\mathbf{q}+\left(\frac{U}{B}\right)\boldsymbol{\psi}_8\dot{\mathbf{q}}+\boldsymbol{\psi}_9\ddot{\mathbf{q}}+\left(\frac{B}{U}\right)\boldsymbol{\psi}_{10}\ddot{\dot{\mathbf{q}}}\right)$$

$$\boldsymbol{\psi}_1=\begin{bmatrix}(\lambda_{L1}\lambda_{L2}\lambda_{L3}(A_0)_{11} & \lambda_{L1}\lambda_{L2}\lambda_{L3}(A_0)_{12}\end{bmatrix}$$

$$\boldsymbol{\psi}_2=\begin{bmatrix}(\lambda_{L1}\lambda_{L2}+\lambda_{L1}\lambda_{L3}+\lambda_{L2}\lambda_{L3})(A_0)_{11}+(\lambda_{L1}\lambda_{L2}\lambda_{L3})(A_1)_{11}+(\lambda_{L2}\lambda_{L3})(F)_{11}+(\lambda_{L1}\lambda_{L3})(G)_{11}+(\lambda_{L1}\lambda_{L2})(H)_{11} \\ (\lambda_{L1}\lambda_{L2}+\lambda_{L1}\lambda_{L3}+\lambda_{L2}\lambda_{L3})(A_0)_{12}+(\lambda_{L1}\lambda_{L2}\lambda_{L3})(A_1)_{12}+(\lambda_{L2}\lambda_{L3})(F)_{12}+(\lambda_{L1}\lambda_{L3})(G)_{12}+(\lambda_{L1}\lambda_{L2})(H)_{12}\end{bmatrix}^T$$

$$\boldsymbol{\psi}_3=\begin{bmatrix}(\lambda_{L1}+\lambda_{L2}+\lambda_{L3})(A_0)_{11}+(\lambda_{L1}\lambda_{L2}+\lambda_{L1}\lambda_{L3}+\lambda_{L2}\lambda_{L3})(A_1)_{11}+(\lambda_{L2}+\lambda_{L3})(F)_{11}+(\lambda_{L1}+\lambda_{L3})(G)_{11}+(\lambda_{L1}+\lambda_{L2})(H)_{11} \\ (\lambda_{L1}+\lambda_{L2}+\lambda_{L3})(A_0)_{12}+(\lambda_{L1}\lambda_{L2}+\lambda_{L1}\lambda_{L3}+\lambda_{L2}\lambda_{L3})(A_1)_{12}+(\lambda_{L2}+\lambda_{L3})(F)_{12}+(\lambda_{L1}+\lambda_{L3})(G)_{12}+(\lambda_{L1}+\lambda_{L2})(H)_{12}\end{bmatrix}^T$$

$$\boldsymbol{\psi}_4=\begin{bmatrix}(A_0)_{11}+(\lambda_{L1}+\lambda_{L2}+\lambda_{L3})(A_1)_{11}+(F)_{11}+(G)_{11}+(H)_{11} & (A_0)_{12}+(\lambda_{L1}+\lambda_{L2}+\lambda_{L3})(A_1)_{12}+(F)_{12}+(G)_{12}+(H)_{12}\end{bmatrix}$$

$$\boldsymbol{\psi}_5=\begin{bmatrix}(A_1)_{11} & (A_1)_{12}\end{bmatrix}$$

$$\boldsymbol{\psi}_6 = \begin{bmatrix} \lambda_{M1}\lambda_{M2}\lambda_{M3}\left(A_0\right)_{21} & \lambda_{M1}\lambda_{M2}\lambda_{M3}\left(A_0\right)_{22} \end{bmatrix}$$

$$\boldsymbol{\psi}_7 = \begin{bmatrix} \left(\lambda_{M1}\lambda_{M2}+\lambda_{M1}\lambda_{M3}+\lambda_{M2}\lambda_{M3}\right)\left(\boldsymbol{A_0}\right)_{21}+\left(\lambda_{M1}\lambda_{M2}\lambda_{M3}\right)\left(A_1\right)_{21}+\left(\lambda_{M2}\lambda_{M3}\right)\left(F\right)_{21}+\left(\lambda_{M1}\lambda_{M3}\right)\left(G\right)_{21}+\left(\lambda_{M1}\lambda_{M2}\right)\left(H\right)_{11} \\ \left(\lambda_{M1}\lambda_{M2}+\lambda_{M1}\lambda_{M3}+\lambda_{M2}\lambda_{M3}\right)\left(\boldsymbol{A_0}\right)_{22}+\left(\lambda_{M1}\lambda_{M2}\lambda_{M3}\right)\left(A_1\right)_{22}+\left(\lambda_{M2}\lambda_{M3}\right)\left(F\right)_{22}+\left(\lambda_{M1}\lambda_{M3}\right)\left(G\right)_{22}+\left(\lambda_{M1}\lambda_{M2}\right)\left(H\right)_{12} \end{bmatrix}^T$$

$$\boldsymbol{\psi}_8 = \begin{bmatrix} \left(\lambda_{M1}+\lambda_{M2}+\lambda_{M3}\right)\left(\boldsymbol{A_0}\right)_{21}+\left(\lambda_{M1}\lambda_{M2}+\lambda_{M1}\lambda_{M3}+\lambda_{M2}\lambda_{M3}\right)\left(A_1\right)_{21}+\left(\lambda_{M2}+\lambda_{M3}\right)\left(F\right)_{21}+\left(\lambda_{M1}+\lambda_{M3}\right)\left(G\right)_{21}+\left(\lambda_{M1}+\lambda_{M2}\right)\left(H\right)_{21} \\ \left(\lambda_{M1}+\lambda_{M2}+\lambda_{M3}\right)\left(\boldsymbol{A_0}\right)_{22}+\left(\lambda_{M1}\lambda_{M2}+\lambda_{M1}\lambda_{M3}+\lambda_{M2}\lambda_{M3}\right)\left(A_1\right)_{22}+\left(\lambda_{M2}+\lambda_{M3}\right)\left(F\right)_{22}+\left(\lambda_{M1}+\lambda_{M3}\right)\left(G\right)_{22}+\left(\lambda_{M1}+\lambda_{M2}\right)\left(H\right)_{22} \end{bmatrix}^T$$

$$\boldsymbol{\psi}_9 = \begin{bmatrix} \left(\boldsymbol{A_0}\right)_{21}+\left(\lambda_{M1}+\lambda_{M2}+\lambda_{M3}\right)\left(A_1\right)_{21}+\left(F\right)_{21}+\left(G\right)_{21}+\left(H\right)_{21} & \left(\boldsymbol{A_0}\right)_{22}+\left(\lambda_{M1}+\lambda_{M2}+\lambda_{M3}\right)\left(A_1\right)_{22}+\left(F\right)_{22}+\left(G\right)_{22}+\left(H\right)_{22} \end{bmatrix}$$

$$\boldsymbol{\psi}_{10} = \begin{bmatrix} \left(A_1\right)_{21} & \left(A_1\right)_{22} \end{bmatrix}$$